

**Slow Speed Orthogonal Machining of Polycrystalline FCC, BCC, & HCP Alloys at
Various Levels of Hardness using Gaseous Coolants**

by

James Michael Carter

A thesis submitted to the Graduate Faculty of
Auburn University
in partial fulfillment of the
requirements for the Degree of
Master of Science

Auburn, Alabama
December 15, 2018

Keywords: orthogonal machining, metal cutting mechanics, quick stop device,
high speed videography, tool wear, gaseous cutting fluid

Copyright 2018 by James Michael Carter

Approved by

Lewis N. Payton, Chair, Associate Research Professor, Mechanical Engineering
Robert L. Jackson, Professor, Mechanical Engineering
Michael Bozack, Professor Emeritus, Physics

Abstract

A statistically designed slow speed orthogonal machining experiment was conducted to compare the effects of various metal-working gases upon the cutting process. Several metals with different crystalline structures and materials conditions were utilized (face centered cubic aluminum alloy 6061 with three tempers (T0, T4 and T6), close packed hexagonal AZ31B at two tempers (H0 and H24), and body centered cubic steel alloy 4130 at three levels of hardness (22, 32, and 42 HR_C). A single tool material of High-Speed Steel (HSS) was utilized with three different tool rake angles (α) of 25°, 30° and 35°. The cutting fluids utilized were air, argon, and nitrogen.

Classic Merchant Force Diagram (MFD) data was collected using a Kistler force Dynamometer and processed using LabVIEW software. The tools were pushed through the 2" long x 0.125" thick piece of stock material at two different depths of 0.004 inches and 0.008 inches. After 10 inches of cut, each tool was studied under a Keyence 3-D microscope in order to quantify the tool wear. High speed, high magnification video was taken of each cut to study all the visible shear angles. The video analysis was completed using KINOVEA video analysis software.

The force data was then used to explore different orthogonal metal working models to validate against literature. Statistical analysis was utilized to determine the relationships between visual shear angles and cutting environment. Analysis was made between tool wear and cutting atmosphere.

Acknowledgements

I want to thank God for the opportunities provided and the drive to accomplish whatever I put my mind to.

I would like to thank my wife and family for always inspiring and showing constant support to never quit.

I want to show my gratitude and thanks to Dr. Lewis Payton, who supported, guided, and lead me through Graduate School even when life got in the way.

I would like to thank my thesis committee members Dr. Robert Jackson and Dr. Michael Bozack for their review and patience in completing my research even after I was required to seek employment away from the university.

I want to thank Dr. Wesley Hunko for his guidance and advice not just with experimentation, but also with general academia. I also want to thank him for the constant support outside of academia in my personal life.

TABLE OF CONTENTS

ABSTRACT	ii
ACKNOWLEDGEMENTS	iii
LIST OF TABLES	vi
LIST OF FIGURES	viii
LIST OF SYMBOLS	x
I. INTRODUCTION	1
II. SCOPE AND OBJECTIVES	3
III. LITERATURE REVIEW	5
HISTORICAL SURVEY	5
CUTTING GEOMETRY WITH A SINGLE EDGE.....	9
THE SHEAR STRAIN MODELS	14
DISLOCATIONS AND METAL CUTTING	24
HIGH MAGNIFICATION PHOTOGRAPHY.....	26
CUTTING FLUIDS	30
IV. MATERIALS, INSTRUMENTS, AND MACHINES.....	36
SAMPLE PREPARATION	51
CUTTING SETUP.....	54
V. EXPERIMENTAL SEQUENCE	56
VIRTUAL QUICK STOP DATA ACQUISITION.....	56
TOOL WEAR ANALYSIS	57
POST PROCESSING	58
VI. INSTRUMENT VALIDATION AND STATISTICAL DESIGN OF EXPERIMENTS	60
MACHINE SETUP.....	60

RUN SETUP	62
VII. DATA RESULTS.....	64
IX. STATISTICAL ANALYSIS	76
ADDITIONAL ANOVA TABLES	92
RESULTS OF THE TOOL WEAR STUDY.....	96
SUMMARIZATION.....	99
X. FUTURE WORK.....	102
XI. REFERENCES	103
APPENDIX A.....	108
APPENDIX B	109
APPENDIX C	110
APPENDIX D.....	134
APPENDIX E	170
APPENDIX F.....	174
APPENDIX G.....	177
APPENDIX H.....	183

LIST OF TABLES

TABLE 1. MATERIAL HARDNESS.....	52
TABLE 2. ALUMINUM AND STEEL ETCHANTS.....	54
TABLE 3. SYMBOLS AND UNITS OF DIRECT MEASUREMENTS.....	64
TABLE 4. SYMBOLS AND UNITS OF CALCULATED MEASUREMENTS.....	66
TABLE 5. ANOVA OF CUTTING FORCE.....	77
TABLE 6. CUTTING FORCE T TEST AIR VS. ARGON.....	78
TABLE 7. CUTTING FORCE T TEST AIR VS. NITROGEN.....	78
TABLE 8. CUTTING FORCE T TEST ARGON VS. NITROGEN.....	79
TABLE 9. ANOVA OF THRUST FORCE FT.....	79
TABLE 10. THRUST FORCE FT T-TEST AIR VS ARGON.....	80
TABLE 11. THRUST FORCE FT T-TEST AIR VS NITROGEN.....	81
TABLE 12. THRUST FORCE T-TEST ARGON VS NITROGEN.....	81
TABLE 13. ANOVA OF SHEAR ANGLE ϕ	82
TABLE 14. SHEAR ANGLE T-TEST AIR VS. ARGON.....	83
TABLE 15. SHEAR ANGLE ϕ T-TEST AIR VS. NITROGEN.....	83
TABLE 16. SHEAR ANGLE ϕ T-TEST ARGON VS. NITROGEN.....	84
TABLE 17. ANOVA OF FRICTION FORCE F.....	85
TABLE 18. FRICTION FORCE F T-TEST AIR VS. ARGON.....	85
TABLE 19. FRICTION FORCE F T-TEST AIR VS. NITROGEN.....	86
TABLE 20. FRICTION FORCE F T-TEST ARGON VS. NITROGEN.....	86
TABLE 21. ANOVA FOR NORMAL FORCE N.....	87
TABLE 22. NORMAL FORCE N T TEST AIR VS. ARGON.....	87
TABLE 23. NORMAL FORCE N T TEST AIR VS. NITROGEN.....	88
TABLE 24. NORMAL FORCE N T TEST ARGON VS. NITROGEN.....	88
TABLE 25. ANOVA OF PSI ϕ	89

TABLE 26. PSI T TEST AIR VS. ARGON.....	90
TABLE 27. PSI T TEST AIR VS. NITROGEN	90
TABLE 28. PSI T TEST ARGON VS. NITROGEN	91
TABLE 29: ANOVA OF MERCHANT’S FS.....	92
TABLE 30: ANOVA MERCHANT’S FN.....	93
TABLE 31:ANOVA OF PAYTON FS	93
TABLE 32: ANOVA OF PAYTON'S FN.....	94
TABLE 33: ANOVA OF COEFFICIENT OF FRICTION (M).....	94
TABLE 34: ANOVA OF RESULTANT.....	95
TABLE 35: ANOVA FOR SPECIFIC HORSEPOWER	95
TABLE 36. VOLUME OF TOOL MATERIAL REMOVED	96
TABLE 37. NITROGEN V. ARGON T-TEST.....	97
TABLE 38. AIR V. NITROGEN T-TEST	97
TABLE 39. AIR V. ARGON T-TEST	98
TABLE 40: RANKED ANOVA EFFECTS FOR EACH ANALYSIS	99
TABLE 41: HPS T TEST AIR VS. ARGON.....	100
TABLE 42: HPS T TEST AIR VS. NITROGEN.....	100
TABLE 43: HPS T TEST ARGON VS. NITROGEN	101

LIST OF FIGURES

FIGURE 1. SHEAR PLANE ANGLE AND TOOL RAKE ANGLE.....	7
FIGURE 2. ORTHOGONAL MACHINING CUT	9
FIGURE 3. TYPE 1,2, & 3 CHIPS RESPECTIVELY.....	10
FIGURE 4. ORTHOGONAL CUTTING PROCESS	11
FIGURE 5. MERCHANT FORCE DIAGRAM [22].....	12
FIGURE 6. MERCHANT'S OBSERVATION OF CHIP FORMATION [26].....	14
FIGURE 7. MERCHANT'S STACK OF CARDS MODEL [14]	15
FIGURE 8. OKUSHIMA AND HITOMI'S MODEL [30].....	17
FIGURE 9. ZOREV'S MODEL OF A THICK ZONE.....	18
FIGURE 10. OXLEY'S PARALLEL-SIDED SHEAR ZONE MODEL [32]	19
FIGURE 11. VAN LUTTERVELT'S STATIONARY SHEAR ZONE MODEL [33].....	20
FIGURE 12. HUANG'S OBSERVATION OF FLOW IN SHEAR ZONE [34]	21
FIGURE 13. HUANG'S "NEW" STACK OF CARDS MODEL.....	23
FIGURE 14. ELEVATED VIEW OF EQUIPMENT SETUP	38
FIGURE 15. QUICK STOP WORKPIECE HOLDER.....	39
FIGURE 16. KISTLER DUAL MODE AMPLIFIERS	40
FIGURE 17. NATIONAL INSTRUMENTS USB-6008	41
FIGURE 18. MODIFIED LOAD LIFT CAMERA STAND	41
FIGURE 19. DRS TECHNOLOGIES LIGHTNING RDT CAMERA.....	42
FIGURE 20. CINCINNATI ARROW VMC 750 CNC MILL.....	43
FIGURE 21. BRIDGEPORT VERTICAL MILLING MACHINE.....	44
FIGURE 22. DO-ALL VERTICAL BAND SAW	45
FIGURE 23. WILTON BELT SANDER	46
FIGURE 24. ROCKWELL HARDNESS TESTER	47
FIGURE 25. MTS Q TEST 100 TENSILE TESTER.....	48
FIGURE 26. TENSILE TESTING JAWS WITH SPECIMEN INSERTED	49

FIGURE 27. KEYENCE VHX 1000 E DIGITAL MICROSCOPE.....	50
FIGURE 28. ASTM E8 SUB-SIZE SPECIMEN DIMENSIONS	53
FIGURE 29. WORKPIECE IN POSITION	54
FIGURE 30. EXAMPLE OF FORCE DATA	59
FIGURE 31. UNEXAMINED FRAME OF VIDEO.....	68
FIGURE 32. EXAMINED FRAME OF VIDEO	69
FIGURE 33. SHEAR ZONE GEOMETRY	70
FIGURE 34. CHIP TO TOOL INTERACTION ZONE	71
FIGURE 35. TOOL SHOWING SIGNS OF FAILING.....	72
FIGURE 36. 3D IMAGE OF TOOL AFTER 80 INCHES OF CUT IN AIR ENVIRONMENT	73
FIGURE 37. AREA OF TOOL-CHIP INTERFACE.....	74
FIGURE 38. TOOL WEAR ZONE WITH SCALE.....	75
FIGURE 39. BOXPLOT OF CUTTING FORCE DIVIDED BY RUN	76

LIST OF SYMBOLS

α	Tool Rake Angle
φ	Onset of Shear Plane Angle
ψ	Shear Front Angle
β	Mean Friction Angle Tool Face
μ	Friction Coefficient
t_{ord}	Ordered Depth of Cut
t_o	Uncut Chip Thickness
t_c	Cut Chip Thickness
w	Width of the Cut Chip
r_c	Ratio of Chip to Un-cut Chip thickness
F_c	Horizontal Cutting Force
F_t	Vertical Cutting Force
F	Frictional Force upon Chip
N	Normal Force upon Chip
R	Resultant Force upon Chip
F_s	Shear Force on the Plane
F_n	Normal Force on the Plane
A_s	Area of the Shear Plane
τ_s	Shear Stress on the Shear Plane
γ	Shear Strain (also ε in some works)

V	Cutting Velocity
V_c	Chip Velocity
V_s	Shear Velocity
HP	Horsepower
HP_s	Specific Horsepower
P	Power Required to Cut
MRR	Metal Removal Rate
U	Specific Total Cutting Energy
U_f	Specific Friction Energy
U_s	Specific Shear Energy
σ_s	Normal Stress
L	chip contact length on tool face

I. Introduction

Heat generated in the tool during the machining process has been known to be a major reason for tool failure during machining. Taylor mentions the following as the main actions that contribute to tool wear. [1]

- Pressure created when the chip slides over the tool
- The speed with which the chip slides over the tool
- The coefficient of friction between the chip and tool surface.

Longevity of tool life can be related to these three items. The question then becomes what the best way is to reduce or control the temperature of the chip-tool interface to reduce tool wear. The most prominent way to reduce temperatures in a machining application is with the application of a liquid coolant. These coolants are referred to as a metal working fluid (MWF).

The National Institute for Occupational Safety and Health (NIOSH) classifies metal cutting fluids as follows [2]:

1. Straight oil (neat oil) MWFs are severely solvent-refined petroleum oils (lubricant-base oils) or other animal, marine, vegetable, or synthetic oils used singly or in combination and with or without additives. Straight oils are not designed to be diluted with water.
2. Soluble oil (emulsifiable oil) MWFs are combinations of 30% to 85%severely refined lubricant-base oils and emulsifiers that may include other

performance additives. Soluble oils are diluted with water at ratios of 1-part concentrate to 5 parts water.

3. Semi-synthetic MWFs contain a lower amount of severely refined lubricant-base oil in the concentrate (5% to 30%), a higher proportion of emulsifiers, and 30% to 50% water. The transparent concentrate is diluted with 10 to 40 parts water.

4. Synthetic MWFs contain no petroleum oils and may be water-soluble or water dispersible. The synthetic concentrate is diluted with 10 to 40 parts water.

Each MWF consists of many different chemicals and can cause significant health risks if un-monitored. Water based MWF's, while common and readily available, can harbor bacteria and fungi. The water-based type can also accelerate a corrosive atmosphere for chips and causes an issue with both chip and coolant disposal [2].

These issues open the doors for alternative MWFs to be explored and their effects on the tool, chip, and forces associated with the machining process. This study looks at the effects of using three different gases on the cutting process.

II. Scope and Objectives

The goal of this thesis is to conduct orthogonal machining experiments to study the effect of gaseous cutting fluids on the resulting cutting forces and shear angles in Magnesium AZ31B, Aluminum 6061, and 4130 Steel. A detailed observation of the orthogonal metal cutting process was made possible using an all-digital high speed videographic quick stop device. The high speed videographic quick stop device consists of a high-speed digital camera synchronized to force measurements from a dynamometer. Precise feed control is also made possible by utilizing a variable frequency drive (VFD) electric motor to move the workpiece underneath the cutting tool. National Instrument's LabVIEW software was used to create a virtual instrument for automatic data collection and organization. These updates to previous virtual quick stop devices permit more precise control over the orthogonal machining process than ever before.

The objectives of the experiment included:

- 1) Develop a better understanding of the metal cutting process
- 2) Measure the Shear Plane Angle (ϕ), Shear Front Angle (ψ), and other geometries of interest directly from the images obtained
- 3) Capture high resolution still images of the metal cutting process during cutting that clearly show the geometries of interest for future publication
- 4) Investigate how the crystal structure of the metal to be machined affects the resulting geometries of interest and cutting forces
- 5) Determine the effect of gaseous cutting fluids on tool wear during the orthogonal machining process.

- 6) Perform tensile tests of the specimens to be machined for precise non-theoretical data of each specimen undergoing study
- 7) Publish the data set in a format (as appendices) which other researchers may use as a quality resource in their studies

III. Literature Review

Historical Survey

Modern machines for metal cutting as they are seen now have existed since the late 1840's and early 1850's. With these more modern machines came various attempts to study and quantify the variables of machining metal. It was during this time that the first scientific papers on metal cutting appeared.

The earliest reference that could be found relating to scientific studies of metal cutting, Cocquilhat in 1851, concentrated his work on rotating his workpiece on a drill. From these studies, he was able to apply the knowledge to other interests [3]. Utilizing the work per unit volume of material removed and assuming wages and working days, he was able to calculate the cost of digging tunnels, cutting marble, and trench digging.

The first experiments in which the influence of tool geometry was studied were reported by Joessel in 1864 [4]. Forces were obtained in lathe cutting and drilling by measuring the torque required to turn the machine while cutting, care being taken to subtract the torque required to overcome the friction of the machine. The effects of depth of cut, speed, and rake angle were studied. References to "cutting fluids" are also found in his work (linseed oil, quicklime and nitric acid to name a few), although no explanation of their benefit was attempted.

The first attempts to study chip formation are those of Time in 1870 and Tresca in 1873 [5] [6]. Time was the first to correctly model the process ahead of the tool as one of shear, although he may be criticized for his viewpoint that the chip formation took place by fracturing of the metal on successive shear planes rather than by plastic deformation.

This is understandable though since the plastic deformation of metals in operations other than cutting was only beginning to be investigated at the time.

Mallock produced a set of drawings of polished and etched chips in 1881 which rival modern photomicrographs in quality [7]. He deduced that the cutting process was one of shear along a sharply defined shear plane with friction occurring along the tool face. With Time, he thought of fracture as occurring on the successive shear planes and described the chip as a “metallic slate.” Mallock observed that the friction between the chip and the tool decreased when a “cutting fluid” was applied. His drawings clearly show that when cutting copper, the use of soap and water as a cutting fluid increased the shear plane angle, which is most easily described as a line from the tip of the tool to the back of the undeformed chip, Figure 1. He was also the first to attempt to categorize the bluntness of the leading edge of the tool (the cutting edge) as a factor.

In 1892, Haussner was successful in building the first instrument which could directly measure the forces involved in metal cutting [8]. In this planning dynamometer, the work was restrained by a stiff spring. Deflections of the spring were magnified, and a record was drawn by the dynamometer of the force against the distance of the cut. Although he was successful only in measuring the force horizontally along the cut, this was a major advancement. He also noted the earliest comments on what appears to be the built up edge in stating that “with ductile materials, after cutting starts, chips welded to the tool and were very hard to separate.” He may also have been the first to deduce the presence of a normal stress along the shear plane, concluding that the elements were not “freely sheared but is under a normal pressure”.

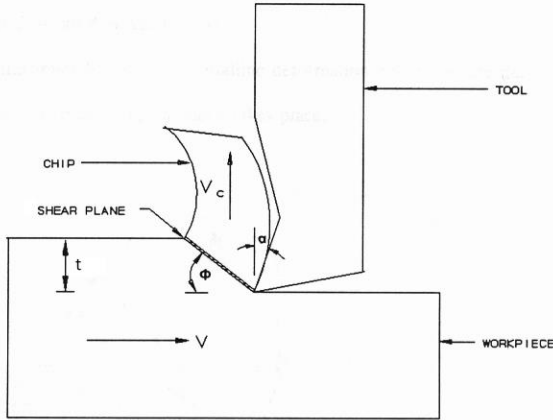


Figure 1. Shear Plane Angle and Tool Rake Angle

Zvorykin published an extensive review of planning in 1893 using his new hydraulic dynamometer [9]. He concurred with Haussner that the resultant force was not necessarily in the cutting direction. Assuming that the force in the direction of the cutting velocity would be a minimum led him to conclude the first attempt to predict the shear plane angle of Figure 1 in terms of the tool rake angle α and friction angle β .

$$f = 45 + \frac{a}{2} - \frac{b}{2} - \frac{bc}{2} \quad \square \quad (1)$$

ϕ corresponds to the shear plane angle, β is the friction angle on the chip and β' is a friction angle for the shear plane itself. This is the first of many formulations of the functional relationship amongst the various angles detailed shortly in an attempt to formulate a predictive relationship based upon the observed geometries at the tool interface. This equation will appear again in the literature review of modern theory, with β' equal to zero:

$$f = 45 + \frac{a}{2} - \frac{b}{2} \quad (2)$$

Equation (2) was derived independently in 1896, in the German engineering handbook "Ingenieur und Maschinenmechanick" [10]. The basis of derivation in that

case was that the shear plane would be the plane of maximum shear stress. The German handbook marks the beginning of the ongoing search for a predictive approach to the shear plane angle which eludes engineers to the current day. It carefully compared equations (1) and (2) at great length, offering reasons for the disagreement. Those equations continued in the literature after the turn of the 20th century. Linder in 1907 and Ernst and Merchant in 1941 obtained equation (1) [11] [12]. Piispanen in 1937 and Merchant in 1945 obtained equation (2) [13] [14]. The development of the many versions of this predictive equation will be detailed at great length in the Shear Zone Section of the literature review since one of the goals of the experiment is to compare the various models through a statistical analysis of the results.

Force analysis would continue to improve to the current day dynamometers and began to be joined with photographic studies in the “Roaring Twenties” when Coker and Chakko carried out experiments in 1922, and Coker in 1925 carried out a series of photo elastic experiments on the action of cutting tools [15] [16]. They were able to show in their photographs that there were zones of approximately radial compression and tension ahead of and behind a line going forward from the tool point, which corresponds to the plane defined by the angle ϕ in Figure 1. His photographs were not taken during cutting however, but during a stoppage of the tool. Ishi in 1929 and Schwerd were the first to study the cutting process while cutting was actually in progress [17] [18]. Photographs were also taken through a microscope by Boston which presented detailed appearance of the metal cutting process [19]. Their photographs were instrumental in the thought processes of the metal cutting investigators of the 1940’s and continue to be highly regarded today by photographic experts in the metal cutting field.

It was also at this time that one of the first experiments examining hardness was conducted by in 1926 by Herbert [20]. He showed that the chip material was harder than the work material and demonstrated that metal cutting involved intense strain hardening which could only come about through the mechanisms of plastic flow.

Cutting Geometry with a Single Edge

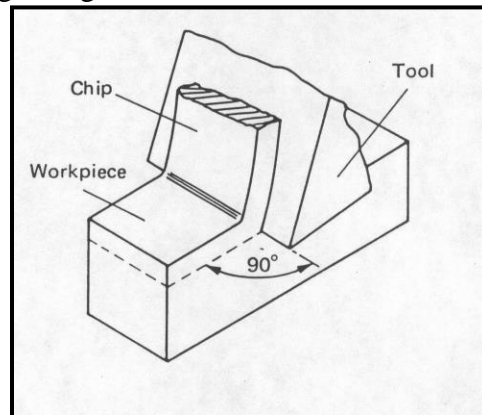


Figure 2. Orthogonal Machining Cut

Orthogonal cutting such as depicted in Figure 2 is seldom used in practice, although it remains the simplest model for scientific analysis. Nearly all practical cutting processes are oblique, where the leading tool edge is inclined to the relative velocity vector between the tool and work. Even in today's computer age, modeling such a difficult geometry remains a daunting task. Thus, it is necessary to consider how the mechanics of the orthogonal cutting can be extended and altered to describe oblique cutting. Beginning in the 1940s, the Orthogonal Machining Process (OMP) of Figure 2 became the basis upon which subsequent models and discussions were based. The commonly used phraseology is provided in the List of Symbols. Most of the derived equations are summarized in Appendix 1. A complete discussion of the model and the formulas derived from it are beyond the scope of this experiment, but excellent reviews may be found in Degarmo,

Black and Kohser's text or the work of Shaw, Trent or Wright [21] [22] [23] [24]. A short discussion is however necessary to set up the shear zone review and discussion.

There are three basic chip types formed during the orthogonal machining process as first denoted by Ernst [25]. Type 1 is a discontinuous or segmented chip type; Type 2 is continuous and smooth; Type 3 is continuous with a buildup of chip material between the tool and chip which is commonly referred to in the literature as "built-up edge" or BUE. All of the models discussed hereafter assume a Type 2 chip.

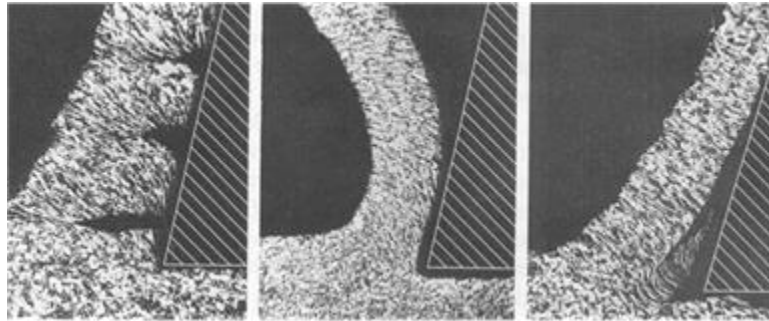


Figure 3. Type 1,2, & 3 Chips Respectively

The modern era of metal cutting research began with the nearly simultaneous work of M.E. Merchant and V. Piispanen during the years leading up to and during World War II. These two men independently proposed the classic force relationships that are used to describe the OMP model.

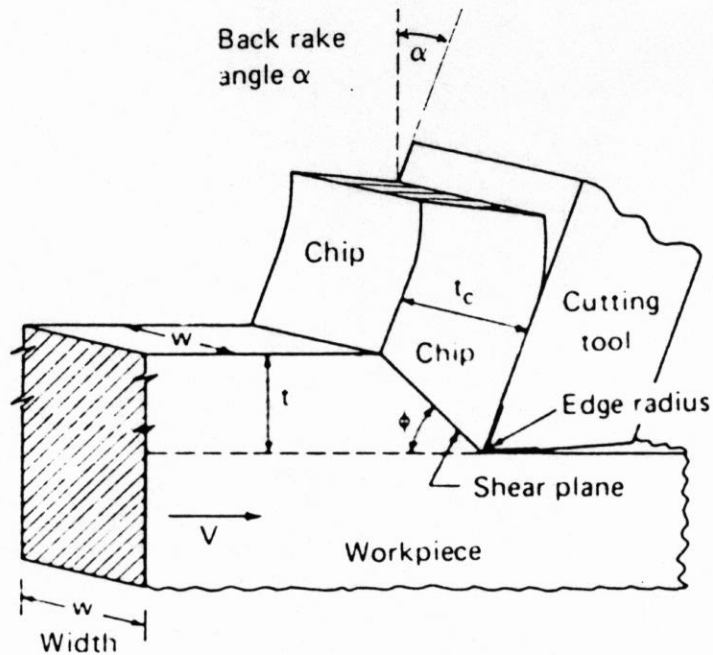


Figure 4. Orthogonal Cutting Process

Figure 4 depicts the commonly accepted symbology of the Merchant and Piispanen model, detailed in the List of Symbols. Basically, the shearing process occurs on a single plane extending from the edge of the cutting tool to the free surface of the workpiece. This plane is commonly referred to as the “shear plane”. The shear angle ϕ is measured from the horizontal to the plane as depicted in Figure 4 and varies depending upon the particular cutting conditions. The shape of the zone on or around this plane has been the topic of intense academic interest since publication of the models in the 1940s occurred. Before beginning the review of the many “shear zone” models, a basic review of the process which led to the development of the geometric force relationships of Appendix 1 will be made using the nomenclature of the List of Symbols. This list is considered to be “American” and must be converted when comparing it to European or Asian cutting models.

Both Merchant and Piispanen independently developed similar concepts for a force diagram which illustrates the geometrical relationship between the cutting force

components during orthogonal machining. This has become the fundamental basis allowing the formulation of the relationships detailed in Appendix A. Both researchers viewed the chip as an independent body held in mechanical equilibrium by the two equal and opposing resultant forces \mathbf{R} and \mathbf{R}' . The force \mathbf{R} is due to the force exerted by the workpiece on the chip. The force \mathbf{R} is composed of two components; the shearing force along the shear plane (\mathbf{F}_s) and a force normal to the shear plane (\mathbf{F}_n). The force \mathbf{R} may also be resolved into two other components, the cutting force (\mathbf{F}_c) and the thrust force (\mathbf{F}_t). Figure 5 shows these relationships in what is now commonly referred to as the Merchant force diagram.

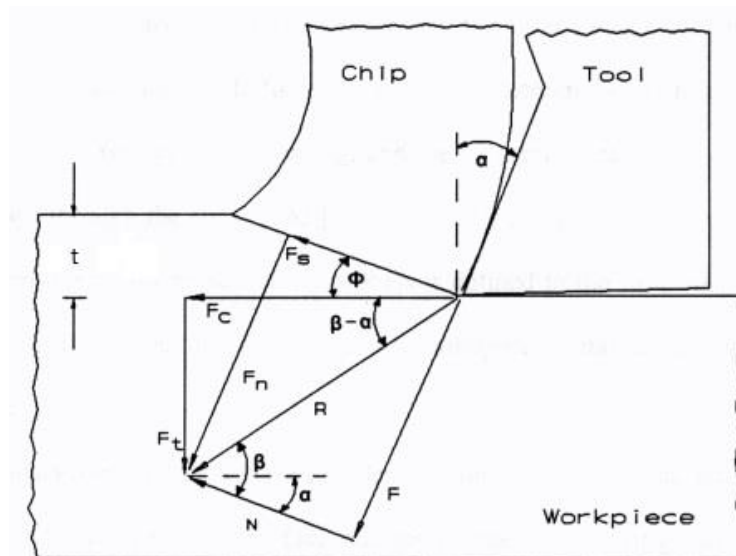


Figure 5. Merchant Force Diagram [22]

The Merchant force diagram applies the opposing force concept of the free body diagram of the chip to the orthogonal cutting process shown in Figures 2, 4 and 6. The force \mathbf{R}' is the force that is exerted upon the chip by the cutting tool. It may be resolved into two components, \mathbf{F} and \mathbf{N} , where \mathbf{F} is the friction force between the chip and the cutting tool and \mathbf{N} is the force normal to the chip and the cutting tool. The forces \mathbf{F}_c and

\mathbf{F}_t are easily measured during the orthogonal cutting experiments using a force dynamometer. The force due to friction \mathbf{F} can then be calculated from the measurement of the cutting and thrust forces as shown in the following equation:

$$F = F_c \times \sin \alpha + F_t \times \cos \alpha \quad (3)$$

The coefficient of friction μ that acts between the cutting edge of the tool and the chip is defined by the following equation:

$$\mu = \frac{F}{N} = \tan \beta \quad (4)$$

The angle β is between friction force \mathbf{F} and the normal force \mathbf{N} as shown in Figure 5. Merchant's orthogonal model permitted the calculation of values such as equations (3), (4), (5) and the others in Appendix A using forces readily measurable with modern dynamometers. The angle β is particularly important in the various predictive shear strain models as shall be demonstrated and investigated.

The resultant \mathbf{R} , which is equal, opposite and collinear with \mathbf{R}' may be resolved into \mathbf{F}_n and \mathbf{F}_s using the measurement of the cutting and thrust forces as with the following equation:

$$F_s = F_c \times \cos \phi - F_t \times \sin \phi \quad (5)$$

Merchant's and Piispanen's work have permitted the quantification of forces at and along the tool-chip interface (Appendix 1). This has formed the basis for modern attempts to develop a predictive mechanism for the shear front plane by establishing their own version of equations (1) and (2) using the geometry of Figure 5. This marks the beginning of the modern "shear zone" investigation.

The Shear Strain Models

The Merchant model of orthogonal cutting permitted the development of expressions for flow stress, shear energy, temperature and chip morphology such as those listed in Appendix A. Shear strain, as well as shear stress, was described in his model but has not been as successful in predicting results. Various models for the shear process have been proposed in the machining literature. These models may be divided into two broad categories, the thin-zone and thick-zone models. Neither model is completely successful, but each has its proponents. The thin-zone model appears to be most successful in describing cutting at a high speed, whereas the thick-zone model is most often used to describe the machining process at very low cutting speeds.

Merchant's model represented the shear zone as a single plane, or thin-zone model. The angle of inclination of the shear plane to the cutting direction was defined by the angle ϕ . Merchant observed that the crystal structure of the material was elongated by the shear process and gave the direction of crystal elongation the direction ψ .

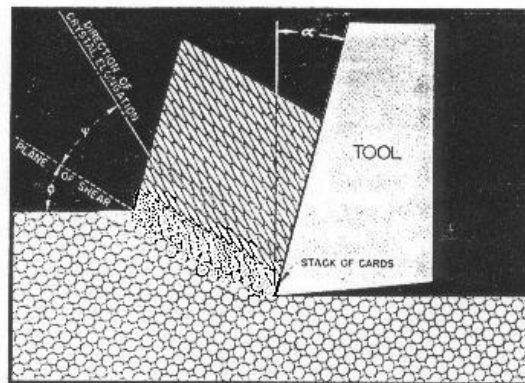


Figure 6. Merchant's Observation of Chip Formation [26]

Merchant did not develop the plastic deformation aspect of his observations. Both Merchant and Piispanen used a “deck of cards” concept to visualize the shear zone process,

where the shear mechanism during chip formation can be illustrated by the incremental displacement of cards in a stack (Figure 7). Each card moves forward a small amount in respect to the next card in the stack as the cutting process occurs. Merchant proposed that the crystalline structure of the metal was elongated by the shear process, and that the direction of elongation was in a different direction than the shear plane [27].

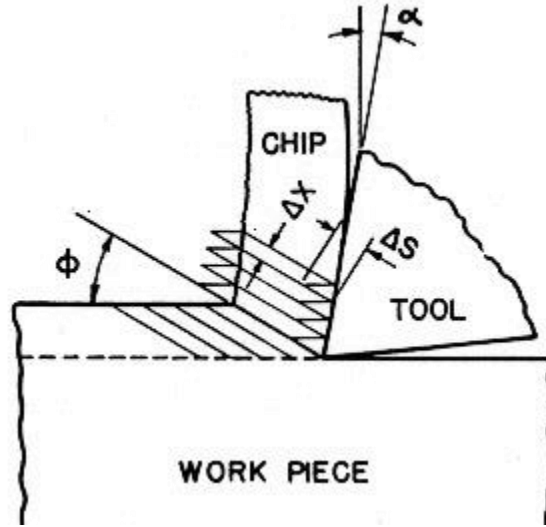


Figure 7. Merchant's Stack of Cards Model [14]

The thickness of each card element was ΔX , and each element in the model was displaced through distance ΔS with respect to its adjacent neighbor. Therefore, the shear strain, γ , could be expressed as $\gamma = \Delta S / \Delta X$. From the geometry of his stack of cards, Merchant thus developed the following equation:

$$\gamma = \frac{\cos \alpha}{\sin \phi \times \cos(\phi - \alpha)} \quad (6)$$

Ernst and Merchant [12] would eventually observe that the angle between the resultant force **R** and the shear plane was thus given by:

$$\phi = 45 + \frac{\alpha}{2} - \frac{\beta}{2} \quad (7)$$

Equation (7) was the first of many modern attempts to derive a functional angle relationship $f(\alpha, \beta)$ of some type. It has come to be referred to as the Ernst and Merchant solution [28]. Although independently derived, this is again the result Zvorykin published in 1893 as equation 2 in this review.

Lee and Shaffer, in their 1951 paper, examined the geometry by considering that a part of the chip would behave as an ideal plastic solid [29]. Using Mohr diagrams, they developed the following relationship amongst the angles of the Merchant model:

$$\phi = 45 + \alpha - \beta \quad (8)$$

Both equation (7) and (8) suggest a strong interaction between the frictional angle and the tool rake angle in determining the shear plane angle. This has not proven to be a very satisfactory observation. Eggleston et al noted in his detailed review of the observations of the angle relationships that neither the Ernst and Merchant formulation, based upon the minimum energy criterion, nor the ideal plastic-solid solution of Lee and Shaffer, nor the mathematical derivations of Hill agree with all the experimental observations [28].

Merchant's model has been extensively examined, published and cited as the first thin-zone model. It has been seriously criticized by some academics because of its inability to describe the actual deformation process in machining. For example, a particle moving along the cutting direction into the shear plane must abruptly change direction at the plane and then flow in the direction of the chip. This represents a discontinuity in the tangential component of velocity on the shear plane, requiring an infinite acceleration across the shear

plane. An examination of the actual shape of the deformation zone is one of the goals of this experiment and a further review of the many shear zone models is continued below.

Okushima and Hitomi developed a simplified thick-zone model in 1961 which is depicted as Figure 8 [30]. The suggested a very large transitional zone AOB.

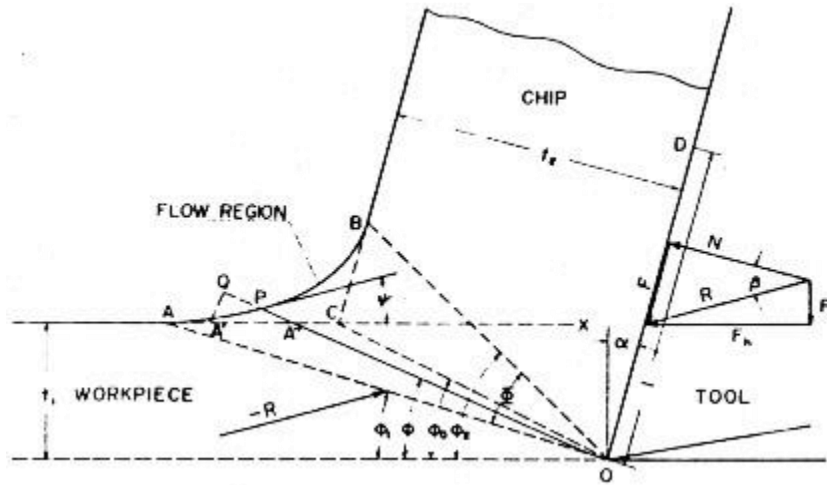


Figure 8. Okushima and Hitomi's Model [30]

The AOB zone existed for plastic deformation of metal between the rigid region of the workpiece and the plastic region of the steady chip as it moved away up the tool face. Plastic deformation began to occur at the starting boundary line of the shear zone, OA, and the plastic strain gradually increased as the cut progressed. Shear strain inside the shear zone AOB was expressed as follows:

$$\gamma = \cot\phi - \cot(\phi - \Psi) \quad (9)$$

Here ϕ is the inclination angle of the arbitrary radial plane, and ψ is the tangent to the free surface (curve between A and B in Figure 8) with the machined surface. This model predicted that the shear strain was zero at the lower boundary of the shear zone and obtained the maximum at the upper boundary of the shear zone.

In 1966, Zorev proposed the thick zone model detailed in Figure 9. Line OL defined the initial boundary of the zone and OM the final boundary of the shear zone. Inside the shear zone LOM, there was a family of shear lines along which shear deformations were formed [31]. Work material passed through the shear zone and was subjected to increasing shear strain:

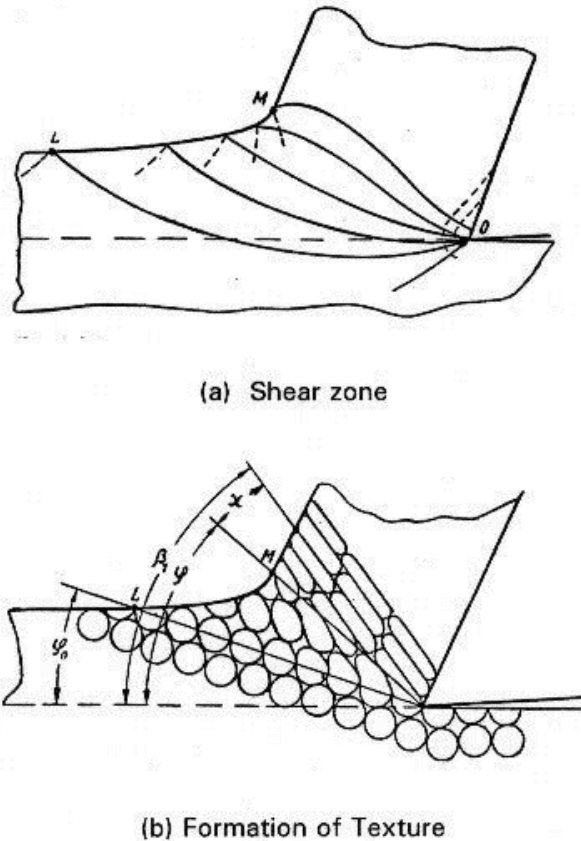


Figure 9. Zorev's Model of a Thick Zone

The initial boundary of shear zone is similar to the onset shear plane proposed by Black in a later paper. The direction of shear deformation was tangent to each line. The shear direction was approximately parallel to the initial boundary of the shear zone.

Zorev's expression of the shear strain is the same as equation (9) above. The texture of the chip formation, due to shear deformation, changed from an equiaxial structure into

It was assumed that one half of the total strain in the shear zone occurred at the centerline, AB. The shear strain in the plane defined by AB was taken as

$$\gamma_{ab} = \frac{\cos\alpha}{2 \times \sin\phi \times \cos(\phi - \alpha)} \quad (12)$$

A “stationary” shear zone model was presented by Van Luttervelt in 1977 as depicted in Figure 11 [33]. This model is similar to Oxley’s parallel sided shear zone model.

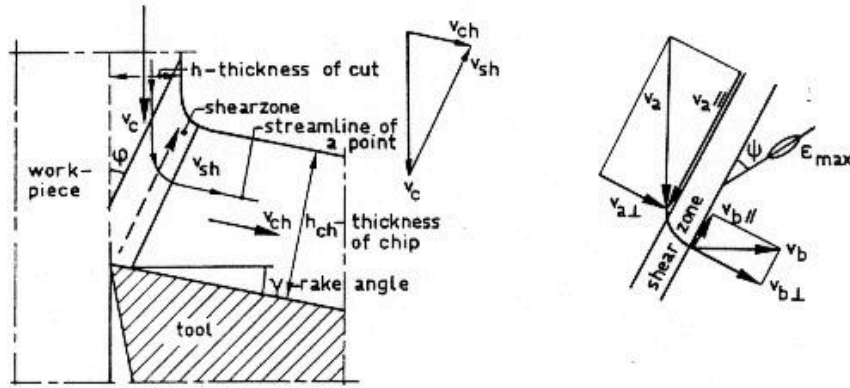


Figure 11. Van Luttervelt's Stationary Shear Zone Model [33]

The material entered the shear zone with velocity V_a , which might be resolved into two components, one parallel to the shear zone and the other perpendicular to the shear zone. The material left the zone with a velocity V_b , which could also be decomposed into its parallel and perpendicular components. The shear strain within the zone was derived from these components as:

$$\gamma = \frac{\cos(2 \times \phi - \alpha)}{\sin\phi \times \cos(\phi - \alpha)} \quad (13)$$

The direction of maximum elongation described in Van Luttervelt's model is the same as in Oxley's model.

Another shear zone model was suggested in 1996 by Huang, working as a graduate student for J.T. Black [34]. During a review of experiment using high speed magnification to observe the cutting of aluminum, Huang developed a new "stack of cards" model and a new shear strain equation of orthogonal machining [35]. In reviewing the tapes made by Briggs, he observed that the material deformed in a totally different fashion than that which had been described in the machining literature. The plastic deformation of material as observed by Huang and Black is depicted in Figure 12.

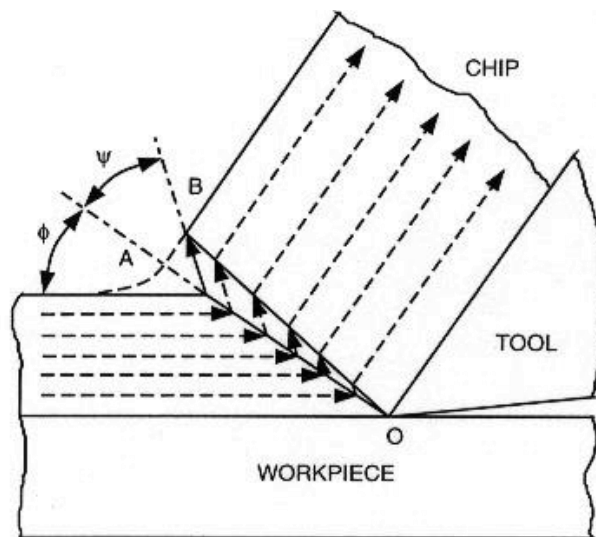


Figure 12. Huang's Observation of Flow in Shear Zone [34]

As the material in the workpiece moves from left to right, toward the cutting tool along the cutting direction, it approaches the shear zone, designated by the triangle AOB. When the material encounters the onset shear plane AO, it changes direction and appears to move at an inclination angle, ψ , to the plane. This is the shearing of the metal caused by the massive movement of many dislocations. Upon reaching the plane BO, the shearing process stops,

and the material changes direction a final time and moves in a direction parallel to the tool face. The shape of AOB is triangular and the onset shear plane is flat. The material encounters plane AO simultaneously and shear is in mass all along the boundary. This onset of shear fronts creates the shear plane and defines the lower boundary of the shear zone. Thus, ϕ has been more properly termed by Black as the Onset of Shear Plane angle [36]. The termination of the shear fronts forms the upper boundary of the shear zone as noted by Black and Briggs [37]. The shear fronts are inclined at an angle, ψ , originating from the plane connecting the tool tip to the free surface. His reasoning behind this movement was the presence of dislocations in the material. Figure 13 details the angular relationships as derived by Huang.

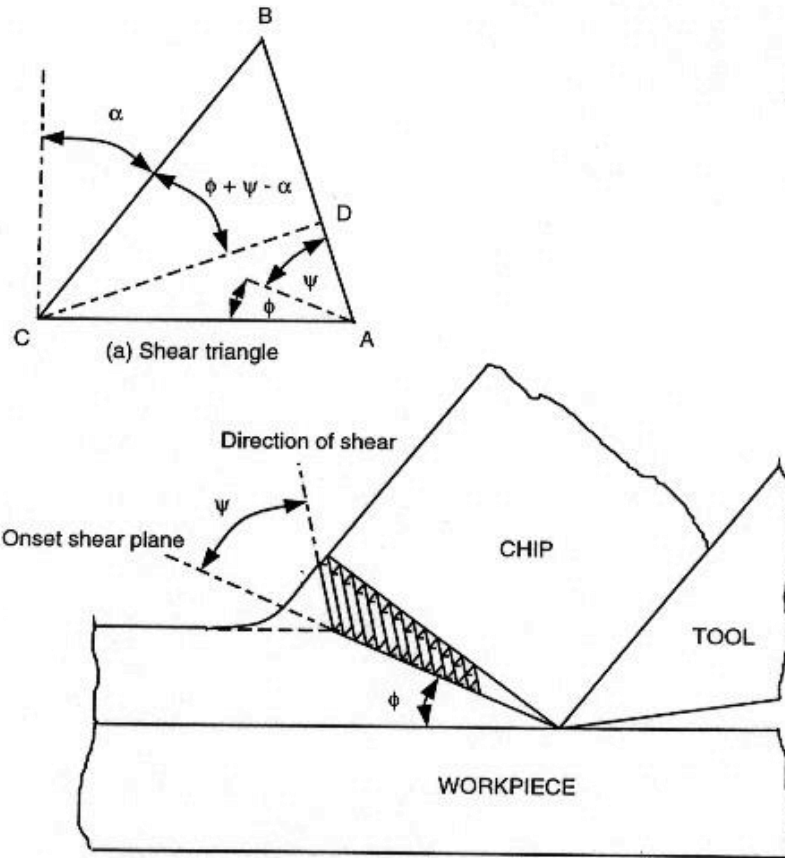


Figure 13. Huang's "New" Stack of Cards Model

Huang's model is significantly different than Merchant's model. In the new card model, an element shears at the direction ψ relative to the onset shear plane. (In Merchant's model, an element shears in the direction of the shear plane ϕ . In Zorev's model the work material shears tangentially to a shear line that is approximately parallel to the initial shear plane.) Using minimum energy criteria Huang developed the following relationships for ψ and γ :

$$\phi = 45 - \psi + \frac{\alpha}{2} \quad (14)$$

$$\gamma = \frac{2 \times \cos \alpha}{1 + \sin \alpha} \quad (15)$$

Reference details all the mathematical derivations of Huang's work as does a later appendix [34]. He explains the movement at the shear plane in terms of dislocation theory.

Dislocations and Metal Cutting

Dislocations have been a major field of study in material engineering and applied physics for over seventy years now, but metal cutting researchers have not typically addressed hardness, dislocation density or dislocation movement in their work with a few noted exceptions. Dieter gives an excellent overview of dislocation theory in general as it applies to material [38]. His integrated overview of the effects of cold rolling in his discussion of metallurgical structure will prove useful later in discussing the conclusions of this experiment.

Research on the effects of material hardness in metal cutting since the efforts of Taylor at the turn of the century and Herbert in the 1920's has been sparse. P.K. Wright made a great contribution to this area in 1982 when he suggested that the work hardening characteristics of the material are the most dominating influence on shear angle in machining [39]. The friction angle and the tool/chip contact interface are important, but not governing factors in his review of available data sets. He was not able to develop a predictive theory from his analysis, but he believed that it would be possible to predict a " ϕ range" for a material. He ignored the effects of the frictional constraints at the chip-tool interface in his analysis.

Von Turkovich discussed dislocation theory as it applied to shear stress in his 1967 paper [40]. Although he was primarily concerned with high speed machining in this paper, he believed that shear stress computation in a Type 2 Chip was possible using the materials elastic constant $G(T)$, the materials characteristic Burger's vector (b) and the dislocation density.

Ramalingham and Black showed that the important variables involving dislocations are the "number and orientation of slip systems, certain characteristic dislocation parameters as the stacking fault energy, the interaction of dislocations with vacancies and solute atoms" in the scanning and transmitting electron microscopy studies of α brass [41]. In their microscopic studies, they cut the material with diamond blades and studied the recrystallization at a molecular level.

Black proposed a model in 1979 for the plastic deformation that occurs in metal cutting [36]. He demonstrated that the magnitude of the flow stress and the onset of shear angle ϕ correlated to the stacking fault energy of the material being cut. His resultant flow stress model predicts a catastrophic shear front, or shear plane, ahead of the tool, created by the annihilation and subsequent heat generation as the metastable cells in his model rearrange themselves. The model observes that dislocations sources originate near the tool tip, driving dislocations into the cell networks. There is a rapid buildup of applied stress levels as the number of dislocations increase, causing a hardening effect at the tip of the tool [42].

Black's paper notes that more than one shear front would be crossing the material from the tool tip to the free surface at any one point in time, comparing this effect to waves at the seashore. Waves from the ocean will intersect a jetty on the beach at many different

points along the length of the jetty, but always at the same angle. This is a good analogy to the deformation observed by Black Huang in aluminum as they developed the “new stack of cards” model. Note that there are many cards sitting on the “onset of shear plane at angle ψ . The onset angle ϕ is dictated by other material properties. Black’s theory predicted that as work-hardening increased; the resistance to the onset of shear will increase. This delay in the initiation of shear would translate into an increase in the onset shear plane angle ϕ . If measuring techniques existed for the angle ψ , one could examine the relationships stated in equations (7), (8) and (14) as well as the shape of the shear zone.

Black and Krishnamurthy conducted a small experiment where they examined the relationships between hardness and shear stress in 6061-T6 aluminum [43]. They noted that shear stress varied with the material hardness over the four samples. They were widely spaced, with varying hardness produced by annealing the as received aluminum. Their results suggested that dislocations could possibly explain the differences which they had observed. In particular, when the aluminum was softened by heat treating, the dislocation density was reduced as predicted by Cottrell and others. This reduces the amount of pinning in the material, allowing more mobility which translates into a lower yield stress. This is also discussed in Dieter [38].

High Magnification Photography

The observation of the shear zone and the geometries associated with it is a challenging task. The deformation process is a complicated one occurring under very high rates of strain in a small area, making it extremely difficult to measure the shear strain expressions experimentally.

Photography and optics have advanced dramatically since Coker's photo elastic attempts in the 1930's. With the advent of scanning electron microscopy techniques, the fundamental structure of various chips that developed during micromachining has been observed at very high levels of magnification by Black, Ueda and Iwata, and others [44] [45]. This, coupled with advances in high speed film and digital imaging such as the Briggs experiment, permits a detailed study of the deformation zone ahead of the tool [35].

Cook and Shaw used magnified cinematography as early as 1951 to analyze the shear process [46]. They observed a thick shear zone and at various times two shear zones. One zone (the primary zone) extended from the tip of the tool along the shear plane while the secondary zone at times appeared adjacent to the tool face. They noted that the frequency of the two zones was "perhaps" more pronounced when cutting materials that strain harden easily and produce thick chips.

Agrawal and Amstead examined the cutting of mild steels with a FASTEX high speed motion camera in the 1960s [47]. They detected the presence of Built Up Edges (BUE), crack formations, and deformation ahead of and below the tool. Their study would also indicate that the shear zone region was not a simple, narrow zone problem. Agrawal and Amstead recognized that their system had technique problems common to all photographers: control of lighting, vibration, movement of the target, focal length, depth of field and magnification.

Oxley conducted experiments with cinematography through a microscope up to 50X to directly observe the cutting zone [48]. These were instrumental in his formulations of the Oxley shear zone model.

Komanduri and Brown recorded at rates up to 3000 frames per second to study chip formation at high (180 sfpm) rates of speed [49]. They encountered the standard problems that Agrawal, Amstead and others encountered when trying to trade off magnification for depth of field. Lighting was a significant problem in their experiment.

Black and James were more successful using high speed motion pictures to record at up to 4000 frames per second as they analyzed the results of their Quick Stop Device (QSD) experiments for orthogonal machining [50]. They were instrumental in studying the disengagement process of the chip from the tool.

J.H.L. attempted to study the commencement of cutting (the incipient stage) using a high-speed camera and a stroboscope [51]. The qualities of the films produced were not consistent and set-up was very difficult and time consuming.

Wernicke used a microscope and a high speed 16 mm camera to study the chip formation process and the initialization of the BUE [52]. He produced a very good video of the overall process that has good classroom value, but the quartz plate technique used to provide optical contrast and limit lateral deformation of the chip limited the ability to observe the microscopic deformation of the chip. Still, this was an excellent advancement in the use of lighting, with a wide range of cutting speeds being observed.

Briggs used a high quality Kodak Ektapro Imaging System (using the EM Model 1012 Processor) and an Infinity K2 Lens with an intensified Imager to conduct an experiment examining some of the classical factors (α , depth of cut, V , tool contact length, and temperature) in an experiment whose primary video objective was to produce a classroom video for metal cutting [35]. The tapes produced of the shear zone were without doubt the best produced to date and formed the basis without further experimentation of

Black and Huang's "new" deck of cards model. The existence of a definitive, easily viewed zone of plastic deformation was strongly supported by his studies of aluminum. The primary drawback with the system being used was the cost and availability. The unit was borrowed, and its usage was limited to a very small amount of time. Since then, simpler video cameras at a fraction of the cost have emerged on the top end of the consumer market that may be useful in a continued study of the shear zone.

Scanning Electron Microscope (SEM) technology has been invaluable in establishing the role of dislocations in the cutting process. Black studied single and polycrystals using the SEM and published the work [44]. Von Turkovich and Black used SEM in studies of chip and workpiece deformation [53]. Ramalingham and Black developed the first in-situ machining technique (machining microscopically within the SEM itself on a stage they developed) and observed the formation of shear fronts and heterogeneous plastic flow during chip formation [41]. It also established the validity of post cut (static) examination of chip morphology to explain the mechanics of chip formation. Black and Cohen would later extend in-situ techniques to measure, for the first time, shear velocity directly, along with chip velocity, shear strain and the strain rate [54]. Their measured velocities were comparable to the calculated velocities of standard orthogonal mechanics from the equations listed in Appendix 1. Scanning electron microscopy is important also because it permits the before and after analysis of dislocation generation during work hardening by the tool face.

Cutting Fluids

Cutting fluids were first documented in 1907 by Taylor stating that in 1883 it was found that utilizing a heavy stream of water on the chip at point of removal from bulk material resulted in an increase in work done of 30 to 40% [1]. In the same address, it was reported that, in the year 1894-95, a heavy stream of water was used on the tool nose while cutting wrought iron and steel increased the cutting speed by 33%. Before this discovery toolmakers advised that water not be used on the tools during use. Since that time many different cutting fluids have been utilized ranging from water to synthetic/ non-synthetic fluids and oils. Downsides became apparent when separation of chip from coolant became prevalent. Along with disposal of coolant as a hazardous material, severe health hazards were encountered by workers exposed to these coolants. [2] This triggered the creation of more rules, administrative procedures, and governance regarding the use and disposal of cutting fluids. This scenario opened the door to exploration of coolants that were more user friendly while still increasing efficiency.

Most commonly a lubricating/coolant fluid is used as a flood onto the tool at the interface between the tool and the chip. While Trent has provided metallographic evidence to show that the lubricant cannot penetrate the whole of the contact area, Williams et al claim that cutting lubricants reduce frictional forces through reduction of the tool-chip contact length [55] [56].

Niebusch, R, B., and Strieder, E, H., [57] in 1950 conducted experiments based off the “rule of thumb”, ‘gallons of cutting fluid per minute = maximum horsepower required for cut’. They concluded that adequate supply of coolant on the cutting tool ended in tool

life improvement of 100%. The experiment also resulted in a better surface finish, greater accuracy, and reduced airborne pollutants.

Rowe, G, W., and Smart, E, F. utilized oxygen as a cutting fluid in the dry machining of mild steel and stated that oxygen is effective in reducing cutting forces [58]. They concluded that there is a marked change in the chip formation criteria when using oxygen as built up edge is avoided in this case where as it was observed in dry machining and vacuum chamber machining. Kim, S, W., Lee, D, W., Kang, M, C., and Kim, J, S., conducted studies to determine the effect of compressed cold air system in machining of difficult to cut metals such as hardened steel, die steel (HRC 42) nickel based alloys etc [59]. Tool wear was measured using a CCD camera and a tool makers microscope. The results showed that when machining Die steel the tool life improved when using compressed air than dry environment and went up 3.5 times when comparing compressed air with flood coolant, the former being more efficient. The authors also note that the compressed air environment did not create any significant improvements in machining Inconel 718 (HRC 43) at a speed of 210 m/min when compared to flood of dry environments and they attribute such an observation to that the severe thermal friction taking place when machining at such high speeds and the inability of the coolant to infiltrate the tool chip interface [59].

Williams, J, E., Smart, E, F., and Milner, D, R., [56] conducted experiments to assess the effect of carbon tetrachloride (CCl₄ spray cooling) in machining operations of varied materials. Materials that are considered brittle, such as magnesium or grey cast iron showed little to no effect from the CCl₄. However, in pure metals and single-phase alloys the cutting forces were lower at machining speeds under 100 feet per minute and increased

thereafter as the softening of chip due to heating is reduced. The effect was higher at rake angles of 6 degrees when compared to a 35-degree tool as the tool chip contact area decreased with decrease in tool face force. However, in machining two phase alloy elements a similar trend was observed but formation of built up edge was absent when machining under low cutting speeds [56].

Cryogenic cutting conditions while cutting Ti-6Al-4V were studied under Hong, Shane, Y., Ding, Yucheng., and Jeong, Woo-cheol. [60] , in 2001. They developed a new system for liquid nitrogen to be introduced to the workpiece using a two-nozzle system. One nozzle on the rake face very close to the tool-chip interface by placing it on the chip breaker. The second nozzle placed on the clearance face of the tool. Both nozzles supplied liquid nitrogen at variable flow rates. They determined the liquid nitrogen reduced feed force and coefficient of friction, however it increased cutting force due to the cooler work material making it harder to cut.

Dahlman, Patrik., and Escursell, Marcel. [61], in 2003 employed the technique of high-pressure jet-assisted cooling to machine decarburized steel. They first examined the wear and surface finish closely using a Scanning Electron Microscope and then used a microscope fitted with a digital camera and imaging software to measure wear. Surface roughness was measured by a rubber-replica method in which a mixture of rubber was applied to the surface and allowed to polymerize which was examined under a Wyko optical reflecting equipment. High pressure jet assistant cooling improved the surface finish of the work by 80% along with a reduction in tool wear.

Cakir, O., Kiyak, M., and Altan, E. [62]., in 2004 investigated the effects of cutting fluids to provide quantitative results about the cutting force, thrust force and the surface

roughness. A 5% emulsion type cutting fluid was used as liquid coolant and compressed oxygen, nitrogen and carbon dioxide gas stored in cylinders at their normal temperatures were used. They used tubes ending with nozzles and fitted with suitable pressure regulators to direct the gases and the coolant at the cutting edge of the tool. The response curve of the mean cutting force and the thrust force showed that all gaseous and flood coolant is different from the dry cutting and also increases with increase in feed. Later Cakir analyzed the response of the shear plane angle under varying depth of cut. This showed an appreciable increase in the shear angle in the gaseous and flood coolant environment leading to smaller shear area and reduced cutting forces as compared to dry cutting environment.

Stanford, M., and Lister, P. M. [63], recognized a relationship between cutting atmosphere and tool wear. Using the case hardening steel En32, the cutting durations were varied between 20 and 80 seconds utilizing different cutting environments including semi-synthetic flood cooling, dry cutting, compressed air, and compressed nitrogen. Cutting speeds were between 200 m/min and 600 m/min. They determined that a Nitrogen rich environment reduced the flank wear up to 55% in both coated and uncoated tools.

In 2006 the effects of minimum quantity lubrication (MQL) on tool wear and surface finish was studied by Dhar, N. R., Kamruzzaman, M., and Ahmed, M., [64]. They machined 4340 steel by turning a solid piece utilizing a carbide insert under different cutting conditions such as like dry, wet (flood) and MQL. These were mixed with compressed air at 60 ml/hr. Tool wear and surface finish was measured using a metallurgical microscope, a scanning electron microscope, and a contact profilometer. Their experiment showed minimum flank wear during the MQL as well as improved

surface finish. They determined the improved surface finish was due to the less damaged tool tip.

In 2006 Su, Y., He, N., Li, L., and Li, X. L., [65], conducted high speed milling experiments on Ti -6Al-4V to determine the effects of different cutting environments on tool wear during the process. The cutting occurred during a milling operation at 400 m/min. Different cutting environments like dry, flood, nitrogen, nitrogen oil mist, compressed cold nitrogen and oil mist (-10 °C) were investigated with the tool nozzle positioned at entry and exit of the tool. Different wear phenomena occurred during the machining process like flank wear, notch wear and nose wear were observed and measured using a toolmakers microscope. The results showed that cold compressed nitrogen gas oil mist environment resulted in 2.93 times improved tool life than dry cutting and nitrogen gas oil mist improved the tool life by 1.93 times.

A 2007 experiment by Su, Y., He, N., Li, L., Iqbal, A., Xiao, M. H., Xu, S., and Qiu, B. G. [66] used cooled air while turning Inconel 718 with coated carbide insert. Three different environments including dry, cooling air (-20° C) and a combination of cooling air (-20° C) and MQL were used at a speed of 76 m/min. Tool wear and surface finish was measured using a tool makers microscope. This showed a 124% improvement of tool life while using MQL. Cool air (-20° C) showed a 78% improvement over dry machining. The same paper also reports the results of high-speed milling experiment carried out on AISI D2 steel (62 HRC) at cutting speed of 175 m/min showed that the cooling air environment improved the tool life by 130%.

Sreejith, P. S., [67] published the results of the study on effects of different lubricating environments in machining Aluminum 6061. The turning experiment was

conducted using a 15° rake angle, diamond coated carbide tool insert at a speed of 400 m/min. Surface roughness was measured using a profilometer and the tool wear was measured using a toolmakers microscope. Cutting environments included dry, flooded and MQL. The experiment showed that the cutting forces were lower for flood cooling. They attributed the lower cutting forces to lower adhesion of the chip to the tool reducing cutting forces.

Payton, L. N., and Sripathi, P. [68] conducted orthogonal tube turning experiments on aluminum 6061 T6 alloy with a high-speed steel tool under 4 different cutting environments including nitrogen, cold compressed air, Kool-Mist and dry. This was a cut performed at 640 rpm. The cold compressed air environment recorded marginally low cutting force and thrust force values closely followed by nitrogen environment, with spray coolant (kool mist) in the third position. The tool wear was recorded in terms of surface roughness of the affected area of the tool measured using a non-contact type profilometer. The results showed that the tool wear was least when the cutting was performed under nitrogen cutting environments.

Vishnu [69] in 2013 showed the relationships between nitrogen and cutting forces again but varied pressures and flows. The experiment was again on a lathe and showed the reduction in cutting forces due to the cutting environment changes from dry machining. In machining of AISI 1020 alloy steel with uncoated carbide tool it was observed that, the environment had significant impact on the cutting and thrust force values. Use of liquid nitrogen in the above scenario decreased the forces significantly with nitrogen performing almost closer to liquid nitrogen while use of cold compressed air resulted in slightly higher values with the highest observed for dry environment.

IV. Materials, Instruments, and Machines

This section describes the materials, instruments and machines that were used in the experiment.

The materials chosen for this experiment were aluminum 6061, 4130 steel, and AZ31B magnesium. The aluminum has three different tempers for 3 different hardness's (T0, T4, and T6 tempers). The 4130 steel was hardened in the DML for 3 different hardness's at 22, 32, and 42 HRC. The magnesium was only available in two different tempers (H0 and H24) for two different hardness's. The initial hardness temper or level of hardness is also listed for each material as they were specifically chosen prior to ordering.

Magnesium AZ31B

- Temper H0 and H24 (certified)

Aluminum 6061

- Temper T0, T4 and T6 (certified)

4130 Steel

- Hardness: 22 HRC (as received, annealed) ,32 HRC (hardened), 42 HRC (hardened)

The equipment used to prepare all samples, perform orthogonal cuts, analyze data, and analyze materials are listed below in no particular order.

CINCINNATI No. 2 HM Horizontal Milling Machine

BALDOR 1/8 Horsepower Three Phase Induction Electric Motor

WOOD'S E-Trac AC Inverter

Quick-Stop Workpiece Holder

HSS Stick Tools, (0.75 x 0.75 inches) at Various Rake Angles

KISTLER Dual Mode Amplifier

KISTLER Dynamometer

NATIONAL INSTRUMENTS USB-6008

DOLAN JENNER Fiber-Lite A-200

STOCKER AND YALE Imagelite Lite Mite Model 20

Fiber Optic Ring Light

Modified Load Lift Camera Stand

Cross Slide Vice

DRS TECHNOLOGIES Lightning RDT Camera

INFINITY InfiniVar Lens

NATIONAL INSTRUMENTS LabVIEW

XCITEX Midas 2.0 Video Capture Software

The following equipment was used to prepare the various magnesium, aluminum, and steel specimens to the appropriate dimensions and properties before undergoing the orthogonal machining process. This list also includes any machinery used to create any custom fixtures or tooling required as well as the material testing equipment used to obtain the material properties of the final specimens. Software used for design and post processing of data also listed.

CINCINNATI Arrow VMC-750 CNC Mill

BRIDGEPORT Vertical Milling Machine

SOUTHBEND Lathe

DO-ALL Vertical Band Saw

WILTON Belt Sander

ROCKWELL Hardness Tester

MTS Q Test 100 Tensile Tester

DASSAULT SYSTEMS Solidworks Modeling Software

AUTODESK HSMWorks CAM Software

MATHWORKS MATLAB

MICROSOFT Excel 2010

KINOVEA Motion Analysis Software

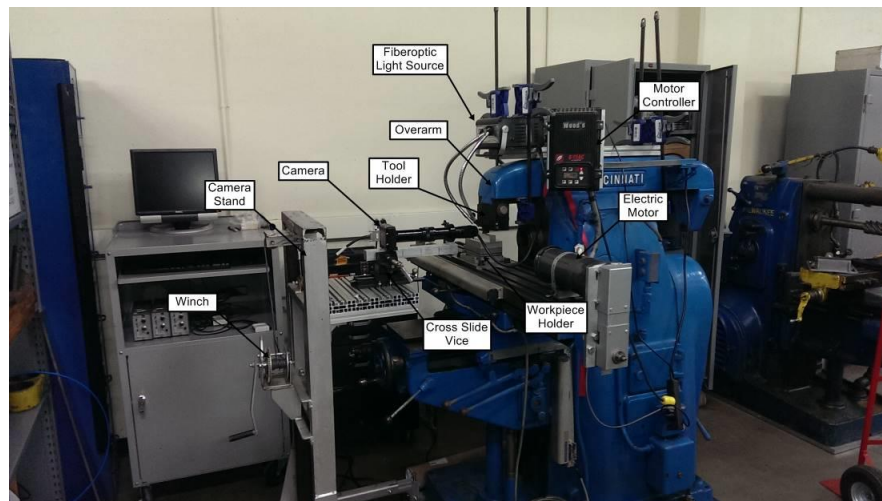


Figure 14. Elevated View of Equipment Setup

An elevated view of the testing area is shown in Figure 14 above. The major components are notated. A computer cart containing the data acquisition PC is seen in the left-hand corner. The cart also holds the NI USB modules as well as the amplifiers for the dynamometer. The user must first start the data acquisition programs and start the camera

recording before moving to the near side making sure not to hit the camera stand in the process to start the motor controller. This location was necessary due to cable lengths and proximity to the power bus located on the wall.

Figure 15 shows the workpiece holder with the camera moved out of the way. The workpiece holder was made from aluminum and covers the entire dynamometer face and attaches to it with socket head cap screws. The socket head cap screws are recessed into the block to allow more room for the camera lens to get close to the specimen. The slot cut into the top of the workpiece holder is just over 4 inches long to hold a 4-inch-long specimen.

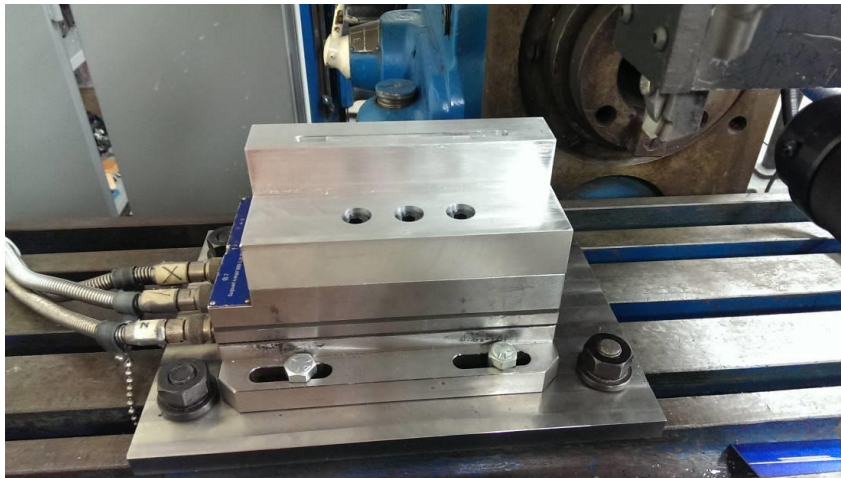


Figure 15. Quick Stop Workpiece Holder

The back side of the holder has ten threaded holes for set screws that apply a clamping force onto the specimen undergoing testing. The work piece holder had finite element analysis run to ensure that the holder would not yield during the tests. The dynamometer itself is attached to a steel plate that is then attached to the horizontal milling table using T-nuts and bolts.

The tools used were $\frac{3}{4}$ by $\frac{3}{4}$ high speed steel tools ground to the correct angles of 25°, 30°, and 35°. The tools were all ordered from the same batch and each tool was the same except for the tool angle that was cut into the face. Tools were precision ground to the required angles locally.



Figure 16. Kistler Dual Mode Amplifiers

The Kistler dual mode amplifiers can be seen in Figure 16 above. Each axis of the dynamometer has its own amplifier. All of the functions for the amplifiers are located on the front as shown for easy operation.



Figure 17. National Instruments USB-6008

The National Instruments USB-6008 can be seen on the above. Two of these data acquisition device was used for many different purposes. The rotary encoder connected to one and the other one took in the amplifier signals for data logging. The device that took in the data from the amplifiers also output a signal to the high-speed camera letting it know when to start recording. This allowed software triggers to be defined for to aid in the capture of images for processing.



Figure 18. Modified Load Lift Camera Stand

The camera stand can be seen in full in Figure 14. Figure 18 shows a close up view of the camera and how it is attached to the custom-made camera stand. Notice how the stand has a modular table that allows many different attachments. The cross-slide vise is mounted to the camera stand table with bolts and nuts that slide into the T-slot grooves in the table. The camera is attached to a rectangular piece of aluminum which is clamped in the cross-slide vise. The piece of aluminum extends out to support the weight of the camera lens as well. The cross-slide vise made adjusting the camera position on a very fine scale a much easier task.



Figure 19. DRS Technologies Lightning RDT Camera

The DRS high speed camera can be seen above with some of the hardware specifications marked.



Figure 20. Cincinnati Arrow VMC 750 CNC Mill

The Cincinnati CNC milling machine was used to cut out the tensile samples from each specimen as well as size the samples to the correct thicknesses before cold rolling. G-code was generated on a separate PC and then loaded via USB stick onto the CNC machine.



Figure 21. Bridgeport Vertical Milling Machine

The Bridgeport milling machine shown in Figure 21 (above) was used to get the specimens to the correct size to fit into the work piece holder for all test runs.



Figure 22. Do-All Vertical Band Saw

The vertical band saw seen in Figure 22 was used to initially rough cut out the specimens from the raw metal stock.



Figure 23. Wilton Belt Sander

The belt sander was used to remove burrs from specimens while undergoing the machining down to thickness to make sure that they sat flat in the vice resulting in perfectly flat pieces.



Figure 24. Rockwell Hardness Tester

Figure 24 shows the Rockwell hardness tester used to test the aluminum and steel samples. The appropriate tip was placed in the tester for a Rockwell B test. The screw handle was turned to raise the sample to be tested into the testing tip. The lever on the side is then pulled which releases the load required for the test. Once the load has been fully applied another lever is pulled which removes the force and the deflection is shown on the dial on the front of the machine. This dial has values that correspond directly to the Rockwell B scale.



Figure 25. MTS Q Test 100 Tensile Tester

The tensile testing machine used can be seen in Figure 25. It is an MTS Q Test 100. The 100 stands for 100kN force that it is rated to apply. A load cell is attached to the upper section of the tester which is attached to ball screws on both sides that move it up and down. Various jaws or fixtures can be attached to the upper section. The tensile testing machine moves at a constant displacement rate and records the forces applied to the load cell.



Figure 26. Tensile Testing Jaws with Specimen Inserted

The jaws used for the tensile testing of the metal samples were of the screw clamping type. A screw collar is tightened which clamps down on the piece. The jaws are designed so that as the pulling force increases the clamping force does as well. Figure 26 shows the jaws clamping a sub-size specimen.

The Keyence 3-D microscope provided a multitude of options and measurements during the tool wear analysis.



Figure 27. Keyence VHX 1000 E digital microscope.

A dress out was necessary due to the microscope being located in a clean room. A micro-vice was utilized for portability and used to hold the tool to be inspected at the correct angle. The microscope is capable of “self-leveling” the image but efforts were made to be as close to parallel to the platform as possible. Once the tool to be examined was in place, images and measurements were taken of the tools wear location. These images and measurements were saved to a flash drive. There is also an image viewer that is available for download from Keyence that makes manipulation of the images possible while away from the microscope.

V. Construction and Methodology of the Experiment

Sample Preparation

Three different workpiece materials were studied in this experiment: Magnesium AZ31B, Aluminum 6061, and 4130 Steel. Each material arrived in a different initial state. The magnesium arrived as a pre-cut 1/8-inch by 2-inch by 36-inch piece. The magnesium had a pickled finish and was manufactured to AMS 4382 and AMS 4377 standards and included material certification. The aluminum was manufactured to meet ASTM B209 standards. The aluminum 6061 T4 and 6061 T0 arrived as a 1/8-inch x 12-inch x 12-inch piece of square stock. The aluminum 6061 T6 arrived in 1/8-inch x 2-inch x 72-inch bar stock. The 4130 steel arrived as a 1/8-inch x 12-inch x 24-inch pieces of rectangular stock. The final size of all specimens to be tested needed to be 1/8-inch x 2-inch x 2-inches. The aluminum and steel stock were cut on a horizontal band saw to just over size in length. The magnesium was rough cut to size using a foot shear. The aluminum and magnesium were then ready to have samples cut from the parent stock material. The steel still needed to be heat treated to its own hardness. The steel arrived at 22 HRC as tested using the Rockwell Hardness tester, a sample was cut, and temperature and quenching liquid was specified in the Specialty ASM Carbon and Alloy Steels handbook for tempering steel to different hardness's. This method was verified by using multiple samples and determining the process was successful in creating a steel with the desired hardness.

A Rockwell C hardness test has the most appropriate range for the steel. All hardness values were converted to the Brinell hardness scale as its range covers all hardness's of all samples. A table below lists the hardness values of all samples and their duplicates. Names include the metal and temper.

Table 1. Material Hardness

Hardness			
Material	HRB	HRC	Brinell
6061-T0			30
6061-T4			65
6061-T6	55		95
Magnesium AZ31B-H0			56
Magnesium AZ31B-H24			73
4130-22	99	22	237
4130-32	107	32	302
4130-42	113	42	390

A Bridgeport vertical milling machine was used to ensure all the samples were made to 2 inches by 4 inches in preparation for tensile test removal and polishing, and also resized material to 2 inches by 2 inches for orthogonal cutting analysis. The Cincinnati CNC machine was utilized again to mill out the tensile test specimens for each specimen. The tensile test design conformed to the ASTM E8 sub-size specimen standard. Figure 31 illustrates the dimensions of the ASTM E8 sub-size specimen.

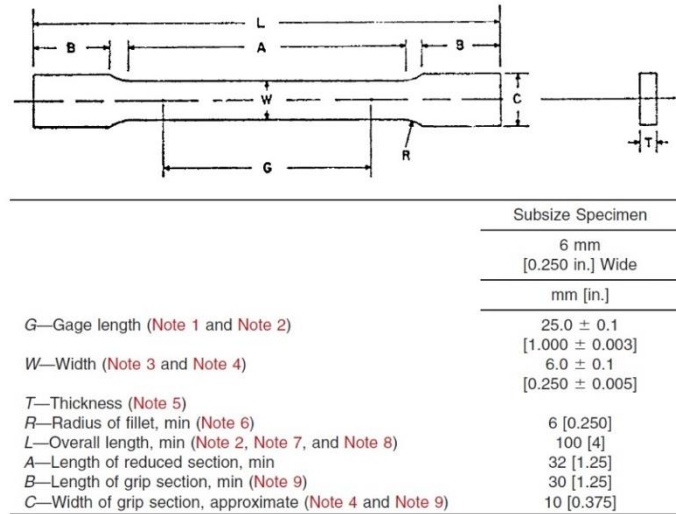


Figure 28. ASTM E8 Sub-size Specimen Dimensions

The sanding process began by putting the samples in the Bridgeport milling machine and making a light pass with the fly cutter. This reduced the sanding required significantly. After the fly cutting operation the samples were sanded using various grit sandpapers. A sanding/grinding machine was used with a water wash to remove debris from the sanding. The samples were sanded first with 180 grit paper, followed by 240, 320, 400, 500, 600, 1000, and finally 2000 grit. After sanding, a polishing compound was used to complete the almost mirror finish. At this point the samples had reached an almost mirror finish and were ready for etching.

The aluminum and steel workpieces were etched to provide optimum reflective characteristics and definition to the material microstructure. Chemical etchants were prepared for the aluminum and steel samples according to Table 2.

Table 2. Aluminum and Steel Etchants

Water	Nitric Acid	Silver Nitrate
H ₂ O	HNO ₃	AgNO ₃
250 ml	250 ml	2.5 grams

Cutting Setup

The now prepared samples were ready to undergo the orthogonal machining process. The workpiece to be cut was placed in the workpiece holder that was attached to the dynamometer and held in place with up to ten set screws.

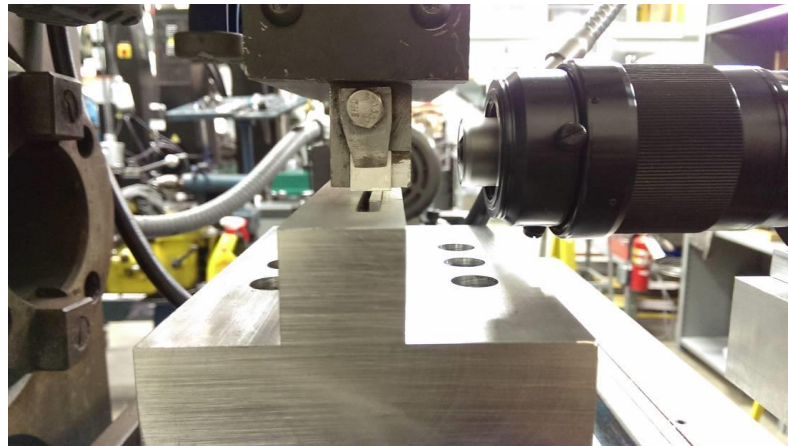


Figure 29. Workpiece in Position

Figure 28 shows a workpiece in the workpiece holder looking down the y axis. The position of the sample underneath the cutting tool is near the front edge of the tool and the

camera is in position to record the run. The camera is shown with the fiber optic lights off due to their brightness.

During the experiment, the table fed the workpiece directly into the tool. The dynamometer measured the cutting force (F_c) and the thrust force (F_t), passing its output signal to the charge amplifier. Output from the charge amplifier was then directed to the NI USB-6008 data acquisition modules and recorded using a LabVIEW program. During the experiment, the camera was always focused slightly to the left of the tool tip so as to magnify and record the shear plane region ahead of the tool. Detailed information about the machine setup and instrument validation is included in the next section.

V. Experimental Sequence

Virtual Quick Stop Data Acquisition

Before runs were made on a given day the machine was calibrated. This calibration included checking the camera focus and scale against the micrometer slide as well as a couple test runs in a scrap sample to check for proper machine movement. After calibration a workpiece was selected according to the run number and mounted in the workpiece holder. The cutting tool corresponding to the run number was loaded into the tool holder and tightened down. The cutting tool was then used to remove a small amount of material from the workpiece (less than .005 inches). This topping cut also corrected for any non-parallelism between the cutting tool and the workpiece thus reducing the possibility of a non-uniform feed. The effectiveness of the topping cut was monitored using the Midas software. Once uniform cuts were established, the forces would stabilize across the entire topping cut. This was clear in the LabVIEW graph display.

After the first cut the z-axis was zeroed so that the following cut would be the correct depth from the now perfectly parallel face. The tool was returned to the starting side of the workpiece and readied for a data run. It was now time to turn on the signal amplifiers for the dynamometer. They were switched on and then flipped into recording mode. This starts the transmission of force data to LabVIEW. The LabVIEW data acquisition program was started which takes in the force data and tells the camera when to start recording. The camera was put into recording mode and awaiting the signal from

LabVIEW. The z axis of the horizontal milling machine was adjusted to the desired depth of cut for the run. The feed on the motor controller was then adjusted as well. With everything now in the correct state for the start of a run, the forward feed button is pressed on the motor controller. This started moving the tool into the workpiece generating a force signal which in turn started the data recording.

As soon as the run was completed the camera video was saved and the tool moved back to the starting position. The force data was saved automatically with an auto-incrementing file name format. All force data and images are time stamped from the system clock to the nearest millisecond. This time stamp from the same clock is critical to synchronizing the force data with the images of the material undergoing shear.

The process continued through all of the required data runs. If there was any error in the recording process the run would be repeated until the desired number of replicated was achieved for each set of parameters.

Tool Wear Analysis

The tool wear analysis portion only used a single tool angle and a single specimen material concentrate on the effects of the atmosphere on the volumetric tool wear. The process is identical to the Virtual Quick Stop data acquisition. The difference is that the tool in question would be taken to the Keyence 3D microscope after 10 inches of material was cut with the tool. Wear measurements were recorded at the microscope and the tool returned to the holder. Care was taken to ensure that no adjustments to the machine occurred so that the same portion of the tool was used to cut the specimen every time. This ensured that the wear would not be spread over the cutting surface and made data capture of the volumetric loss easier to identify and measure. This process was repeated 5 times for

a total of 50 cuts or 100 inches of material cut. After the entire sequence was completed for either Air, Nitrogen, or Argon a new tool would be inserted, and the atmosphere would be changed. The process would then be repeated until cutting occurred in all three atmospheres. Force data was taken as the cuts were completed for analysis later.

Post Processing

The post processing of all the data was done using various programs selected for their performance in their respective areas of data processing. LabVIEW was utilized to convert the data generated by the data collection program into an Excel format. This data was exported to another Excel file for use to calculate the resultant forces, strains, and stress according to Merchant's model. Kinovea is a video analysis program that was used to measure the angles of interest as well as the tool angle and uncut chip thicknesses. The programs used will be detailed next.

Kinovea has the ability to measure, distance, speed, and acceleration of points in video. By using these capabilities, the speed was verified.

LabVIEW produced data files of the force measurements from the dynamometer in a proprietary .TDM file format. A LabVIEW program incremented through all the .TDM force data files and generated a formatted Excel file. The full program can be viewed in Appendix 5.

MATLAB incremented through all Excel files generated by the previous LabVIEW file and displays a graph of the cutting force data.

The figure below shows a plot that is displayed to select the appropriate range of data for average force calculation.

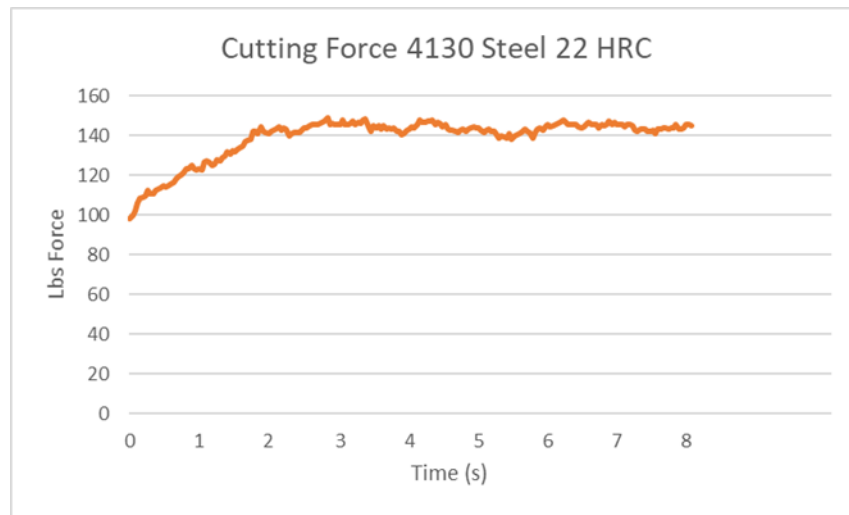


Figure 30. Example of Force data

Once all data was recorded, Excel was utilized to take the mean of the force, so an average force could then be recorded. The first 2 seconds on average were thrown out due to a lack of steady state force. A separate Excel spread sheet was then used to keep record of all average forces. To measure the shear angle from the video, KINOVEA video analysis software was used. The individual frames or the video could be marked for the software to measure the onset of shear angle. The analysis software also allowed for psi to be measured. The Keyence 3d microscope was utilized for the tool wear study. Each image taken at the microscope was measured for width of wear, length of wear, and depth of wear using the microscope software to achieve the measurements. All measurements were recorded in Excel where comparisons of forces with the atmosphere as the variable would be possible. Also, the volume of material removed from the tool was calculated and comparisons were made.

VI. Instrument Validation and Statistical Design of Experiments

Machine Setup

The goal of instrument validation is to verify that the High Speed Videographic Quick Stop Device for Orthogonal Machining is a valid instrument for making orthogonal cuts at predetermined parameters and its ability to record the resulting information. This study is valid for the quick stop device as it exists in its current form in 2016. Any modifications to the system will require a reevaluation of the machine and its capabilities.

The foundation of the virtual quick stop device is a Cincinnati Milacron horizontal milling machine. The horizontal milling machine is used as a rigid base for making the orthogonal cuts. The machine itself is never powered up as none of the powered functions of the machine are utilized. It is an extremely massive, stable bed for the experiment.

A 1/8 horsepower Baldor three-phase induction electric motor is used to move the milling table in the x direction underneath the stationary tool holder. The Baldor electric motor is connected to a Wood's E-Trac motor controller. This motor controller permits precise speed control of the motor using a variable frequency drive (VFD). The frequency at which this motor controller sends power to the motor directly controls the motor RPM. The formula for calculating the RPM of an electric motor using VFD is calculated as

$$n = 120 \left(\frac{f}{P} \right) \quad (16)$$

where n is the RPM, f is the frequency of the power, and P is the number of pole pairs in the electric motor. A 20/1 gear reducer is installed on the motor to increase the torque

provided by the motor. The speed of the motor is monitored in real time using a rotary encoder.

The tool holder is attached to the overarm dovetail of the horizontal milling machine. If the horizontal milling machine was being used for traditional milling, an arbor support would attach to the overarm dovetail. The overarm is designed to incur very high loads during normal horizontal milling operations and is extremely rigid and perfectly parallel to the milling table making it an ideal platform to attach the tool holder to. The overarm is adjustable in the y direction to reduce the distance of the tool holder from the main base. This distance was minimized to increase rigidity even further. The tool holder is designed to hold a 3/4" high speed steel (HSS) tool that has been ground to a specified angle to the milling table below. The tool is also held perfectly perpendicular to the table motion so that it is a true orthogonal cut with all force being exerted into the piece in a single plane.

A workpiece holder was designed to attach to the Kistler dynamometer and also provide maximum clamping force on the sample being cut. The dynamometer is attached to the milling table via a steel adapter plate that fixes into the milling tables T-slots. This fixture ensures that the workpiece will be perfectly parallel to the x direction of the table.

The camera for recording the deformation of the workpiece during cutting is attached to a custom-made stand. The stand is a load lift modified to allow the fixture of various attachments. A cross slide vice has been attached to the load lift table which allows the camera to be precisely moved in the x and y directions for easy camera positioning. A winch on the back of the lift moves the camera in the z direction.

Run Setup

The correct initial setup of the machine is necessary for repeatable measurements to be made on any given day. The setup begins by positioning the camera and calibrating the focus and scale. This is accomplished by moving the camera stand into position in front of the tool holder. The cross-slide vice can be used for fine adjustments in the x direction and the height should be adjusted using the winch. Insert a tool into the tool holder and tighten the screws that hold the tool in place. It is important to make sure that the tool is inserted all the way up into the tool holder for repeatable tool rigidity. Insert a workpiece into the workpiece holder and tighten it down with the set screws. It is important to make sure that the sample is firmly contacting the bottom of the workpiece slot during tightening of the set screws.

Place the calibration slide against the workpiece with the etched side against the material. This places the scale on the same plane as the workpiece. Move the workpiece holder underneath the tool and raise it until the top of the calibration slide is just touching the tool. This will keep the slide from falling. Be sure not to crush the slide while raising the workpiece holder.

Start the Midas software on the computer connected to the camera and make sure you can see a live feed. Turn on the fiber optic ring light to provide enough light for the camera at the high magnification. The camera lens has two adjustment knobs. One is for the zoom level and the other for focusing. Adjust the camera lens zoom to the maximum level and the focus to the closest setting. When the object is in focus at these settings the camera is achieving the maximum zoom possible by the lens. Move the camera in the y direction until the micrometer scale comes into focus. The y-direction of the horizontal

mill table can be adjusted as well to bring the scale into focus as long as the workpiece remains underneath the tool. Once the scale is clearly visible do not move the camera or adjust the zoom or focus of the camera lens until all runs are completed for the session. Record the scale for a couple seconds. This video will be used for a pixel to inch ratio. This ratio can be calculated in the Midas software or later in an external program. Carefully remove the micrometer scale from against the workpiece.

Raise the workpiece underneath the tool so that both can be observed by the camera. Run the motor in reverse until the tool is just to the side of the workpiece. Adjust the workpiece holder to remove 0.002" of material. The adjustment of the workpiece can be measured using a dial indicator attached to the milling machine base and then contacting the milling table. Check the depth of cut for the first cut with the video from the camera. This provides a check for the dial indicator. Set the motor controller to the desired run speed and make a pass with the tool. This will establish a perfectly parallel plane between the workpiece and tool for the rest of the runs. Once the cut is completed lower the workpiece just enough so that when it is run in reverse to start the next run the tool does not slide back over the workpiece. If necessary, the workpiece can be refocused by moving the milling table to bring the piece into better focus. As long as the camera has not been adjusted, when the sample is in focus it will be at the same scale as when it started.

VII. Data Results

The experimental data was collected, during which time the process was carefully monitored for any irregularities or obvious discrepancies. The following types of data were collected through direct measurement (electronically for the forces and stresses, and optically for the angles).

Table 3. Symbols and Units of Direct Measurements

Data	Symbol	Units
Tool Rake Angle	α	degrees
Uncut Chip Thickness	t_o	inches
Cut Chip Thickness	t_c	inches
Horizontal Cutting Force	F_c	pounds force (lbf)
Vertical Cutting Force	F_t	pounds force (lbf)
Shear Plane Angle	ϕ	degrees
Shear Front Angle	ψ	degrees
Ultimate Stress	F_u	pounds force (ksi)

During initial selection of the parameters to be used it appeared that the three tool angles selected would produce nice type 2 chips for all materials at all hardnesses. It was discovered during testing that this was not the case. The 25-degree tool would not reliably produce type 2 chips in the aluminum, steel, and softer magnesium specimens. The 25-degree tool would produce nice type 2 chips every now and then but often it would plow into the material making it unsuitable for subsequent runs. This caused considerable time delays and made it practically impossible to collect a reliable data set for analysis at some points. During these instances the data was thrown out and the cut was re-done to get data that was acceptable. During the experiment it was also noted that during some runs the tool underwent minor deflections in some materials.

Using the data collected during the experiment it was possible to calculate the values of primary interest in metal cutting using the relationship derived by Merchant, Payton, and others. The table below lists the values that were calculated.

Table 4. Symbols and Units of Calculated Measurements

Data	Symbol	Units
Chip Thickness Ratio	r_c	none
Friction Force Upon Chip	F	newtons
Normal Force Upon Chip	N	newtons
Shear Force on Plane	F_s	newtons
Normal Force on Plane	F_n	newtons
Mean Friction Angle at Tool	β	degrees
Area of Shear Plane	A_s	in ²
Shear Stress on Shear Plane	τ_s	MPa
Friction Coefficient	μ	none
Shear Strain	γ	none
Resultant Force	R	newtons
Resultant Shear Stress	R_τ	MPa

Results of the Videographic Study

The virtual quick stop videographic analysis proved very capable of doing the analysis intended. Video of each run was captured in real time resulting in a massive amount of data for each run. The video of each run had its share of useful and unusable images. As the tool progressed through the material the material would often move in and out of focus during the duration of the cut. This was due to the material specimens either

not being perfectly flat or being bent slightly out of flat when it was being secured in the workpiece holder.

After each run completed a portion of the video from the run was saved for further analysis. The selection was determined by the focus of the image and a clear view of the shear plane. As force data was recorded during the entire cut, there was sufficient force data for any range of image selection. Figure 29 illustrates a sample of the force data collected during a run sequence.

The range of images was exported as a video file which would be analyzed with software during post processing. During post processing individual images were selected from the video file which best represented the shear plane during the cut and when forces has stabilized. An example of the image taken from the video is shown below.

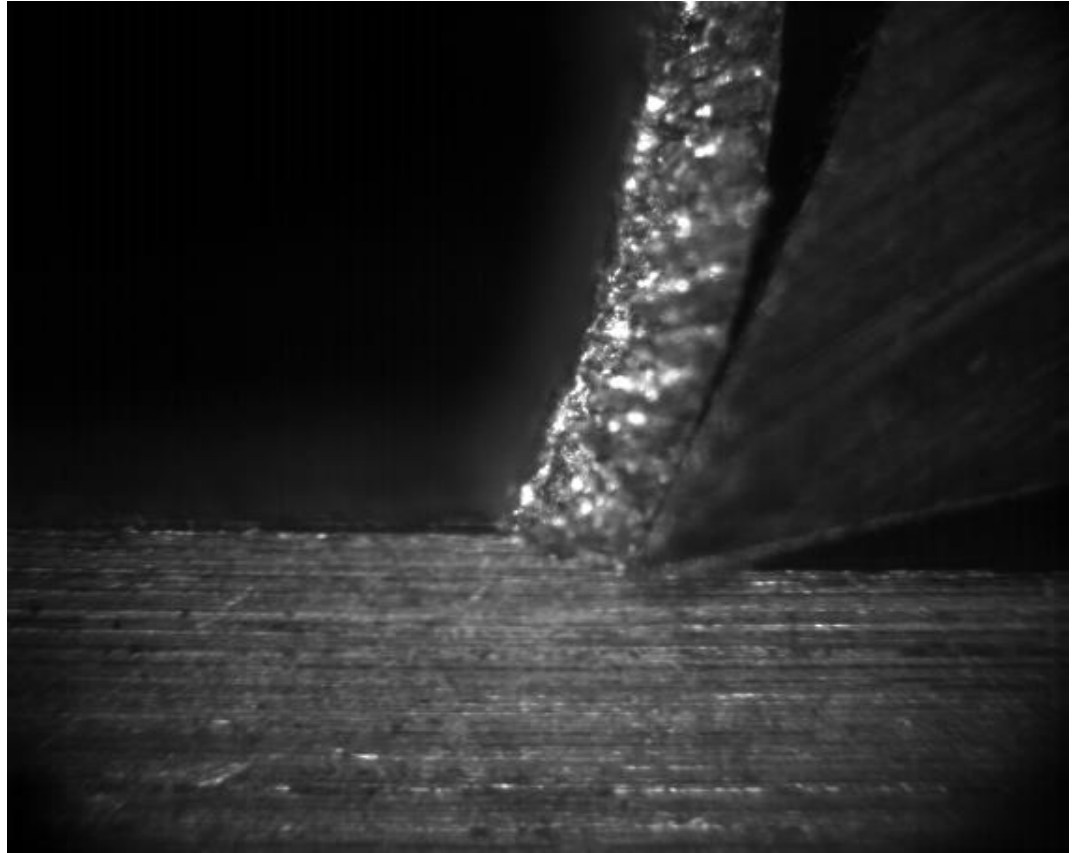


Figure 31. Unexamined Frame of Video

This individual image was used to measure the angles of interest as well as the tool angle and depth of cut. Measured shear angles were compared with the calculated values of Merchant's model with extremely good effect. This system of measurement greatly reduced the time required and decreased the margin of error typically associated with measuring the angles of interest using traditional methods. An example of the examined frame of video is shown below. The depth of cut, chip thickness, and shear angle were all measured in the same picture.

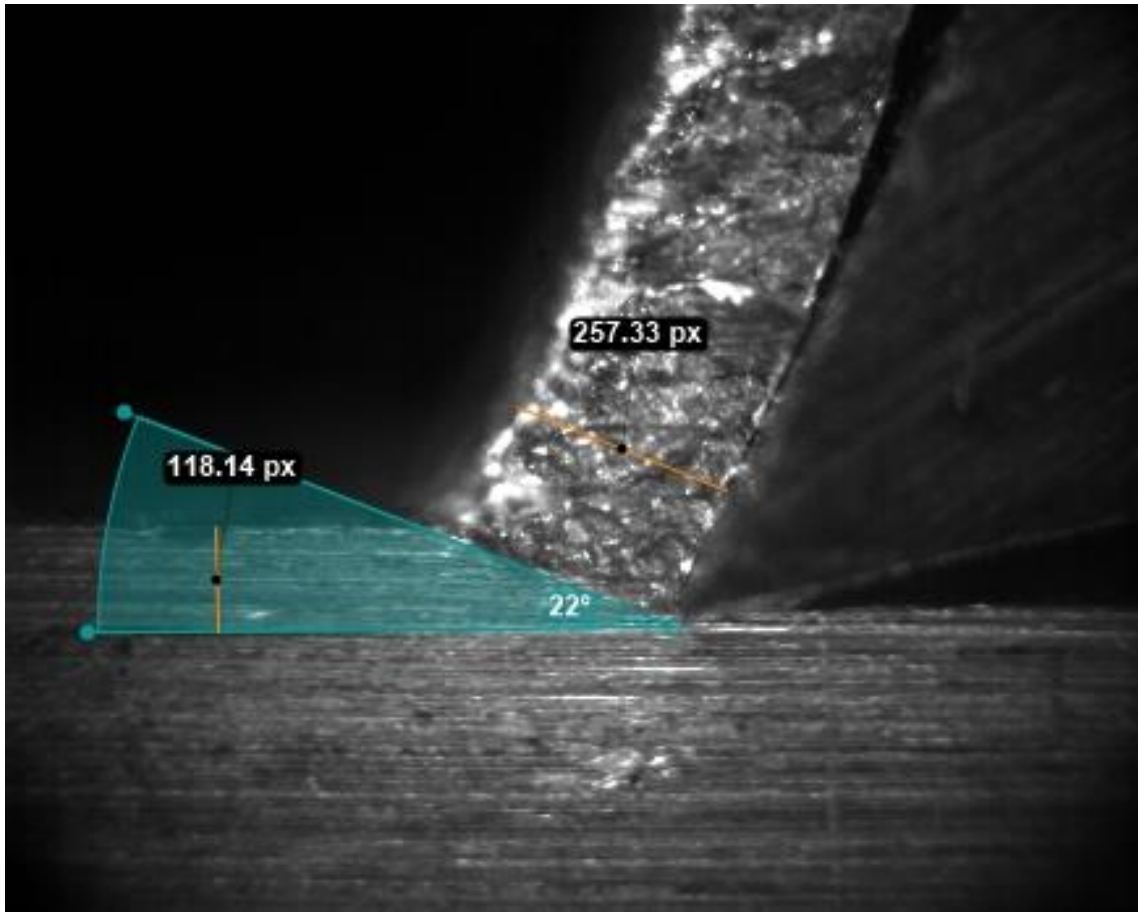


Figure 32. Examined Frame of Video

The depth was cut was observed to vary up to ± 0.0005 inches and is attributed to slight slack in the lead screw controlling the z axis of the horizontal milling machine.

The figure below illustrates the observed geometry of the shear zone in all materials. .

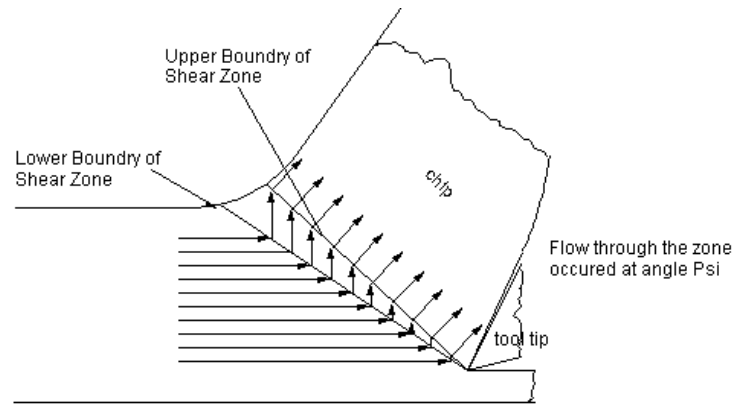


Figure 33. Shear Zone Geometry

This geometry is consistent with the observations of Briggs, Huang and Black, and Payton [35] [70] [71]. The movement of the crystals into and through the shear zone follows the Huang model of movement. The large amount of data collected was prepared for statistical analysis to be detailed in the next section.

Results of Tool Wear Microscopy

Tool wear microscopy was performed using the Keyence 3D microscope and provided the ability to get volumetric loss of the tool. The resulting images of the tool show a clearly defined interaction zone between the tool and the chip. This zone is shown in the image below.

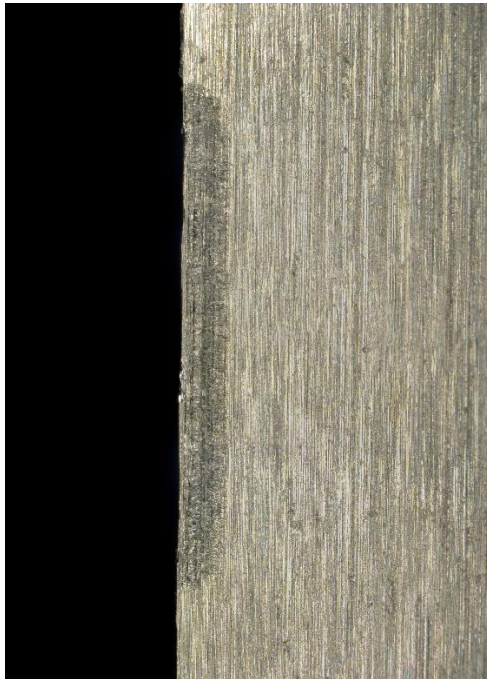


Figure 34. Chip to tool interaction zone

Since each tool was never sharpened the tool/chip interface consistently turned more and more ragged. Each tool eventually showed signs of failing as tool wear continued. The image below shows the tool as pieces are broken off and missing.

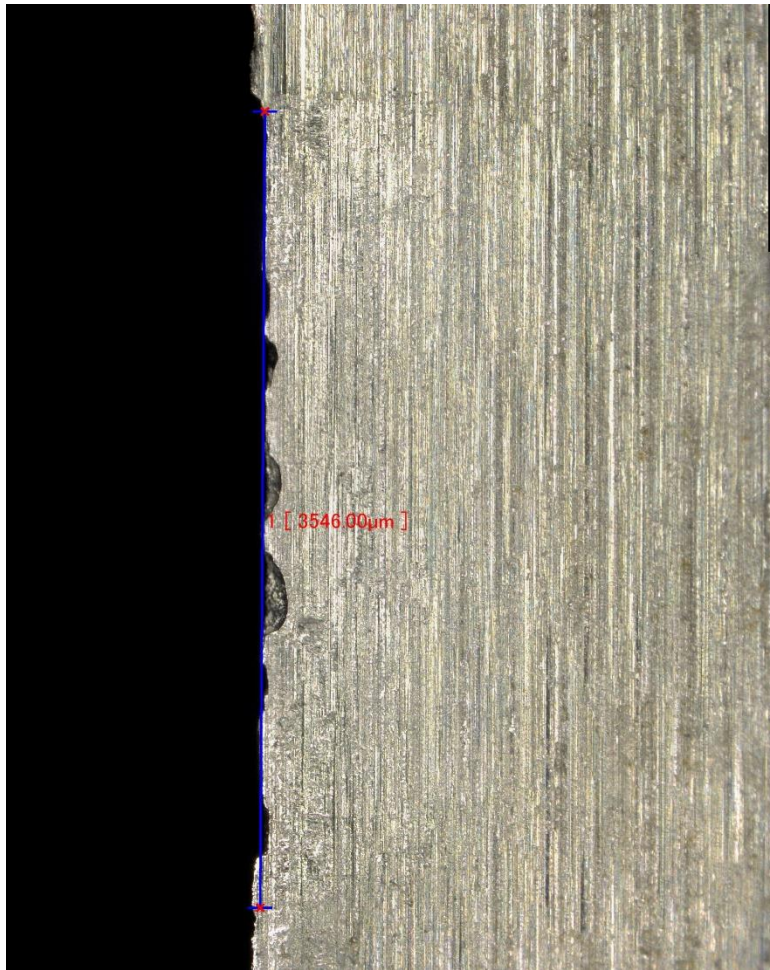


Figure 35. Tool Showing Signs of Failing

3D images of the tool wear zone were also taken and were utilized for data analysis.

An example of the 3D picture is given below.

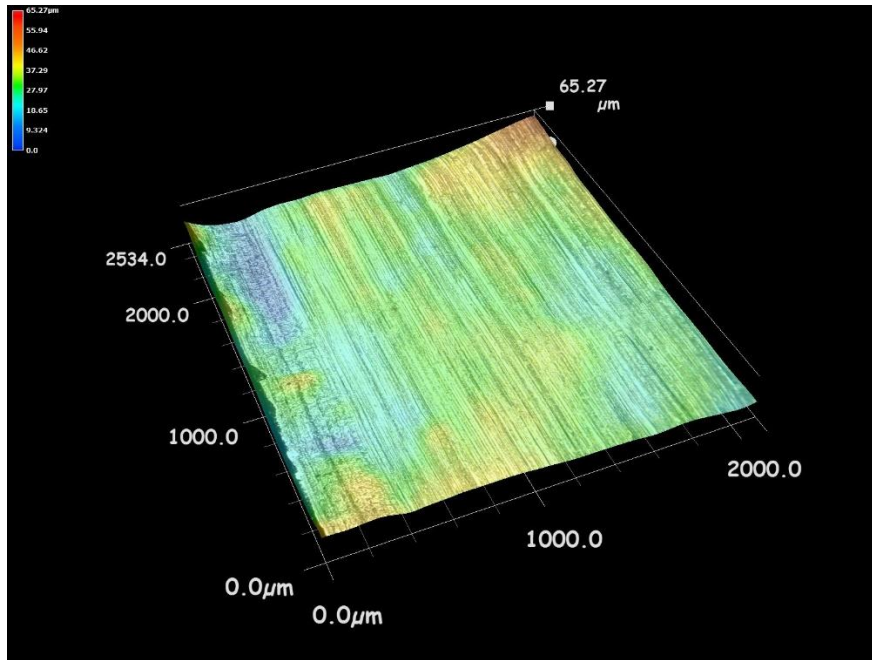


Figure 36. 3D image of tool after 80 inches of cut in air environment

Utilizing the Keyence 3D microscope measurements and data were recorded. The measurements and data recorded include the width of the wear area, length from the tool edge, and the depth of material removed. The following image shows the area of the tool-chip interface measurement.

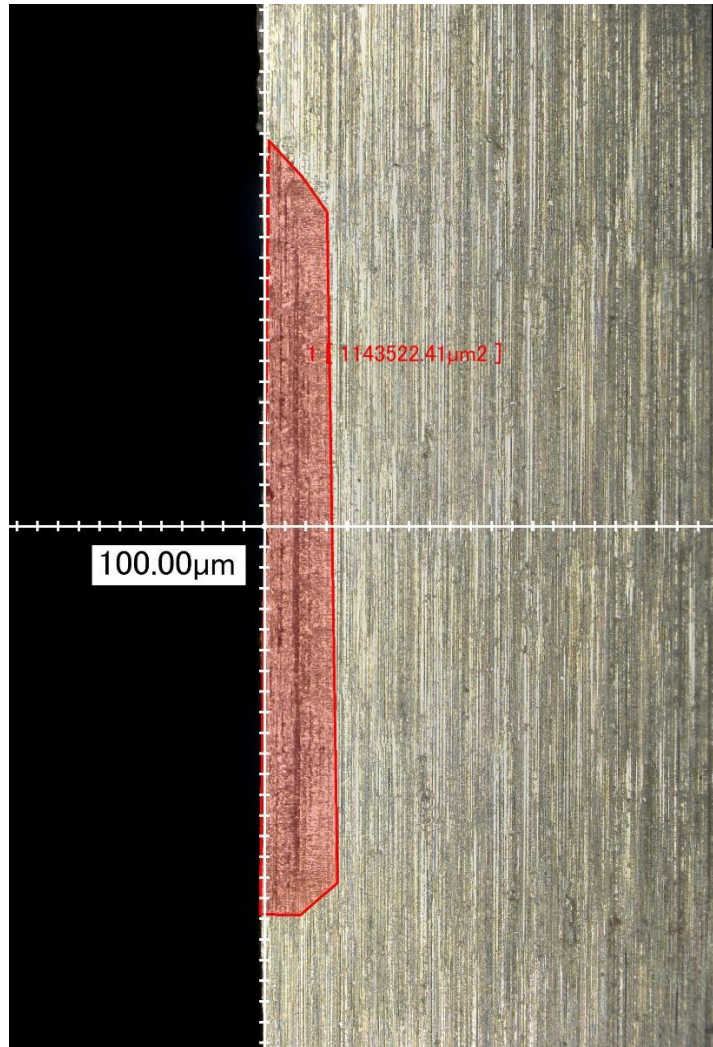


Figure 37. Area of Tool-Chip Interface

Profiles were taken and recorded after every 20 inches of cut. Each profile was recorded into a Comma Separated Values file (.CSV) directly from the microscope. The profiles were leveled and compared to see if a visible dip was shown where tool wear occurred. This allowed the data to be manipulated in Excel for comparison.

Pictured below is a picture showing the tool-chip interface with a scale next to it for size comparison. This was a typical image and showed clearly the darkened area where the chip interacted with the tool.

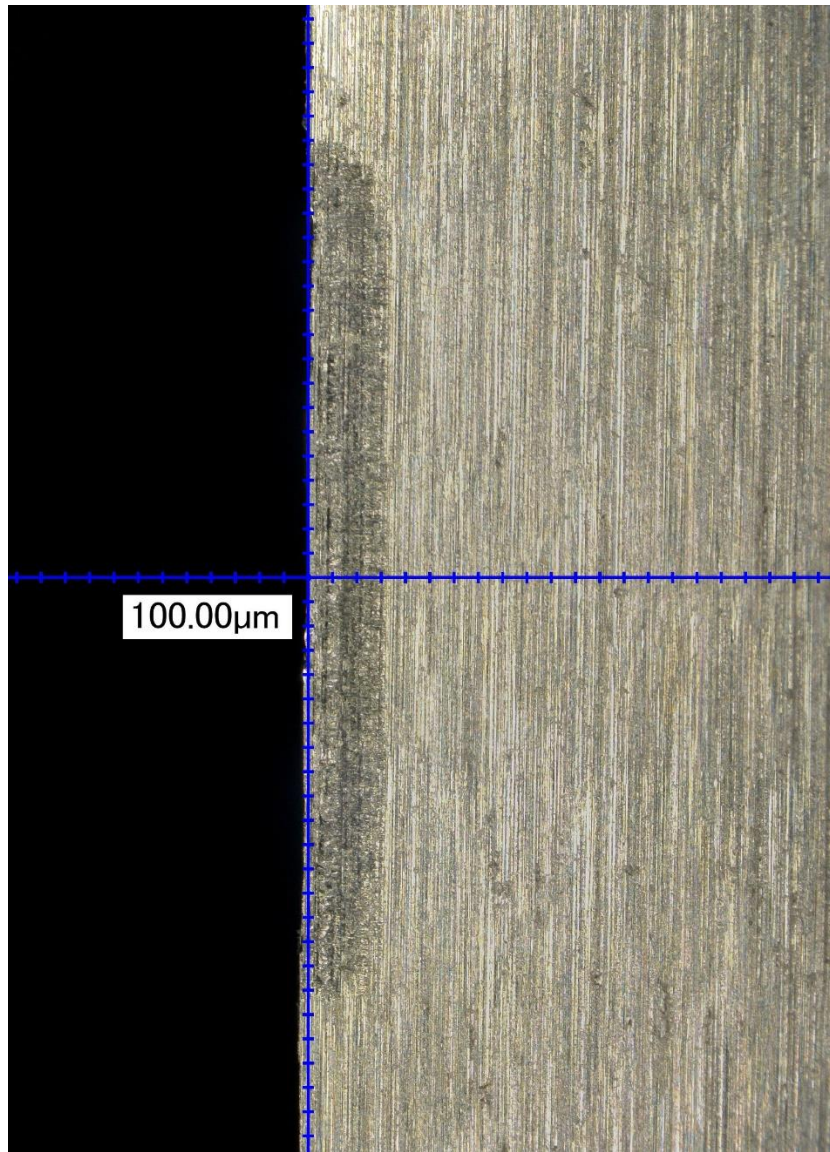


Figure 38. Tool wear zone with scale

IX. Statistical Analysis

Statistical analysis was performed on the data collected from the dynamometer and optical methods. This experiment produced large amounts of data on the forces predicted by Merchant's model. In addition, the angle measurements α , β , ϕ , and ψ tied to these forces were available for analysis. The statistical software packages Design-Ease7 and Design Expert 11 were utilized to examine the data collected and to compare the predictive models for the angles of interest. The comparative effect of the gases on the tool wear were also scrutinized.

The following box plot shows three typical replicate runs side by side by. This optically verifies the typical repeatability of every factor level combination attempted in the experiment.

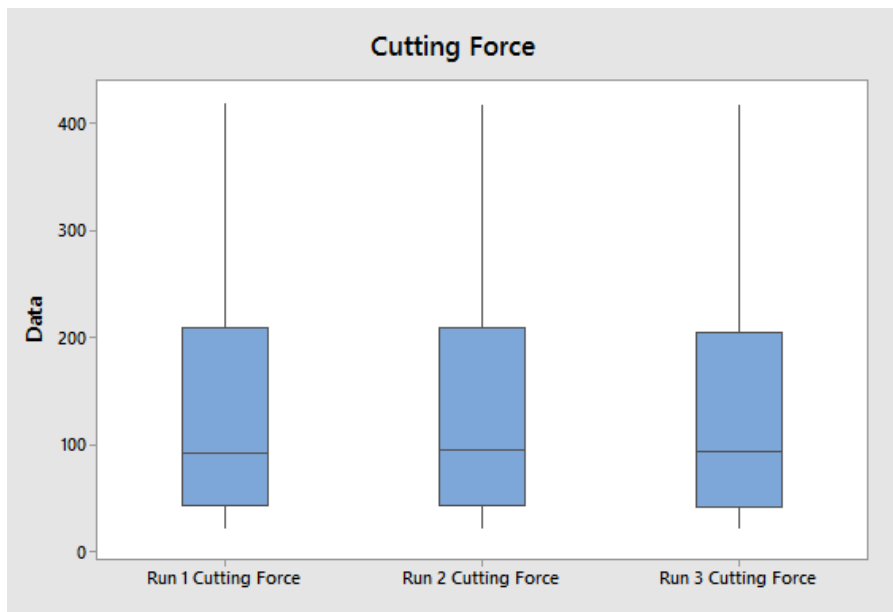


Figure 39. Boxplot of Cutting Force divided by Run

The following table shows the ANOVA of the cutting forces F_c . The model F-value of 401.86 implies the model is significant. There is only a 0.01% chance that an F-value this large could occur due to noise. P-values less than 0.0500 indicate model terms are significant. In this case hardness, depth of cut, and tool angle are significant model terms. The table shows that the cutting atmosphere had no effect in the cutting force. With a P-value of 0.0948, the atmosphere had no statistical effect unlike the other three variables, of material hardness, depth of cut, and tool angle.

Table 5. ANOVA of Cutting Force

ANOVA for selected factorial model

Response 1: cutting force

	Source	Sum of Squares	df	Mean Square	F-value	p-value	
	Block	88.64	2	44.32			
	Model	5.702E+06	12	4.752E+05	401.86	< 0.0001	significant
	A-hardness	4.951E+06	7	7.073E+05	598.14	< 0.0001	
	B-atmosphere	5603.02	2	2801.51	2.37	0.0948	
	C-depth of cut	7.111E+05	1	7.111E+05	601.37	< 0.0001	
	D-Tool angle	34577.39	2	17288.69	14.62	< 0.0001	
	Residual	4.931E+05	417	1182.46			
	Cor Total	6.195E+06	431				

The following t-tests comparing the cutting force with Air vs. Argon, Air vs. Nitrogen, and Argon vs. Nitrogen correlate with the ANOVA shown in Table 5. The P-value of 0.68 on the Air vs. Argon T-test shows there is not a significant difference.

Table 6. Cutting Force T Test Air vs. Argon

	<i>cutting force (lbs force) Air</i>	<i>cutting force (lbs force) Argon</i>
Mean	138.3823817	144.0736406
Variance	13379.48827	14623.00382
Observations	144	145
Pooled Variance	14003.41245	
Hypothesized Mean	0	
df	287	
t Stat	-0.408797031	
P(T<=t) one-tail	0.341496744	
t Critical one-tail	1.650180211	
P(T<=t) two-tail	0.682993488	
t Critical two-tail	1.968264113	

The same can be said of the Air vs. Nitrogen T-test. The P- value of 0.56 shows there is not a significant difference.

Table 7. Cutting Force T Test Air vs. Nitrogen

	<i>cutting force (lbs force) Air</i>	<i>cutting force (lbs force) Nitrogen</i>
Mean	138.3823817	146.513803
Variance	13379.48827	15062.68639
Observations	144	144
Pooled Variance	14221.08733	
Hypothesized Mean Difference	0	
df	286	
t Stat	-0.578583856	
P(T<=t) one-tail	0.281662671	
t Critical one-tail	1.650198896	
P(T<=t) two-tail	0.563325342	
t Critical two-tail	1.968293255	

The last comparison was to determine of the Argon vs. Nitrogen showed a significant difference. The table below shows there is not a significant difference in cutting force when varying Nitrogen or Argon.

Table 8. Cutting Force T Test Argon vs. Nitrogen

	<i>cutting force (lbs force)</i> <i>Argon</i>	<i>cutting force (lbs force)</i> <i>Nitrogen</i>
Mean	144.0736406	146.513803
Variance	14623.00382	15062.68639
Observations	145	144
Pooled Variance	14842.0791	
Hypothesized Mean Difference	0	
df	287	
t Stat	-0.170250219	
P(T<=t) one-tail	0.432466655	
t Critical one-tail	1.650180211	
P(T<=t) two-tail	0.864933311	
t Critical two-tail	1.968264113	

The same can be said for the Shear Angle and Friction Force, but not the Thrust Force. The following ANOVA table of the Thrust Force F_t shows that the Atmosphere does have a significant effect on the thrust force.

Table 9. ANOVA of Thrust Force F_t

ANOVA for selected factorial model

Response 2: thrust force

Source	Sum of Squares	df	Mean Square	F-value	p-value	
Block	27.21	2	13.60			
Model	5.225E+05	12	43542.26	316.12	< 0.0001	significant
A-hardness	4.747E+05	7	67809.64	492.31	< 0.0001	
B-atmosphere	2838.88	2	1419.44	10.31	< 0.0001	
C-depth of cut	23249.91	1	23249.91	168.80	< 0.0001	
D-Tool angle	21750.86	2	10875.43	78.96	< 0.0001	
Residual	57436.66	417	137.74			
Cor Total	5.800E+05	431				

This shows that there is an effect between the atmosphere and the thrust force F_t . T-Tests were then performed to show the differences between Air vs. Argon, Air vs. Nitrogen, and Argon vs. Nitrogen to determine which were different.

Table 10. Thrust Force F_t T-Test Air vs Argon

	<i>thrust force (lbs force) Air</i>	<i>thrust force (lbs force) Argon</i>
Mean	33.42698332	38.42891453
Variance	1064.63298	1448.030333
Observations	144	144
Pearson Correlation	0.980772981	
Hypothesized Mean Difference	0	
df	143	
t Stat	-6.832820257	
P(T<=t) one-tail	1.109E-10	
t Critical one-tail	1.655579143	
P(T<=t) two-tail	2.218E-10	
t Critical two-tail	1.976692198	

The p value shown above displays a significant difference in the thrust force F_t when swapping between Air and Argon. The table below shows the comparison between Air and Nitrogen.

Table 11. Thrust Force F_t T-Test Air vs Nitrogen

	<i>thrust force (lbs force) Air</i>	<i>thrust force (lbs force) Nitrogen</i>
Mean	33.42698332	39.25481957
Variance	1064.63298	1527.846773
Observations	144	144
Pearson Correlation	0.982043422	
Hypothesized Mean Difference	0	
df	143	
t Stat	-7.475357409	
P(T<=t) one-tail	3.53103E-12	
t Critical one-tail	1.655579143	
P(T<=t) two-tail	7.06206E-12	
t Critical two-tail	1.976692198	

This p-value Of 7.06E-12 also shows a significant difference between Air and Nitrogen. The last T-test shows the comparison between Argon and Nitrogen in the thrust force F_t .

Table 12:Thrust Force T-Test Argon vs Nitrogen

	<i>thrust force (lbs force) Argon</i>	<i>thrust force (lbs force) Nitrogen</i>
Mean	38.42891453	39.25481957
Variance	1448.030333	1527.846773
Observations	144	144
Pearson Correlation	0.991432678	
Hypothesized Mean Difference	0	
df	143	
t Stat	-1.923199244	
P(T<=t) one-tail	0.028221217	
t Critical one-tail	1.655579143	
P(T<=t) two-tail	0.056442433	
t Critical two-tail	1.976692198	

This last t-test shows the P-value of 0.056 being greater than the α value of 0.05. Therefore there is no significant difference between Argon and Nitrogen in the thrust force F_t .

This reaffirms the ANOVA results that gaseous cutting fluids have an effect on the thrust force, although there is no significant difference in the thrust force when comparing Argon and Nitrogen.

Only when comparing the thrust forces of the Air environment against either the Argon or Nitrogen environment does it show a statistically significant difference.

With the positive correlation between the Thrust Force F_t and the Atmosphere, the results for the shear angle compared. However, the ANOVA for the Onset of Shear Angle ϕ showed no correlation of the atmosphere and the directly measured Onset of Shear ϕ . The following ANOVA Table shows no correlation.

Table 13. ANOVA of Shear Angle ϕ

ANOVA for selected factorial model

Response 3: Shear Angle

Source	Sum of Squares	df	Mean Square	F-value	p-value	
Block	3.73	2	1.87			
Model	76443.43	12	6370.29	619.97	< 0.0001	significant
A-hardness	75740.36	7	10820.05	1053.04	< 0.0001	
B-atmosphere	47.67	2	23.84	2.32	0.0996	
C-depth of cut	37.10	1	37.10	3.61	0.0581	
D-Tool angle	618.30	2	309.15	30.09	< 0.0001	
Residual	4284.71	417	10.28			
Cor Total	80731.87	431				

The following T-tests compare the shear angle of Air vs. Argon, Air vs. Nitrogen, and Argon vs. Nitrogen.

Table 14. Shear Angle T-Test Air vs. Argon

	<i>measured shear angle (degrees) air</i>	<i>measured shear angle (degrees) Argon</i>
Mean	33.49983333	32.73625
Variance	186.8933455	190.2870823
Observations	144	144
Pooled Variance	188.5902139	
Hypothesized Mean Difference	0	
df	286	
t Stat	0.471805623	
P(T<=t) one-tail	0.318712641	
t Critical one-tail	1.650198896	
P(T<=t) two-tail	0.637425282	
t Critical two-tail	1.968293255	

The P- value of 0.63 shows that any difference is not significant. The following table shows the t test between Air and Nitrogen.

Table 15. Shear Angle ϕ T-Test Air vs. Nitrogen

	<i>measured shear angle (degrees) air</i>	<i>measured shear angle (degrees) Nitrogen</i>
Mean	33.49983333	33.17388889
Variance	186.8933455	187.6164771
Observations	144	144
Pooled Variance	187.2549113	
Hypothesized Mean Difference	0	
df	286	
t Stat	0.202112523	
P(T<=t) one-tail	0.419986224	
t Critical one-tail	1.650198896	
P(T<=t) two-tail	0.839972449	
t Critical two-tail	1.968293255	

This also shows no significant difference in shear angle when using Air or Nitrogen. The last comparison is between Argon and Nitrogen.

Table 16. Shear Angle ϕ T-Test Argon vs. Nitrogen

	<i>measured shear angle (degrees) Argon</i>	<i>measured shear angle (degrees) Nitrogen</i>
Mean	34.78351394	35.21771515
Variance	772.6552045	751.3750875
Observations	144	144
Pooled Variance	762.015146	
Hypothesized Mean Difference	0	
df	286	
t Stat	-0.133467487	
P(T<=t) one-tail	0.44695877	
t Critical one-tail	1.650198896	
P(T<=t) two-tail	0.89391754	
t Critical two-tail	1.968293255	

The frictional force **F** ANOVA shown below has two significant factors and 2 insignificant factors according to the analysis. The Model F-value of 401.98 implies the model is significant. P-values less than 0.0500 indicate model terms are significant. In this case Hardness and depth of cut are significant model terms. This shows that the frictional force is statistically dependent on the material being cut and depth of cut instead of the atmosphere or tool angle.

Table 17. ANOVA of Friction Force F

ANOVA for selected factorial model

Response 4: Friction Force

Source	Sum of Squares	df	Mean Square	F-value	p-value	
Block	1218.62	2	609.31			
Model	6.391E+07	12	5.325E+06	401.98	< 0.0001	significant
A-hardness	5.842E+07	7	8.346E+06	629.99	< 0.0001	
B-atmosphere	48432.77	2	24216.39	1.83	0.1620	
C-depth of cut	5.409E+06	1	5.409E+06	408.26	< 0.0001	
D-Tool angle	25012.55	2	12506.28	0.9440	0.3899	
Residual	5.524E+06	417	13248.16			
Cor Total	6.943E+07	431				

The following T tests show there is no significant difference between Air vs. Argon.

Table 18. Friction Force F T-Test Air vs. Argon

	<i>Friction Force (Newtons) air</i>	<i>Friction Force (Newtons) Argon</i>
Mean	433.8778298	465.7199446
Variance	139100.6085	166631.2464
Observations	144	144
Pooled Variance	152865.9274	
Hypothesized Mean Difference	0	
df	286	
t Stat	-0.691055304	
P(T<=t) one-tail	0.24504565	
t Critical one-tail	1.650198896	
P(T<=t) two-tail	0.490091299	
t Critical two-tail	1.968293255	

Air vs Nitrogen T test did not show a significant difference as shown in the table below.

Table 19. Friction Force F T-Test Air vs. Nitrogen

	<i>Friction Force (Newtons) air</i>	<i>Friction Force (Newtons) Nitrogen</i>
Mean	433.8778298	475.6535722
Variance	139100.6085	172926.6353
Observations	144	143
Pooled Variance	155954.278	
Hypothesized Mean Difference	0	
df	285	
t Stat	-0.896053306	
P(T<=t) one-tail	0.185490251	
t Critical one-tail	1.650217713	
P(T<=t) two-tail	0.370980503	
t Critical two-tail	1.968322603	

Argon vs Nitrogen did not show a significant difference in the friction force when tested during a t test.

Table 20. Friction Force F T-Test Argon vs. Nitrogen

	<i>Friction Force (Newtons) Argon</i>	<i>Friction Force (Newtons) Nitrogen</i>
Mean	465.7199446	475.6535722
Variance	166631.2464	172926.6353
Observations	144	143
Pooled Variance	169767.8963	
Hypothesized Mean Difference	0	
df	285	
t Stat	-0.204215361	
P(T<=t) one-tail	0.41916548	
t Critical one-tail	1.650217713	
P(T<=t) two-tail	0.83833096	
t Critical two-tail	1.968322603	

By observing the friction force the normal force of the chip to the tool face is the next logical step to analyze. The normal force ANOVA can be seen below. This shows that the atmosphere did not have an effect on the normal force.

Table 21. ANOVA for Normal Force N

ANOVA for selected factorial model

Response 5: Normal Force

Source	Sum of Squares	df	Mean Square	F-value	p-value	
Block	1846.69	2	923.35			
Model	5.898E+07	12	4.915E+06	328.70	< 0.0001	significant
A-hardness	4.993E+07	7	7.134E+06	477.08	< 0.0001	
B-atmosphere	13713.69	2	6856.85	0.4586	0.6325	
C-depth of cut	7.989E+06	1	7.989E+06	534.26	< 0.0001	
D-Tool angle	1.042E+06	2	5.208E+05	34.83	< 0.0001	
Residual	6.235E+06	417	14952.67			
Cor Total	6.522E+07	431				

The following T tests compared the normal force of air against the normal force of Argon. There was no significant difference in the normal force.

Table 22. Normal Force N T Test Air vs. Argon

	<i>Normal Force (Newtons) air</i>	<i>Normal Force (Newtons) Argon</i>
Mean	461.1992298	472.2225388
Variance	146763.7504	154417.2346
Observations	144	144
Pooled Variance	150590.4925	
Hypothesized Mean Difference	0	
df	286	
t Stat	-0.241034635	
P(T<=t) one-tail	0.404850489	
t Critical one-tail	1.650198896	
P(T<=t) two-tail	0.809700978	
t Critical two-tail	1.968293255	

The following table shows the results of the normal force when comparing Air vs Nitrogen. There was no significant difference in the Normal forces.

Table 23. Normal Force N T Test Air vs. Nitrogen

	<i>Normal Force (Newtons) air</i>	<i>Normal Force (Newtons) Nitrogen</i>
Mean	461.1992298	479.8929876
Variance	146763.7504	157796.5817
Observations	144	143
Pooled Variance	152260.8102	
Hypothesized Mean Difference	0	
df	285	
t Stat	-0.405798896	
P(T<=t) one-tail	0.34259743	
t Critical one-tail	1.650217713	
P(T<=t) two-tail	0.68519486	
t Critical two-tail	1.968322603	

The following table shows more of the same as there is no significant difference in the Nitrogen vs. Argon Normal force as well.

Table 24. Normal Force N T Test Argon vs. Nitrogen

	<i>Normal Force (Newtons) Argon</i>	<i>Normal Force (Newtons) Nitrogen</i>
Mean	472.2225388	479.2243464
Variance	154417.2346	156757.4887
Observations	144	144
Pooled Variance	155587.3616	
Hypothesized Mean Difference	0	
df	286	
t Stat	-0.150622297	
P(T<=t) one-tail	0.440189924	
t Critical one-tail	1.650198896	
P(T<=t) two-tail	0.880379848	
t Critical two-tail	1.968293255	

The ANOVA of Psi ψ (as depicted in figure 34) was interesting due to the model being significant. The Model F-value of 58.76 implies the model is significant. There is

only a 0.01% chance that an F-value this large could occur due to noise. P-values less than 0.0500 indicate model terms are significant. In this case only hardness is a significant model term. This indicates that Psi is only dependent to the material. No outside influence from the atmosphere, depth of cut, or tool angle had an effect statistically.

Table 25. ANOVA of Psi ψ
ANOVA for selected factorial model

Response 7: Psi

	Source	Sum of Squares	df	Mean Square	F-value	p-value	
	Block	196.95	2	98.47			
	Model	1.049E+05	12	8738.35	58.76	< 0.0001	significant
	A-hardness	1.043E+05	7	14904.03	100.22	< 0.0001	
	B-atmosphere	26.37	2	13.18	0.0887	0.9152	
	C-depth of cut	198.48	1	198.48	1.33	0.2486	
	D-Tool angle	307.18	2	153.59	1.03	0.3569	
	Residual	62015.42	417	148.72			
	Cor Total	1.671E+05	431				

With this data the experiment moved to the tools themselves to determine the wear and if the atmosphere showed a difference in the amount of tool material removed during the cut. The following tables show the T tests of Psi when varying the atmosphere. There is no significant difference shown.

Table 26. Psi T Test Air vs. Argon

	<i>Psi (measured degrees) air</i>	<i>Psi (measured degrees) Argon</i>
Mean	26.41411882	28.17433242
Variance	241.1125618	1179.17592
Observations	144	144
Pooled Variance	710.1442407	
Hypothesized Mean Difference	0	
df	286	
t Stat	-0.5604777	
P(T<=t) one-tail	0.287796214	
t Critical one-tail	1.650198896	
P(T<=t) two-tail	0.575592429	
t Critical two-tail	1.968293255	

The T Test comparing Psi when using Air and Nitrogen is shown below. There is no significant difference.

Table 27. Psi T Test Air vs. Nitrogen

	<i>Psi (measured degrees) air</i>	<i>Psi (measured degrees) Nitrogen</i>
Mean	26.41411882	28.7545844
Variance	241.1125618	1554.420418
Observations	144	144
Pooled Variance	897.7664896	
Hypothesized Mean Difference	0	
df	286	
t Stat	-0.662806582	
P(T<=t) one-tail	0.253994122	
t Critical one-tail	1.650198896	
P(T<=t) two-tail	0.507988243	
t Critical two-tail	1.968293255	

The T Test comparing Psi when using Argon and Nitrogen is shown below. There is no significant difference.

Table 28. Psi T Test Argon vs. Nitrogen

	<i>Psi (measured degrees)Argon</i>	<i>Psi (measured degrees) Nitrogen</i>
Mean	28.17433242	28.7545844
Variance	1179.17592	1554.420418
Observations	144	144
Pooled Variance	1366.798169	
Hypothesized Mean Difference	0	
df	286	
t Stat	-0.133177447	
P(T<=t) one-tail	0.447073351	
t Critical one-tail	1.650198896	
P(T<=t) two-tail	0.894146703	
t Critical two-tail	1.968293255	

Additional ANOVA Tables

The following ANOVA tables are shown in no particular order but are included in the summary Table at the end. All α values are 0.05. The Following ANOVA is for Merchant's **F_s**. The ANOVA table shows the hardness, depth of cut, and Tool angle as significant. It does not show the atmosphere as significant.

Table 29: ANOVA of Merchant's F_s

Response 8: F_s Merchant

	Source	Sum of Squares	df	Mean Square	F-value	p-value	
	Block	2797.02	2	1398.51			
	Model	5.156E+07	12	4.297E+06	281.87	< 0.0001	significant
	A-hardness	4.308E+07	7	6.154E+06	403.69	< 0.0001	
	B-atmosphere	49160.34	2	24580.17	1.61	0.2006	
	C-depth of cut	7.752E+06	1	7.752E+06	508.50	< 0.0001	
	D-Tool angle	6.845E+05	2	3.422E+05	22.45	< 0.0001	
	Residual	6.357E+06	417	15244.48			
	Cor Total	5.792E+07	431				

The following ANOVA table shows Merchant's **F_n**. All of the factors of the ANOVA except for the atmosphere.

Table 30: ANOVA Merchant's Fn

Response 9: Fn Merchant

	Source	Sum of Squares	df	Mean Square	F-value	p-value	
	Block	4177.74	2	2088.87			
	Model	7.243E+07	12	6.036E+06	355.86	< 0.0001	significant
	A-hardness	6.506E+07	7	9.294E+06	547.95	< 0.0001	
	B-atmosphere	1.013E+05	2	50644.19	2.99	0.0516	
	C-depth of cut	6.876E+06	1	6.876E+06	405.40	< 0.0001	
	D-Tool angle	3.955E+05	2	1.978E+05	11.66	< 0.0001	
	Residual	7.073E+06	417	16962.09			
	Cor Total	7.951E+07	431				

The next ANOVA table represents Payton's Fs. This ANOVA table shows hardness, depth of cut, and tool angle as significant. It does not show atmosphere as significant.

Table 31: ANOVA of Payton Fs

Response 10: Fs Payton

	Source	Sum of Squares	df	Mean Square	F-value	p-value	
	Block	608.65	2	304.33			
	Model	7.234E+06	12	6.028E+05	301.19	< 0.0001	significant
	A-hardness	5.481E+06	7	7.829E+05	391.17	< 0.0001	
	B-atmosphere	2227.08	2	1113.54	0.5563	0.5737	
	C-depth of cut	1.646E+06	1	1.646E+06	822.49	< 0.0001	
	D-Tool angle	1.051E+05	2	52526.07	26.24	< 0.0001	
	Residual	8.347E+05	417	2001.56			
	Cor Total	8.069E+06	431				

The following ANOVA table shows Payton's Fn. All factors of the model including atmosphere are significant.

Table 32: ANOVA of Payton's Fn

Response 11: Fn Payton

	Source	Sum of Squares	df	Mean Square	F-value	p-value	
	Block	528.28	2	264.14			
	Model	1.150E+08	12	9.582E+06	396.96	< 0.0001	significant
	A-hardness	1.010E+08	7	1.443E+07	598.00	< 0.0001	
	B-atmosphere	1.534E+05	2	76718.66	3.18	0.0427	
	C-depth of cut	1.287E+07	1	1.287E+07	533.20	< 0.0001	
	D-Tool angle	9.162E+05	2	4.581E+05	18.98	< 0.0001	
	Residual	1.007E+07	417	24137.95			
	Cor Total	1.250E+08	431				

The next ANOVA table shows the Coefficient of Friction (μ). The hardness, depth of cut, and tool angle are all significant with a p-value less than 0.05.

Table 33: ANOVA of coefficient of friction (μ)

Response 12: μ (Mu)

	Source	Sum of Squares	df	Mean Square	F-value	p-value	
	Block	0.0029	2	0.0015			
	Model	9.58	12	0.7986	148.47	< 0.0001	significant
	A-hardness	5.39	7	0.7700	143.16	< 0.0001	
	B-atmosphere	0.0289	2	0.0144	2.68	0.0694	
	C-depth of cut	1.60	1	1.60	296.73	< 0.0001	
	D-Tool angle	2.57	2	1.28	238.74	< 0.0001	
	Residual	2.24	417	0.0054			
	Cor Total	11.83	431				

The next ANOVA table is the Resultant force **R**. The hardness, depth of cut, and tool angle are all significant. The atmosphere has a P-value of 0.07 which is greater than 0.05 does not show atmosphere as significant.

Table 34: ANOVA of Resultant

Response 13: Resultant

	Source	Sum of Squares	df	Mean Square	F-value	p-value	
	Block	29.91	2	14.96			
	Model	6.156E+06	12	5.130E+05	397.12	< 0.0001	significant
	A-hardness	5.364E+06	7	7.663E+05	593.25	< 0.0001	
	B-atmosphere	6907.62	2	3453.81	2.67	0.0702	
	C-depth of cut	7.330E+05	1	7.330E+05	567.49	< 0.0001	
	D-Tool angle	51517.71	2	25758.86	19.94	< 0.0001	
	Residual	5.386E+05	417	1291.72			
	Cor Total	6.694E+06	431				

The final ANOVA table is for Specific Horsepower. Hardness, atmosphere, depth of cut, and tool angle are all significant in this ANOVA.

Table 35: ANOVA for Specific Horsepower

Response 14: Specific Horsepower

	Source	Sum of Squares	df	Mean Square	F-value	p-value	
	Block	0.2122	2	0.1061			
	Model	8433.54	12	702.80	2102.05	< 0.0001	significant
	A-hardness	8312.22	7	1187.46	3551.68	< 0.0001	
	B-atmosphere	12.13	2	6.07	18.14	< 0.0001	
	C-depth of cut	46.98	1	46.98	140.51	< 0.0001	
	D-Tool angle	62.22	2	31.11	93.04	< 0.0001	
	Residual	139.42	417	0.3343			
	Cor Total	8573.17	431				

Results of the Tool Wear Study

To measure the tool-wear the same experimental set-up as the videographic study was used. During this experiment the tools were taken to the 3-D microscope for measurements to be taken after every ten inches of cutting. Only the 30 degree tool, 6061-T6 aluminum, and the 0.008 in depth of cut were utilized to simplify the runs. Using the microscope, the width, length, and depth of the wear was recorded. A total volume of tool material removed was then calculated for every 10 inches of cut. The results of the measurements can be seen in the table below.

Table 36. Volume of Tool Material Removed

	Contact Length from Edge (inches)	Width of Wear (inches)	Depth of Material Removed (inches)	Volume in Inches ³
air 10	0.012615354	0.13752	0.000298	5.16991E-07
air 20	0.012835827	0.137934	0.000303	5.36462E-07
air 30	0.012924409	0.138938	0.000408	7.32641E-07
air 40	0.013680315	0.137517	0.000531	9.98954E-07
air 50	0.013798425	0.145452	0.00081	1.62568E-06
nit 10	0.021661417	0.13827	0.000814	2.43803E-06
nit 20	0.021977953	0.141272	0.000996	3.09246E-06
nit 30	0.02294252	0.148392	0.001021	3.47598E-06
nit 40	0.020071654	0.139194	0.001082	3.02296E-06
nit 50	0.023466142	0.139606	0.001251	4.0983E-06
arg 10	0.015297638	0.137702	0.000566	1.19229E-06
arg 20	0.015803937	0.140008	0.000763	1.68827E-06
arg 30	0.020595669	0.138437	0.000881	2.51191E-06
arg 40	0.021185039	0.142868	0.000933	2.82387E-06
arg 50	0.030176772	0.140778	0.001	4.24822E-06

A students T-test was performed between each atmospheric test to determine if the amount of volume removed was the same or different with only he atmosphere changing.

The Argon and nitrogen atmospheres statistically showed the same volume of tool material removed.

Table 37. Nitrogen v. Argon T-Test

t-Test: Two-Sample Assuming Equal Variances		
nit vs arg		
	<i>nitrogen</i>	<i>argon</i>
Mean	3.226E-06	2.49291E-06
Variance	3.758E-13	1.38252E-12
Observations	5	5
Pooled Variance	8.792E-13	
Hypothesized Mean Difference	0	
df	8	
t Stat	1.2354276	
P(T<=t) one-tail	0.1258595	
t Critical one-tail	1.859548	
P(T<=t) two-tail	0.251719	
t Critical two-tail	2.3060041	

Table 38. Air v. Nitrogen T-Test

t-Test: Two-Sample Assuming Equal Variances		
air vs nit		
	<i>air</i>	<i>nitrogen</i>
Mean	8.821E-07	3.22555E-06
Variance	2.104E-13	3.75841E-13
Observations	5	5
Pooled Variance	2.931E-13	
Hypothesized Mean Difference	0	
df	8	
t Stat	-6.84364	
P(T<=t) one-tail	6.592E-05	
t Critical one-tail	1.859548	
P(T<=t) two-tail	0.0001318	
t Critical two-tail	2.3060041	

Table 39. Air v. Argon T-Test

t-Test: Two-Sample Assuming Equal Variances		
air vs arg		
	<i>air</i>	<i>argon</i>
Mean	8.82145E-07	2.49291E-06
Variance	2.10417E-13	1.38252E-12
Observations	5	5
Pooled Variance	7.96468E-13	
Hypothesized Mean	0	
df	8	
t Stat	-2.853769689	
P(T<=t) one-tail	0.010677467	
t Critical one-tail	1.859548033	
P(T<=t) two-tail	0.021354933	
t Critical two-tail	2.306004133	

When each was tested against the air cutting fluid, the t-tests showed that the volume of material removed was statistically different between air vs argon, and air vs nitrogen. According to the results of the experiment, air as a cutting fluid removed less material from the tool than using argon, or nitrogen. This proves that at very low cutting speeds, air is a better cutting fluid than argon or nitrogen. This shows that there is a difference between using air as a cutting fluid and using Argon or nitrogen. Statistically, Argon and nitrogen can be used interchangeably as a gaseous cutting fluid while achieving the same result in this experiment.

Summarization

Table 40 summarizes and ranks the observed ANOVA results of this experiment.

Table 40: Ranked ANOVA effects for each Analysis

Analysis	Hardness	Atmosphere	Depth of Cut	Tool Angle
Cutting Force F_c	2	Not	1	3
Thrust Force F_t	1	4	2	3
Friction Force F	1	Not	Not	2
Normal Force N	1	Not	2	Not
Shear Force (Payton) F_s	2	Not	1	3
Shear Force (Merchant) F_s	2	Not	1	3
Normal Shear Plane (Payton) F_n	1	4	2	3
Normal Shear Plane (Merchant) F_n	1	Not	2	3
Onset of Shear ϕ	1	Not	Not	2
Direction of Shear ψ	1	4	2	3
Coefficient of Friction μ	3	Not	1	2
Resultant R	1	Not	2	3
Specific Horsepower HP_s	1	4	2	3

Air vs, Argon shows a significant difference. This correlates with the wear data that showed a significant difference in tool wear when using Air vs. Argon.

Table 41: HPs T Test Air vs. Argon

	<i>HPs Air</i>	<i>HPs Argon</i>
Mean	3.8305201	4.043369601
Variance	8.013300279	9.472483397
Observations	144	144
Pearson Correlation	0.992496568	
Hypothesized Mean Difference	0	
df	143	
t Stat	-5.833130622	
P(T<=t) one-tail	1.74094E-08	
t Critical one-tail	1.655579143	
P(T<=t) two-tail	3.48188E-08	
t Critical two-tail	1.976692198	

The same can be said for Air vs. Nitrogen. This also correlates with the wear data that showed a significant difference in the tool volume lost when using Air vs Nitrogen.

Table 42: HPs T Test Air vs. Nitrogen

	<i>HPs Air</i>	<i>HPs Nitrogen</i>
Mean	3.8305201	4.085633551
Variance	8.013300279	9.786499654
Observations	144	144
Pearson Correlation	0.993087041	
Hypothesized Mean Difference	0	
df	143	
t Stat	-6.664910396	
P(T<=t) one-tail	2.66655E-10	
t Critical one-tail	1.655579143	
P(T<=t) two-tail	5.3331E-10	
t Critical two-tail	1.976692198	

Argon vs. Nitrogen did not show a significant difference just as the wear data did not show a significant difference between Argon and Nitrogen.

Table 43: HPs T Test Argon vs. Nitrogen

	<i>HPs Argon</i>	<i>HPs Nitrogen</i>
Mean	4.043369601	4.085633551
Variance	9.472483397	9.786499654
Observations	144	144
Pearson Correlation	0.993789776	
Hypothesized Mean Difference	0	
df	143	
t Stat	-1.45114284	
P(T<=t) one-tail	0.074465135	
t Critical one-tail	1.655579143	
P(T<=t) two-tail	0.14893027	
t Critical two-tail	1.976692198	

The means of the data when using Argon or Nitrogen are higher than when not.

This is consistent with the increase in tool volume lost when using Argon or Nitrogen.

X. Future Work

This experiment was executed performing low speed feed rates using gases at room temperature. Previous work by Dr. Vishnu Chandrasekaran [69] using chilled gases showed a decrease in tool forces utilizing an oxygen deficient environment. Varying the cutting speed and chilling the various atmospheres could be beneficial to discovering a tipping point for when the benefits of an oxygen deficient environment could begin to be seen.

The wear observations experiment was relatively limited in scope. The relationship between the cutting atmosphere and tool wear needs to be more clearly understood. By varying the cutting speeds from 3.75 in/min to speeds of 200 ft/min a greater assessment of the cutting force and tool wear could be understood.

Investigation of the chip and tool face directly after a cut to determine if the presence of an oxide exists could be beneficial as well. This would determine if the oxide forms during the chip formation or only after the chip is formed. Utilizing oxygen deficient atmospheres vs ample oxygen atmospheres would be ideal, however, analyzing them for the oxide layer would be difficult because you would have to control the atmosphere during chip formation and all the way through to the chip and tool analysis.

XI. References

- [1] Taylor, F. W., "On The Art of Cutting Metals," *Transactions of the ASME*, vol. 28, pp. 70-350, 1907.
- [2] Achutan J. N. C., "<https://www.cdc.gov/niosh/hhe/>," March 2007. [Online]. Available: <https://www.cdc.gov/niosh/hhe/reports/pdfs/2003-0175-3033.pdf>. [Accessed June 2018].
- [3] Colcquihat, M., *Experience sur la Resistance Utile Produites dan le Forage*, vol. 10, Annales des Travaus Publics en Belgique, 1851.
- [4] Joessel H., *Experiments on the Most Favorable Form of Tools in Workshops from the Point of View of Economy of Power*, Annuaire de la Societe des Anciens eleves des Ecoles Imperiales D'Arts et Meteiers, 1865.
- [5] Time, I., *Memoire sur le Rabotage de Metaux*, St. Petersburg, Russia, 1877.
- [6] Tresca, H., "On Further Applications of the Flow of Solids," in *Proceedings of the institution of Mechanical Engineers*, London, 1878.
- [7] Mallock , A., *The Action of Cutting Tools*, vol. 33, London, 1881, p. 127.
- [8] Haussner, A., *Das Holben von Metallen*, Mitteilungne des Technicshc Gewerbe Museums, 1892, p. 117.
- [9] Zvorkin, K., *Rabota I Usilie Neobkhodimyya dlya Oteleniya Metallicheskih Struzhek*, Moscow, Russia, 1893.
- [10] Weibach, H., *Ingeniuer und Maschinenmechanik*, Berlin, 1896.
- [11] Linder. G., *Book Review of Taylor's "On the Art of Cutting Metals"*, vol. 51, 1907, p. 1070.
- [12] Ernst H. and Merchant, E., "Chip Formation, Friction, and High Quality Machined Surfaces," *ASM Symposium*, p. 299, 1941.
- [13] Piispanen ,V., "Lastuntnuodostumiesn Teoriaa," *Teknillinen Aikakauslehti*, vol. 27, p. 315, 1937.
- [14] Merchant, M. E., "Mechanics of the Metal Cutting Proces I. Orthogonal Cutting and a Type 2 Chip," *Journal of Applied Physics*, vol. 16, pp. 318-324, 1945.

- [15] E. Coker and K. Chakko, "Experiments on the Actions of Cutting Tools," in *Proceedings of the Institution of Mechanical Engineers*, London, 1922.
- [16] E. Coker, "Report on the Action of Cutting Tools," in *Proceedings of the institution of Mechanical Engineers*, London, 1925.
- [17] Ishi S., "Macroscopic Kinematographs Applied to Research in Metal Cutting," in *World Engineering Congress*, Tokyo, 1929.
- [18] Schwerd, F., *Filmaufnahmen des Ablaufenden Spans bei Ueblichen und bei Sher Hohen Schnittgeschwindigkeiten*, vol. 80, 1935, p. 233.
- [19] Boston O., "What Happens When Metal is Cut," *Transactions ASME*, vol. 52, p. 119, 1930.
- [20] Herbert, E. G., "Work HARDening Properties of Metals," *Transactions ASME*, vol. 48, p. 705, 1926.
- [21] DeGarmo, E. Paul., Black J. T. and Kohser R. A., *Materials and Processes in Manufacturing*, 7th ed., New York: Macmillan Publishing Company, 1988.
- [22] Shaw, M. C., *Metal Cutting Principles*, Oxford: Clarendon Press, 1984.
- [23] Trent, E. M., *Metal Cutting*, Second ed., London: Butterworth's & Co. Ltd., 1984.
- [24] Trent, E. M. and Wright, P. K., *Metal Cutting*, fourth ed., London: Butterworth's & Heinemann, 1984.
- [25] Ernst, H., "Machining of Metals," in *ASM Symposium*, 1938.
- [26] Merchant, M. E., "Basic Mechanics of the Metal Cutting Process," *Journal of Applied Physics*, vol. 16, pp. 318-324, 1944.
- [27] Merchant, M. E., "Mechanics of the Metal Cutting Process-II. Plasticity Conditions in Orthogonal Cutting," *Journal of Applied Physics*, vol. 16, pp. 318-324, 1945.
- [28] Eggleston, D. M., Herzog, R. and Thomsen, E. G., "Observations on the Angle Relationships in Metal Cutting," *Journal of Engineering for Industry*, pp. 263-279, 1959.
- [29] Lee, E. H. and Shaffer, B. W., "The Theory of Plasticity Applied to a Problem of Machining," *Journal of Applied Mechanics*, vol. 18, no. 4, pp. 405-413, 1951.
- [30] Okushima, K. and Hitomi, K., "An Analysis of the Mechanism of Orthogonal Cutting and Its Application to Discontinuous Chip Formation," *ASME Journal of Engineering for Industry*, pp. 545-556, 1961.
- [31] Zorev, N. N., *Metal Cutting Mechanics*, New York: Peragon Press, 1966.

- [32] Oxley, P., *Mechanics of Machining: An Analytical Approach to Assessing Machinability*, New York: John Wiley & Sons, 1989.
- [33] Luttermelt, C. V., "The Split Shearzone Mechanism of Chip Segmentation," *Annals of the CIRP*, vol. 25, no. 1, pp. 33-38.
- [34] Huang, J., "Theoretical and Numerical Studies of Machining," Auburn University, 1996.
- [35] Briggs, N. D., "Observation of the Orthogonal Machining Process Using High Speed Videography," Auburn University, 1993.
- [36] Black, J., "Flow Stress Model in Metal Cutting," *ASME Journal of Engineering for Industry*, vol. 101, pp. 403-415, 1979.
- [37] Black, J. T. and Briggs, N. D., "High Speed Videographs of the Orthogonal Machining of Aluminium," in *ASME Tribology Symposium*, 1994.
- [38] Dieter, G. E., *Mechanical Metallurgy*, New York: McGraw-Hill Publishing Company, 1998.
- [39] Wright, P., "Predicting the Shear Plane Angle in Machining from Work Material Strain Hardening Characteristics," *Journal of Engineering for Industry*, vol. 104, pp. 285-292, 1982.
- [40] Turkovich, B. F. V., "Dislocation Theory of Shear Stress and Strain Rate in Metal Cutting," in *Proceedings of 8th International M.T.D.R. Conference*, 1967.
- [41] Ramalingham, S. and Black J. T., "On the Metal Physical Considerations in the Machining of Metal," *Journal of Engineering for Industry*, 1971.
- [42] Cottrell, A. H., *Theory of Crystal Dislocations*, London: Gordon and Breach, 1964.
- [43] Black J. T. and Krishnamurthy R., "Effect of Hardness of Flow Stress of Aluminium," Auburn University, unpublished.
- [44] Black J. T., "On the Fundamental Mechanism of Large Strain Plastic Deformation - Electron Microscopy of Metal Cutting Chips," *ASME Journal of Engineering for Industry*, vol. 93, pp. 507-526, 1971.
- [45] Ueda k. and Iwata K., "Chip Formation Mechanism in Single Crystal Cutting of L3 Brass," *Annals of the CLRP*, vol. 29, no. 1, pp. 41-46, 1980.
- [46] Cook N. H. and Shaw M. C., "Visual Metal Cutting Study," *Mechanical Engineering*, pp. 9212-923, 1951.
- [47] Agrawal S. N. and Armstead B. H., "Study Reveals Mechanics of Chip Formation," *Machinery*, pp. 114-119, 1961.

- [48] Oxley, P. L. B., "Shear Strain Solutions in Orthogonal Machining," *International Journal of Machine Tool Design and Research*, vol. 1, pp. 89-97, 1961.
- [49] Komanduri, R. and Brown. R. H., "On the Mechanics of Chip Segmentation in Machining," *Journal of Engineering for Industry*, vol. 103, pp. 33-51, 1981.
- [50] Black, J. T. and James. C. R., "The Hammer QSD - Quick Stop Device for High Speed Machining and Rubbing," *Journal of Engineering for Industry*, vol. 103, pp. 13-21, 1981.
- [51] The. J., "High-Speed Films of the Incipient Cutting Process in Machining at Conventional Speeds," *Journal of Engineering for Industry*, pp. 263-268, 1977.
- [52] Warnecke, G., "A New Method of Visualizing the Cutting Process," in *5th North American Metalworking Research Conference NAMRC*, 1977.
- [53] Von Turkovich, B. F. and Black, J. T., "Micro-Machining of Copper and Aluminium Crystals," *Journal of Engineering for Industry*, pp. 130-134, 1970.
- [54] Cohen, P. H. and Black, J. T., "Strain, Strain Rate, and Shear Velocity Measurement in Metal Cutting," *ASME*, pp. 271-278, 1978.
- [55] Trent, E. M., "Proc. Proceedings Conference Machinability," *Iron and Steel Institute*, pp. 11-18, 1970.
- [56] Williams, J. E., Smart, E. F. and Milner, D. R., "The metallurgy of machining Part 3: The effect of a lubricant and an Assessment of the current understanding of materials behaviour in machining," *Metallurgia*, vol. 81, pp. 89-93, 1970.
- [57] Niebusch, R. B. and Strieder, E. H., "Application of Cutting fluids to Machining Operations," in *Annual Meeting of ASME*, New York, 1950.
- [58] Rowe, G. W. and Smart, E. F., "The importance of oxygen in dry machining of metal on lathe," *British Journal of Applied Physics*, vol. 14, pp. 924-926, 1963.
- [59] Kim, S. W., Kang, M. C., Kim, J. S. and D.W.L., "Evaluation of machinability by cutting environments in high-speed milling of difficult-to-cut materials," *Journal of Materials Processing Technology*, vol. 111, pp. 256-260, 2001.
- [60] Hong, S. Y., Ding Y. and Jeong, W.C., "Friction and cutting forces in cryogenic machining of Ti-6Al-4V," *International Journal of Machine Tools & Manufacture*, vol. 41, pp. 2271-2258, 2001.
- [61] Dahlman, P. and Escursell, M., "High pressure jet-assisted cooling: a new possibility for near net shape turning of decarburized steel," *International Journal of Machine Tools & Manufacture*, 2003.

- [62] Cakir, O., Kiyak, M. and Altan, E., "Comparison of Gases applications to wet and dry cuttings in turning," *Journal of Materials Processing Technology*, Vols. 153-154, pp. 35--41, 2004.
- [63] Stanford, L. and Lister, P. M., "Investigation into the relationship between tool-wear and cutting environments when turning EN32 steel," *Industrial Lubrication and Tribology*, vol. 56, no. 2, pp. 114-121, 2004.
- [64] Dhar, N. R., Kamruzzaman, M. and Ahmed, M., "Effect of minimum quantity lubrication (MQL) on tool wear and surface roughness in turning AISI-4340 steel," *Journal of Materials Processing Technology*, vol. 172, no. 2, pp. 229-304, 2006.
- [65] Su, Y., He, N., Li, L. and X. L. Li, "An experimental investigation of effects of cooling/lubrication conditions on tool wear in high-speed end milling of Ti-6Al-4V," *Wear*, vol. 261, no. 7-8, pp. 760-766, 2006.
- [66] He, Y. Su, He, N., Li, L., Iqbal, A., Xiao, M. H., Xu, S. and Qiu, B. G., "Refrigerated cooling air cutting of difficult-to-cut materials," *International Journal of Machine Tools and Manufacture*, vol. 47, no. 6, pp. 927-933, 2007.
- [67] Sreejith, P. S., "Machining of 6061 aluminium alloy with MQL, dry and flooded lubricant conditions," *Materials Letters*, vol. 62, no. 2, pp. 276-278, 2008.
- [68] Payton, L. N. and Sripathi, P., "Effects of Alternative Metal Working Fluids Upon Tool Face Wear," *ASME Conference Proceedings*, pp. 433-445, 2010.
- [69] Chandrasekaran, Vishnu V., "A Study on Forces, Tool Wear and Surface finish in Orthogonal Machining of Aluminum 6061 T6 alloy and AISI 1020 Steel with HSS and Uncoated Carbide tool inserts under different gaseous cutting environments," Auburn, 2013.
- [70] Huang, J. M. and Black, J. T., "An Evaluation of Chip Separation Criteria for the FEM Simulation of Machining," *Journal of Engineering for Industry*, 1996.
- [71] Payton, L. N., "Orthogonal Machining of Copper using a Virtual Quickstop Device," Auburn University, Auburn, 2000.
- [72] Kim, S. W., W. L. D., Kang, M. C., and Kim, J. S., "Evaluation of machinability by cutting environments in high-speed milling of difficult-to-cut materials," *Journal of Materials Processing Technology*, vol. 111, pp. 256-260, 2001.

Appendix A
Common Formula in Orthogonal Plate Machining Models

$$r_c \equiv \frac{t_o}{t_c} = \frac{t_1}{t_2} = \frac{V_c}{V}$$

$$\phi = \arctan\left(\frac{r_c \times \cos \alpha}{1 - r_c \sin \alpha}\right)$$

$$F = F_c \times \sin \alpha + F_t \cos \alpha$$

$$N = F_c \times \cos \alpha - F_t \times \sin \alpha$$

$$\mu = \frac{F}{N}$$

$$R = \sqrt{F_c^2 + F_t^2}$$

$$\beta = \arctan\left[\frac{F}{N}\right]$$

$$F_s = F_c \times \cos \phi - F_t \times \sin \phi$$

$$F_n = F_c \times \sin \phi - F_t \times \cos \phi$$

$$A_s = \frac{t_o \times w}{\sin \phi} = \frac{t_1 \times w}{\sin \phi}$$

$$\tau_s = \frac{F_s}{A_s}$$

$$HP = \frac{F_c \times V / 12}{33,000}$$

$$MRR = V \times w \times t_o = V \times w \times t_1$$

$$HP_s = \frac{HP}{MRR}$$

$$V_c = \frac{V \times \sin \phi}{\cos(\phi - \alpha)}$$

$$V_s = \frac{V \times \cos \alpha}{\cos(\phi - \beta)}$$

$$U = U_s + U_f = \frac{F_c}{w \times V}$$

$$U_f = \frac{F \times V_c}{w \times V}$$

$$U_s = \frac{F_s \times V_s}{f_r \times t_o \times V}$$

Black and Huang Model Predicts:

$$\varepsilon = \gamma = \frac{2 \times \cos \alpha}{1 + \sin \alpha}$$

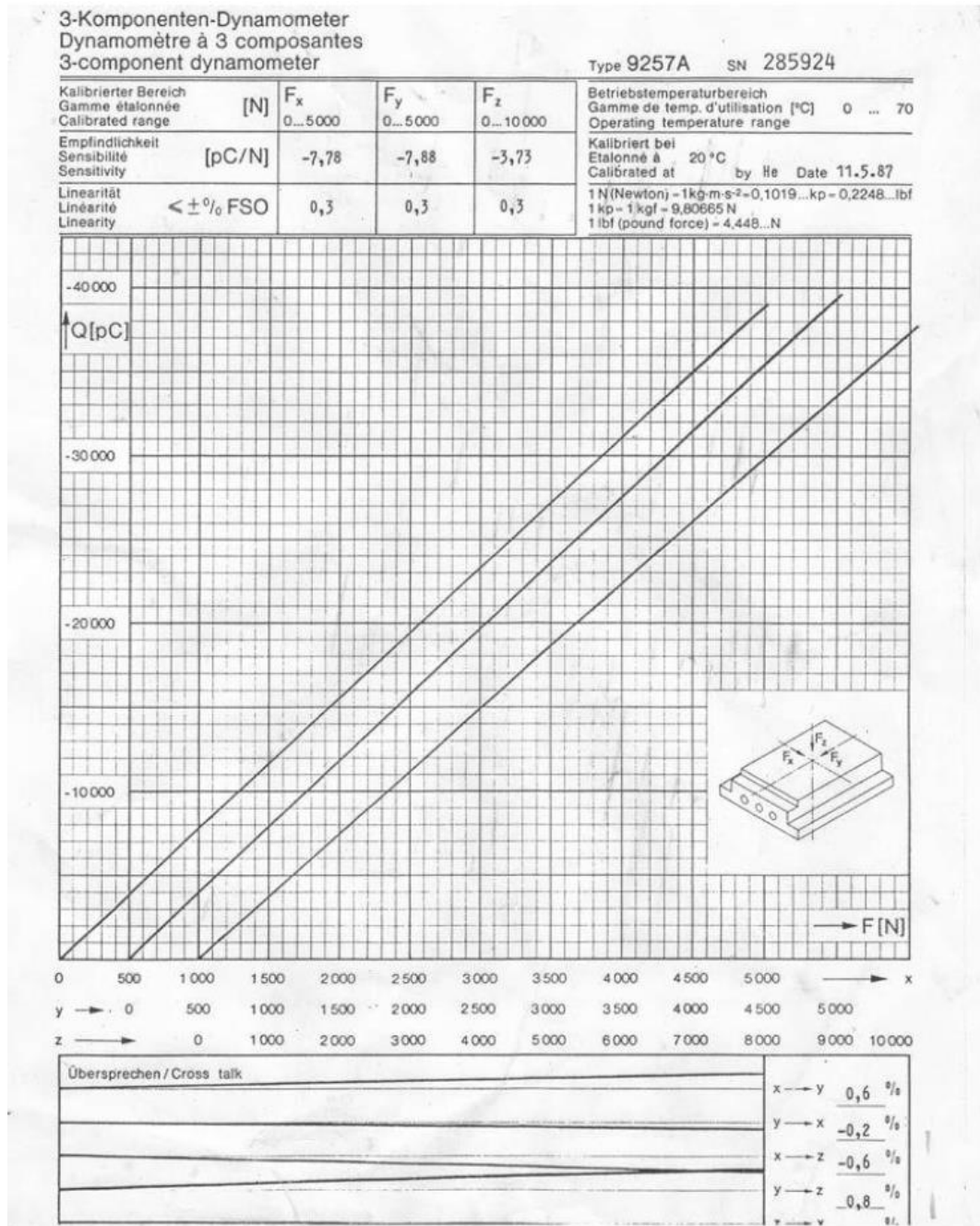
$$\Psi = 45 - \phi + \frac{\alpha}{2}$$

Merchant Model Predicts:

$$\varepsilon = \gamma = \frac{\cos \alpha}{\sin \phi \times \cos(\phi - \alpha)}$$

$$\phi = 45 + \frac{\alpha}{2} - \frac{\beta}{2}$$

Appendix B Relevant Calibration Certificates



Appendix C
Measured Data

run	Medium	Alloy	Material Condition (Hardness)	Depth of Cut	Tool Angle	Replicate	cutting force (lbs force)	thrust force (lbs force)
1	Air	4130	22	0.004	25	1	195.00	52.63
2	Air	4130	22	0.004	30	1	181.21	48.37
3	Air	4130	22	0.004	35	1	138.41	32.50
4	Air	4130	22	0.008	25	1	337.07	82.89
5	Air	4130	22	0.008	30	1	336.03	85.27
6	Air	4130	22	0.008	35	1	271.87	63.49
7	Argon	4130	22	0.004	25	1	198.36	63.49
8	Argon	4130	22	0.004	30	1	200.57	61.30
9	Argon	4130	22	0.004	35	1	167.53	43.76
10	Argon	4130	22	0.008	25	1	366.44	106.65
11	Argon	4130	22	0.008	30	1	379.61	107.21
12	Argon	4130	22	0.008	35	1	301.93	77.19
13	Nitrogen	4130	22	0.004	25	1	196.14	60.39
14	Nitrogen	4130	22	0.004	30	1	210.14	64.83
15	Nitrogen	4130	22	0.004	35	1	176.35	46.37
16	Nitrogen	4130	22	0.008	25	1	367.31	115.67
17	Nitrogen	4130	22	0.008	30	1	350.73	96.73
18	Nitrogen	4130	22	0.008	35	1	326.80	85.12
19	Air	4130	32	0.004	25	1	211.22	72.21
20	Air	4130	32	0.004	30	1	183.87	51.52
21	Air	4130	32	0.004	35	1	171.87	38.93
22	Air	4130	32	0.008	25	1	376.30	102.74
23	Air	4130	32	0.008	30	1	362.36	82.98
24	Air	4130	32	0.008	35	1	331.38	66.77
25	Argon	4130	32	0.004	25	1	213.22	78.61
26	Argon	4130	32	0.004	30	1	220.37	73.30
27	Argon	4130	32	0.004	35	1	190.62	54.60
28	Argon	4130	32	0.008	25	1	383.31	105.60
29	Argon	4130	32	0.008	30	1	384.12	106.27
30	Argon	4130	32	0.008	35	1	335.24	75.05
31	Nitrogen	4130	32	0.004	25	1	233.78	88.08

run	Medium	Alloy	Material Condition (Hardness)	Depth of Cut	Tool Angle	Replicate	cutting force (lbs force)	thrust force (lbs force)
32	Nitrogen	4130	32	0.004	30	1	219.41	74.84
33	Nitrogen	4130	32	0.004	35	1	194.12	54.02
34	Nitrogen	4130	32	0.008	25	1	394.73	110.99
35	Nitrogen	4130	32	0.008	30	1	402.61	113.71
36	Nitrogen	4130	32	0.008	35	1	329.95	74.54
37	Air	4130	42	0.004	25	1	210.94	67.81
38	Air	4130	42	0.004	30	1	192.35	50.17
39	Air	4130	42	0.004	35	1	173.84	36.86
40	Air	4130	42	0.008	25	1	409.79	128.19
41	Air	4130	42	0.008	30	1	381.90	91.15
42	Air	4130	42	0.008	35	1	340.72	82.74
43	Argon	4130	42	0.004	25	1	227.11	91.68
44	Argon	4130	42	0.004	30	1	187.64	56.77
45	Argon	4130	42	0.004	35	1	188.30	58.08
46	Argon	4130	42	0.008	25	1	391.97	128.95
47	Argon	4130	42	0.008	30	1	380.28	102.14
48	Argon	4130	42	0.008	35	1	343.02	80.64
49	Nitrogen	4130	42	0.004	25	1	227.01	91.31
50	Nitrogen	4130	42	0.004	30	1	206.40	69.09
51	Nitrogen	4130	42	0.004	35	1	195.40	56.08
52	Nitrogen	4130	42	0.008	25	1	416.85	143.33
53	Nitrogen	4130	42	0.008	30	1	362.55	97.56
54	Nitrogen	4130	42	0.008	35	1	361.79	98.99
55	Air	Mag	HO	0.004	25	1	25.05	4.83
56	Air	Mag	HO	0.004	30	1	24.45	9.16
57	Air	Mag	HO	0.004	35	1	27.12	1.48
58	Air	Mag	HO	0.008	25	1	39.28	2.01
59	Air	Mag	HO	0.008	30	1	39.86	0.65
60	Air	Mag	HO	0.008	35	1	39.13	-0.39
61	Argon	Mag	HO	0.004	25	1	23.52	4.30
62	Argon	Mag	HO	0.004	30	1	23.56	4.18
63	Argon	Mag	HO	0.004	35	1	26.24	1.38
64	Argon	Mag	HO	0.008	25	1	38.04	1.15
65	Argon	Mag	HO	0.008	30	1	36.68	0.51
66	Argon	Mag	HO	0.008	35	1	37.63	-0.03
67	Nitrogen	Mag	HO	0.004	25	1	24.11	3.97
68	Nitrogen	Mag	HO	0.004	30	1	23.38	3.81

run	Medium	Alloy	Material Condition (Hardness)	Depth of Cut	Tool Angle	Replicate	cutting force (lbs force)	thrust force (lbs force)
69	Nitrogen	Mag	HO	0.004	35	1	25.69	2.33
70	Nitrogen	Mag	HO	0.008	25	1	37.57	1.78
71	Nitrogen	Mag	HO	0.008	30	1	38.32	0.73
72	Nitrogen	Mag	HO	0.008	35	1	37.62	0.35
73	Air	Mag	H24	0.004	25	1	24.80	6.87
74	Air	Mag	H24	0.004	30	1	23.20	8.08
75	Air	Mag	H24	0.004	35	1	23.55	7.86
76	Air	Mag	H24	0.008	25	1	41.72	4.82
77	Air	Mag	H24	0.008	30	1	42.74	5.47
78	Air	Mag	H24	0.008	35	1	42.77	4.55
79	Argon	Mag	H24	0.004	25	1	22.29	6.78
80	Argon	Mag	H24	0.004	30	1	23.84	7.89
81	Argon	Mag	H24	0.004	35	1	24.61	7.17
82	Argon	Mag	H24	0.008	25	1	39.34	3.92
83	Argon	Mag	H24	0.008	30	1	40.13	6.38
84	Argon	Mag	H24	0.008	35	1	39.50	4.66
85	Nitrogen	Mag	H24	0.004	25	1	24.00	6.37
86	Nitrogen	Mag	H24	0.004	30	1	24.15	7.90
87	Nitrogen	Mag	H24	0.004	35	1	24.77	7.55
88	Nitrogen	Mag	H24	0.008	25	1	39.34	4.27
89	Nitrogen	Mag	H24	0.008	30	1	41.64	6.70
90	Nitrogen	Mag	H24	0.008	35	1	40.09	5.15
91	Air	6061	T0	0.004	25	1	66.45	20.23
92	Air	6061	T0	0.004	30	1	61.53	15.82
93	Air	6061	T0	0.004	35	1	51.55	11.60
94	Air	6061	T0	0.008	25	1	111.02	31.75
95	Air	6061	T0	0.008	30	1	89.95	14.27
96	Air	6061	T0	0.008	35	1	89.31	16.23
97	Argon	6061	T0	0.004	25	1	71.17	22.97
98	Argon	6061	T0	0.004	30	1	63.45	17.53
99	Argon	6061	T0	0.004	35	1	53.65	11.56
100	Argon	6061	T0	0.008	25	1	119.24	36.06
101	Argon	6061	T0	0.008	30	1	99.75	22.96
102	Argon	6061	T0	0.008	35	1	94.76	17.50
103	Nitrogen	6061	T0	0.004	25	1	69.82	22.01
104	Nitrogen	6061	T0	0.004	30	1	65.26	18.31
105	Nitrogen	6061	T0	0.004	35	1	52.05	11.87

run	Medium	Alloy	Material Condition (Hardness)	Depth of Cut	Tool Angle	Replicate	cutting force (lbs force)	thrust force (lbs force)
106	Nitrogen	6061	T0	0.008	25	1	116.57	33.56
107	Nitrogen	6061	T0	0.008	30	1	107.31	24.94
108	Nitrogen	6061	T0	0.008	35	1	94.65	16.79
109	Air	6061	T4	0.004	25	1	53.97	14.75
110	Air	6061	T4	0.004	30	1	52.99	13.13
111	Air	6061	T4	0.004	35	1	43.52	7.02
112	Air	6061	T4	0.008	25	1	86.34	21.66
113	Air	6061	T4	0.008	30	1	83.54	15.84
114	Air	6061	T4	0.008	35	1	76.02	10.61
115	Argon	6061	T4	0.004	25	1	52.28	15.22
116	Argon	6061	T4	0.004	30	1	47.25	12.40
117	Argon	6061	T4	0.004	35	1	43.13	8.82
118	Argon	6061	T4	0.008	25	1	98.67	21.42
119	Argon	6061	T4	0.008	30	1	88.90	15.64
120	Argon	6061	T4	0.008	35	1	82.12	11.50
121	Nitrogen	6061	T4	0.004	25	1	54.75	17.07
122	Nitrogen	6061	T4	0.004	30	1	49.82	12.80
123	Nitrogen	6061	T4	0.004	35	1	43.76	8.32
124	Nitrogen	6061	T4	0.008	25	1	97.52	24.46
125	Nitrogen	6061	T4	0.008	30	1	86.70	15.28
126	Nitrogen	6061	T4	0.008	35	1	82.38	11.14
127	Air	6061	T6	0.004	25	1	73.36	16.73
128	Air	6061	T6	0.004	30	1	65.71	10.43
129	Air	6061	T6	0.004	35	1	62.48	6.49
130	Air	6061	T6	0.008	25	1	122.47	25.52
131	Air	6061	T6	0.008	30	1	111.98	15.62
132	Air	6061	T6	0.008	35	1	103.91	7.31
133	Argon	6061	T6	0.004	25	1	75.33	17.69
134	Argon	6061	T6	0.004	30	1	68.98	12.85
135	Argon	6061	T6	0.004	35	1	65.16	6.83
136	Argon	6061	T6	0.008	25	1	139.32	24.84
137	Argon	6061	T6	0.008	30	1	122.73	14.21
138	Argon	6061	T6	0.008	35	1	110.47	8.84
139	Nitrogen	6061	T6	0.004	25	1	72.29	15.43
140	Nitrogen	6061	T6	0.004	30	1	69.49	12.93
141	Nitrogen	6061	T6	0.004	35	1	62.32	6.72
142	Nitrogen	6061	T6	0.008	25	1	126.16	25.16

run	Medium	Alloy	Material Condition (Hardness)	Depth of Cut	Tool Angle	Replicate	cutting force (lbs force)	thrust force (lbs force)
143	Nitrogen	6061	T6	0.008	30	1	126.92	18.42
144	Nitrogen	6061	T6	0.008	35	1	110.20	8.12
145	Air	4130	22	0.004	25	2	188.78	54.15
146	Air	4130	22	0.004	30	2	188.58	49.39
147	Air	4130	22	0.004	35	2	156.58	35.24
148	Air	4130	22	0.008	25	2	344.78	94.15
149	Air	4130	22	0.008	30	2	323.56	82.36
150	Air	4130	22	0.008	35	2	295.63	68.77
151	Argon	4130	22	0.004	25	2	214.00	66.17
152	Argon	4130	22	0.004	30	2	199.64	63.41
153	Argon	4130	22	0.004	35	2	177.46	47.35
154	Argon	4130	22	0.008	25	2	362.26	105.17
155	Argon	4130	22	0.008	30	2	352.32	97.80
156	Argon	4130	22	0.008	35	2	318.88	79.03
157	Nitrogen	4130	22	0.004	25	2	197.01	62.63
158	Nitrogen	4130	22	0.004	30	2	209.08	65.44
159	Nitrogen	4130	22	0.004	35	2	165.91	45.95
160	Nitrogen	4130	22	0.008	25	2	382.55	114.44
161	Nitrogen	4130	22	0.008	30	2	368.30	102.62
162	Nitrogen	4130	22	0.008	35	2	313.01	69.06
163	Air	4130	32	0.004	25	2	212.73	73.37
164	Air	4130	32	0.004	30	2	193.33	51.70
165	Air	4130	32	0.004	35	2	167.96	38.06
166	Air	4130	32	0.008	25	2	406.96	127.45
167	Air	4130	32	0.008	30	2	351.74	88.74
168	Air	4130	32	0.008	35	2	312.75	63.68
169	Argon	4130	32	0.004	25	2	216.34	77.21
170	Argon	4130	32	0.004	30	2	233.62	76.53
171	Argon	4130	32	0.004	35	2	194.41	53.63
172	Argon	4130	32	0.008	25	2	378.92	104.89
173	Argon	4130	32	0.008	30	2	365.04	94.84
174	Argon	4130	32	0.008	35	2	336.42	77.16
175	Nitrogen	4130	32	0.004	25	2	277.99	106.53
176	Nitrogen	4130	32	0.004	30	2	233.95	75.01
177	Nitrogen	4130	32	0.004	35	2	189.46	53.32
178	Nitrogen	4130	32	0.008	25	2	382.38	111.00
179	Nitrogen	4130	32	0.008	30	2	395.03	104.85

run	Medium	Alloy	Material Condition (Hardness)	Depth of Cut	Tool Angle	Replicate	cutting force (lbs force)	thrust force (lbs force)
180	Nitrogen	4130	32	0.008	35	2	340.07	72.03
181	Air	4130	42	0.004	25	2	209.74	67.24
182	Air	4130	42	0.004	30	2	174.43	47.58
183	Air	4130	42	0.004	35	2	161.76	35.02
184	Air	4130	42	0.008	25	2	392.45	126.55
185	Air	4130	42	0.008	30	2	357.09	87.91
186	Air	4130	42	0.008	35	2	352.22	69.25
187	Argon	4130	42	0.004	25	2	244.10	101.10
188	Argon	4130	42	0.004	30	2	201.32	60.71
189	Argon	4130	42	0.004	35	2	207.80	66.83
190	Argon	4130	42	0.008	25	2	415.51	140.58
191	Argon	4130	42	0.008	30	2	353.01	99.57
192	Argon	4130	42	0.008	35	2	354.29	85.36
193	Nitrogen	4130	42	0.004	25	2	218.91	84.97
194	Nitrogen	4130	42	0.004	30	2	196.14	66.03
195	Nitrogen	4130	42	0.004	35	2	180.26	56.07
196	Nitrogen	4130	42	0.008	25	2	400.61	145.29
197	Nitrogen	4130	42	0.008	30	2	365.96	99.55
198	Nitrogen	4130	42	0.008	35	2	373.21	102.14
199	Air	Mag	HO	0.004	25	2	25.56	5.05
200	Air	Mag	HO	0.004	30	2	25.05	9.59
201	Air	Mag	HO	0.004	35	2	24.34	2.66
202	Air	Mag	HO	0.008	25	2	39.52	2.49
203	Air	Mag	HO	0.008	30	2	38.54	1.54
204	Air	Mag	HO	0.008	35	2	38.50	0.50
205	Argon	Mag	HO	0.004	25	2	23.93	3.92
206	Argon	Mag	HO	0.004	30	2	25.14	3.65
207	Argon	Mag	HO	0.004	35	2	25.24	2.12
208	Argon	Mag	HO	0.008	25	2	39.42	1.03
209	Argon	Mag	HO	0.008	30	2	38.67	0.06
210	Argon	Mag	HO	0.008	35	2	38.76	-0.07
211	Nitrogen	Mag	HO	0.004	25	2	23.71	3.97
212	Nitrogen	Mag	HO	0.004	30	2	24.88	3.81
213	Nitrogen	Mag	HO	0.004	35	2	25.35	2.27
214	Nitrogen	Mag	HO	0.008	25	2	39.27	1.01
215	Nitrogen	Mag	HO	0.008	30	2	38.26	0.40
216	Nitrogen	Mag	HO	0.008	35	2	38.29	0.01

run	Medium	Alloy	Material Condition (Hardness)	Depth of Cut	Tool Angle	Replicate	cutting force (lbs force)	thrust force (lbs force)
217	Air	Mag	H24	0.004	25	2	23.95	7.57
218	Air	Mag	H24	0.004	30	2	25.37	8.04
219	Air	Mag	H24	0.004	35	2	24.21	7.92
220	Air	Mag	H24	0.008	25	2	43.75	4.74
221	Air	Mag	H24	0.008	30	2	41.29	6.86
222	Air	Mag	H24	0.008	35	2	40.26	5.48
223	Argon	Mag	H24	0.004	25	2	25.03	6.28
224	Argon	Mag	H24	0.004	30	2	23.56	7.90
225	Argon	Mag	H24	0.004	35	2	23.63	7.18
226	Argon	Mag	H24	0.008	25	2	41.22	3.84
227	Argon	Mag	H24	0.008	30	2	39.21	6.81
228	Argon	Mag	H24	0.008	35	2	39.68	4.78
229	Nitrogen	Mag	H24	0.004	25	2	22.49	6.63
230	Nitrogen	Mag	H24	0.004	30	2	22.91	8.20
231	Nitrogen	Mag	H24	0.004	35	2	24.06	7.24
232	Nitrogen	Mag	H24	0.008	25	2	39.04	4.13
233	Nitrogen	Mag	H24	0.008	30	2	40.82	6.70
234	Nitrogen	Mag	H24	0.008	35	2	41.08	4.43
235	Air	6061	T0	0.004	25	2	72.34	23.80
236	Air	6061	T0	0.004	30	2	64.51	17.78
237	Air	6061	T0	0.004	35	2	52.13	10.61
238	Air	6061	T0	0.008	25	2	120.33	34.53
239	Air	6061	T0	0.008	30	2	97.82	22.36
240	Air	6061	T0	0.008	35	2	94.52	15.73
241	Argon	6061	T0	0.004	25	2	73.04	23.41
242	Argon	6061	T0	0.004	30	2	67.69	18.57
243	Argon	6061	T0	0.004	35	2	52.93	11.39
244	Argon	6061	T0	0.008	25	2	121.70	36.69
245	Argon	6061	T0	0.008	30	2	109.01	25.80
246	Argon	6061	T0	0.008	35	2	86.95	11.15
247	Nitrogen	6061	T0	0.004	25	2	70.62	20.87
248	Nitrogen	6061	T0	0.004	30	2	69.07	19.12
249	Nitrogen	6061	T0	0.004	35	2	56.56	12.35
250	Nitrogen	6061	T0	0.008	25	2	118.76	32.67
251	Nitrogen	6061	T0	0.008	30	2	115.72	26.89
252	Nitrogen	6061	T0	0.008	35	2	94.61	16.55
253	Air	6061	T4	0.004	25	2	49.08	14.91

run	Medium	Alloy	Material Condition (Hardness)	Depth of Cut	Tool Angle	Replicate	cutting force (lbs force)	thrust force (lbs force)
254	Air	6061	T4	0.004	30	2	51.66	13.08
255	Air	6061	T4	0.004	35	2	44.09	6.69
256	Air	6061	T4	0.008	25	2	95.69	24.99
257	Air	6061	T4	0.008	30	2	86.88	16.46
258	Air	6061	T4	0.008	35	2	81.84	11.22
259	Argon	6061	T4	0.004	25	2	52.07	16.11
260	Argon	6061	T4	0.004	30	2	53.12	13.48
261	Argon	6061	T4	0.004	35	2	44.61	8.94
262	Argon	6061	T4	0.008	25	2	97.03	23.44
263	Argon	6061	T4	0.008	30	2	89.00	15.93
264	Argon	6061	T4	0.008	35	2	84.71	11.42
265	Nitrogen	6061	T4	0.004	25	2	50.26	15.81
266	Nitrogen	6061	T4	0.004	30	2	46.34	12.32
267	Nitrogen	6061	T4	0.004	35	2	43.43	8.84
268	Nitrogen	6061	T4	0.008	25	2	97.40	23.91
269	Nitrogen	6061	T4	0.008	30	2	89.70	15.39
270	Nitrogen	6061	T4	0.008	35	2	83.14	11.51
271	Air	6061	T6	0.004	25	2	67.69	15.58
272	Air	6061	T6	0.004	30	2	69.35	12.95
273	Air	6061	T6	0.004	35	2	60.27	7.06
274	Air	6061	T6	0.008	25	2	136.58	27.47
275	Air	6061	T6	0.008	30	2	118.09	11.32
276	Air	6061	T6	0.008	35	2	108.30	7.24
277	Argon	6061	T6	0.004	25	2	75.21	17.96
278	Argon	6061	T6	0.004	30	2	69.46	13.40
279	Argon	6061	T6	0.004	35	2	58.56	6.16
280	Argon	6061	T6	0.008	25	2	129.95	26.10
281	Argon	6061	T6	0.008	30	2	124.95	17.75
282	Argon	6061	T6	0.008	35	2	109.12	8.48
283	Nitrogen	6061	T6	0.004	25	2	74.68	17.13
284	Nitrogen	6061	T6	0.004	30	2	67.55	12.68
285	Nitrogen	6061	T6	0.004	35	2	57.43	6.35
286	Nitrogen	6061	T6	0.008	25	2	130.80	26.00
287	Nitrogen	6061	T6	0.008	30	2	126.82	18.82
288	Nitrogen	6061	T6	0.008	35	2	111.56	8.36
289	Air	4130	22	0.004	25	3	185.88	52.88
290	Air	4130	22	0.004	30	3	193.31	51.69

run	Medium	Alloy	Material Condition (Hardness)	Depth of Cut	Tool Angle	Replicate	cutting force (lbs force)	thrust force (lbs force)
291	Air	4130	22	0.004	35	3	153.71	35.01
292	Air	4130	22	0.008	25	3	344.31	98.30
293	Air	4130	22	0.008	30	3	333.45	84.96
294	Air	4130	22	0.008	35	3	294.08	69.75
295	Argon	4130	22	0.004	25	3	201.83	64.27
296	Argon	4130	22	0.004	30	3	205.48	63.65
297	Argon	4130	22	0.004	35	3	164.63	44.39
298	Argon	4130	22	0.008	25	3	369.61	109.25
299	Argon	4130	22	0.008	30	3	341.26	97.59
300	Argon	4130	22	0.008	35	3	299.30	81.36
301	Nitrogen	4130	22	0.004	25	3	200.51	63.96
302	Nitrogen	4130	22	0.004	30	3	196.78	60.44
303	Nitrogen	4130	22	0.004	35	3	182.36	46.87
304	Nitrogen	4130	22	0.008	25	3	350.15	94.93
305	Nitrogen	4130	22	0.008	30	3	356.13	100.14
306	Nitrogen	4130	22	0.008	35	3	320.00	75.67
307	Air	4130	32	0.004	25	3	219.08	74.28
308	Air	4130	32	0.004	30	3	186.47	52.59
309	Air	4130	32	0.004	35	3	165.58	35.65
310	Air	4130	32	0.008	25	3	384.71	107.27
311	Air	4130	32	0.008	30	3	359.24	86.33
312	Air	4130	32	0.008	35	3	323.01	65.36
313	Argon	4130	32	0.004	25	3	204.70	77.09
314	Argon	4130	32	0.004	30	3	227.03	73.33
315	Argon	4130	32	0.004	35	3	202.88	56.91
316	Argon	4130	32	0.008	25	3	389.18	115.21
317	Argon	4130	32	0.008	30	3	349.02	89.67
318	Argon	4130	32	0.008	35	3	338.15	77.30
319	Nitrogen	4130	32	0.004	25	3	226.17	86.39
320	Nitrogen	4130	32	0.004	30	3	228.47	76.48
321	Nitrogen	4130	32	0.004	35	3	189.14	51.77
322	Nitrogen	4130	32	0.008	25	3	381.05	111.11
323	Nitrogen	4130	32	0.008	30	3	346.54	89.28
324	Nitrogen	4130	32	0.008	35	3	347.01	86.60
325	Air	4130	42	0.004	25	3	188.52	66.39
326	Air	4130	42	0.004	30	3	193.85	51.05
327	Air	4130	42	0.004	35	3	174.99	38.38

run	Medium	Alloy	Material Condition (Hardness)	Depth of Cut	Tool Angle	Replicate	cutting force (lbs force)	thrust force (lbs force)
328	Air	4130	42	0.008	25	3	389.29	123.67
329	Air	4130	42	0.008	30	3	361.80	88.95
330	Air	4130	42	0.008	35	3	344.80	70.88
331	Argon	4130	42	0.004	25	3	215.76	89.70
332	Argon	4130	42	0.004	30	3	187.74	60.39
333	Argon	4130	42	0.004	35	3	213.94	66.53
334	Argon	4130	42	0.008	25	3	415.87	146.57
335	Argon	4130	42	0.008	30	3	369.39	109.11
336	Argon	4130	42	0.008	35	3	363.31	90.10
337	Nitrogen	4130	42	0.004	25	3	226.99	92.07
338	Nitrogen	4130	42	0.004	30	3	200.74	64.82
339	Nitrogen	4130	42	0.004	35	3	195.06	60.51
340	Nitrogen	4130	42	0.008	25	3	410.00	142.13
341	Nitrogen	4130	42	0.008	30	3	369.36	103.71
342	Nitrogen	4130	42	0.008	35	3	352.15	94.45
343	Air	Mag	HO	0.004	25	3	24.21	5.30
344	Air	Mag	HO	0.004	30	3	23.66	4.70
345	Air	Mag	HO	0.004	35	3	22.99	3.14
346	Air	Mag	HO	0.008	25	3	38.01	3.00
347	Air	Mag	HO	0.008	30	3	37.95	1.67
348	Air	Mag	HO	0.008	35	3	37.63	1.13
349	Argon	Mag	HO	0.004	25	3	24.22	3.90
350	Argon	Mag	HO	0.004	30	3	23.50	3.75
351	Argon	Mag	HO	0.004	35	3	26.13	1.85
352	Argon	Mag	HO	0.008	25	3	37.18	1.19
353	Argon	Mag	HO	0.008	30	3	36.92	0.77
354	Argon	Mag	HO	0.008	35	3	36.60	0.46
355	Nitrogen	Mag	HO	0.004	25	3	24.72	3.82
356	Nitrogen	Mag	HO	0.004	30	3	23.12	4.10
357	Nitrogen	Mag	HO	0.004	35	3	25.30	2.19
358	Nitrogen	Mag	HO	0.008	25	3	37.11	1.15
359	Nitrogen	Mag	HO	0.008	30	3	37.21	0.58
360	Nitrogen	Mag	HO	0.008	35	3	36.61	0.37
361	Air	Mag	H24	0.004	25	3	22.83	7.24
362	Air	Mag	H24	0.004	30	3	23.88	8.39
363	Air	Mag	H24	0.004	35	3	26.46	7.64
364	Air	Mag	H24	0.008	25	3	40.72	5.87

run	Medium	Alloy	Material Condition (Hardness)	Depth of Cut	Tool Angle	Replicate	cutting force (lbs force)	thrust force (lbs force)
365	Air	Mag	H24	0.008	30	3	40.76	7.67
366	Air	Mag	H24	0.008	35	3	40.63	5.71
367	Argon	Mag	H24	0.004	25	3	24.43	6.43
368	Argon	Mag	H24	0.004	30	3	23.96	7.98
369	Argon	Mag	H24	0.004	35	3	26.17	6.94
370	Argon	Mag	H24	0.008	25	3	37.74	4.45
371	Argon	Mag	H24	0.008	30	3	41.36	6.87
372	Argon	Mag	H24	0.008	35	3	39.61	4.65
373	Nitrogen	Mag	H24	0.004	25	3	25.54	6.42
374	Nitrogen	Mag	H24	0.004	30	3	24.55	8.13
375	Nitrogen	Mag	H24	0.004	35	3	24.91	7.34
376	Nitrogen	Mag	H24	0.008	25	3	40.63	4.10
377	Nitrogen	Mag	H24	0.008	30	3	40.50	6.69
378	Nitrogen	Mag	H24	0.008	35	3	41.19	4.70
379	Air	6061	T0	0.004	25	3	71.19	23.99
380	Air	6061	T0	0.004	30	3	67.87	18.82
381	Air	6061	T0	0.004	35	3	54.08	12.03
382	Air	6061	T0	0.008	25	3	116.72	35.33
383	Air	6061	T0	0.008	30	3	111.01	25.02
384	Air	6061	T0	0.008	35	3	91.12	17.17
385	Argon	6061	T0	0.004	25	3	69.87	22.20
386	Argon	6061	T0	0.004	30	3	66.64	18.72
387	Argon	6061	T0	0.004	35	3	56.60	11.69
388	Argon	6061	T0	0.008	25	3	113.87	32.64
389	Argon	6061	T0	0.008	30	3	113.48	25.51
390	Argon	6061	T0	0.008	35	3	87.21	15.31
391	Nitrogen	6061	T0	0.004	25	3	71.62	23.22
392	Nitrogen	6061	T0	0.004	30	3	64.16	18.08
393	Nitrogen	6061	T0	0.004	35	3	59.80	13.10
394	Nitrogen	6061	T0	0.008	25	3	119.85	34.89
395	Nitrogen	6061	T0	0.008	30	3	112.97	26.66
396	Nitrogen	6061	T0	0.008	35	3	94.61	16.02
397	Air	6061	T4	0.004	25	3	52.30	16.07
398	Air	6061	T4	0.004	30	3	49.40	13.14
399	Air	6061	T4	0.004	35	3	43.08	8.93
400	Air	6061	T4	0.008	25	3	96.46	24.63
401	Air	6061	T4	0.008	30	3	91.32	16.73

run	Medium	Alloy	Material Condition (Hardness)	Depth of Cut	Tool Angle	Replicate	cutting force (lbs force)	thrust force (lbs force)
402	Air	6061	T4	0.008	35	3	82.43	11.79
403	Argon	6061	T4	0.004	25	3	51.47	15.88
404	Argon	6061	T4	0.004	30	3	47.23	12.50
405	Argon	6061	T4	0.004	35	3	45.27	7.02
406	Argon	6061	T4	0.008	25	3	88.17	22.28
407	Argon	6061	T4	0.008	30	3	85.80	15.71
408	Argon	6061	T4	0.008	35	3	81.81	11.53
409	Nitrogen	6061	T4	0.004	25	3	53.37	16.25
410	Nitrogen	6061	T4	0.004	30	3	51.37	12.86
411	Nitrogen	6061	T4	0.004	35	3	45.69	9.47
412	Nitrogen	6061	T4	0.008	25	3	101.26	24.76
413	Nitrogen	6061	T4	0.008	30	3	86.87	15.44
414	Nitrogen	6061	T4	0.008	35	3	81.74	11.92
415	Air	6061	T6	0.004	25	3	73.45	17.40
416	Air	6061	T6	0.004	30	3	68.95	13.32
417	Air	6061	T6	0.004	35	3	55.16	6.70
418	Air	6061	T6	0.008	25	3	136.80	27.46
419	Air	6061	T6	0.008	30	3	119.23	17.51
420	Air	6061	T6	0.008	35	3	112.17	8.19
421	Argon	6061	T6	0.004	25	3	77.72	18.23
422	Argon	6061	T6	0.004	30	3	68.49	12.00
423	Argon	6061	T6	0.004	35	3	57.99	6.66
424	Argon	6061	T6	0.008	25	3	135.83	27.26
425	Argon	6061	T6	0.008	30	3	125.86	18.53
426	Argon	6061	T6	0.008	35	3	113.52	9.00
427	Nitrogen	6061	T6	0.004	25	3	73.40	17.08
428	Nitrogen	6061	T6	0.004	30	3	69.84	13.26
429	Nitrogen	6061	T6	0.004	35	3	60.01	6.78
430	Nitrogen	6061	T6	0.008	25	3	136.93	27.12
431	Nitrogen	6061	T6	0.008	30	3	127.60	18.55
432	Nitrogen	6061	T6	0.008	35	3	111.69	9.15

run	Resultant (lbs force)	measured shear angle (degrees)	Psi (measured degrees)	Friction Force (Newtons)	Normal Force (Newtons)
1	202.0	21.3	35.5	578.8	687.2
2	187.6	24.9	38.4	589.4	590.5
3	142.2	26.4	35.5	471.6	421.4
4	347.1	21.9	39.0	967.8	1203.1
5	346.7	20.1	40.7	1075.8	1104.8
6	279.2	30.8	29.8	925.0	828.7
7	208.3	20.1	36.7	628.9	680.3
8	209.7	25.0	39.5	682.2	636.3
9	173.2	26.8	33.2	586.9	498.8
10	381.6	23.4	33.2	1118.8	1276.8
11	394.5	21.6	36.1	1257.3	1223.9
12	311.6	27.3	30.9	1051.6	903.2
13	205.2	25.9	24.1	612.2	677.2
14	219.9	25.6	30.4	717.1	665.3
15	182.3	33.7	27.5	618.9	524.3
16	385.1	23.5	22.9	1156.8	1263.4
17	363.8	24.6	29.8	1152.7	1136.0
18	337.7	27.5	28.6	1143.9	973.6
19	223.2	27.1	41.3	688.2	715.8
20	191.0	25.1	40.7	607.4	593.7
21	176.2	29.7	35.0	580.3	526.9
22	390.1	25.7	36.1	1121.6	1323.9
23	371.7	30.5	32.7	1125.6	1211.4
24	338.0	28.8	33.8	1088.8	1037.1
25	227.2	21.0	28.1	717.7	711.8
26	232.2	24.5	32.7	772.5	685.9
27	198.3	27.5	29.8	685.3	555.3
28	397.6	26.0	28.1	1146.3	1346.8
29	398.6	25.1	37.8	1263.7	1243.4
30	343.5	31.7	33.8	1128.8	1030.1
31	249.8	21.8	27.5	794.6	776.9
32	231.8	19.3	32.7	776.3	678.8
33	201.5	28.4	39.5	692.1	569.5
34	410.0	28.5	32.1	1189.5	1382.7
35	418.4	24.8	35.5	1333.5	1298.1
36	338.3	25.9	30.9	1113.4	1012.1
37	221.6	29.8	35.5	669.9	722.9

run	Resultant (lbs force)	measured shear angle (degrees)	Psi (measured degrees)	Friction Force (Newtons)	Normal Force (Newtons)
38	198.8	20.5	29.8	621.1	629.4
39	177.7	34.1	29.8	577.8	539.4
40	429.4	28.6	32.1	1287.1	1411.1
41	392.6	28.0	29.2	1200.5	1268.5
42	350.6	29.5	24.6	1170.8	1030.4
43	244.9	27.8	32.7	796.5	743.3
44	196.0	30.0	23.5	636.0	596.6
45	197.1	36.6	33.2	692.1	538.0
46	412.6	27.9	35.0	1256.7	1337.8
47	393.8	25.5	29.8	1239.3	1237.8
48	352.4	27.3	25.8	1169.0	1044.1
49	244.7	29.1	40.1	794.9	743.5
50	217.7	26.3	31.5	725.2	641.5
51	203.3	35.4	22.3	702.9	568.9
52	440.8	32.6	30.4	1361.5	1411.1
53	375.5	28.6	24.1	1182.2	1179.7
54	375.1	25.3	22.3	1283.8	1065.7
55	25.5	53.0	2.0	66.6	91.9
56	26.1	50.2	9.9	89.6	73.8
57	27.2	47.8	7.3	74.6	95.0
58	39.3	54.6	-0.5	82.0	154.6
59	39.9	51.0	3.5	91.2	152.1
60	39.1	51.7	3.7	98.4	143.6
61	23.9	45.7	12.2	61.5	86.8
62	23.9	52.0	8.0	68.5	81.5
63	26.3	51.9	-0.7	72.0	92.1
64	38.1	53.6	-3.4	76.1	151.2
65	36.7	49.7	-4.9	83.5	140.1
66	37.6	52.2	1.5	95.9	137.2
67	24.4	51.1	3.2	61.3	89.7
68	23.7	44.4	-19.7	66.7	81.6
69	25.8	47.4	-0.8	74.0	87.7
70	37.6	50.5	-1.6	77.8	148.1
71	38.3	54.0	-4.7	88.0	146.0
72	37.6	54.2	-4.5	97.2	136.2
73	25.7	58.1	11.6	74.3	87.0
74	24.6	50.8	-0.7	82.7	71.4

run	Resultant (lbs force)	measured shear angle (degrees)	Psi (measured degrees)	Friction Force (Newtons)	Normal Force (Newtons)
75	24.8	53.3	-1.9	88.7	65.8
76	42.0	61.6	3.9	97.8	159.1
77	43.1	58.7	4.3	116.1	152.5
78	43.0	62.4	2.5	125.7	144.3
79	23.3	65.6	-3.9	69.2	77.1
80	25.1	58.1	-7.0	83.4	74.3
81	25.6	50.6	-9.7	88.9	71.4
82	39.5	59.7	0.3	89.8	151.2
83	40.6	61.3	-1.7	113.8	140.4
84	39.8	62.7	1.1	117.7	132.0
85	24.8	58.9	-8.5	70.8	84.8
86	25.4	57.6	-0.5	84.1	75.5
87	25.9	58.3	1.2	90.7	71.0
88	39.6	59.6	0.9	91.2	150.6
89	42.2	62.4	1.4	118.4	145.5
90	40.4	62.1	-1.5	121.1	132.9
91	69.5	15.1	35.5	206.5	229.9
92	63.5	14.9	44.1	197.8	201.8
93	52.8	17.0	37.8	173.8	158.2
94	115.5	15.6	48.7	336.7	387.9
95	91.1	18.5	44.1	255.0	314.8
96	90.8	20.5	43.0	287.0	284.0
97	74.8	17.4	41.8	226.4	243.7
98	65.8	16.6	44.1	208.6	205.4
99	54.9	20.5	39.5	179.0	166.0
100	124.6	17.0	43.0	369.5	412.9
101	102.4	18.4	47.0	310.3	333.2
102	96.4	18.6	40.1	305.5	300.7
103	73.2	18.8	43.5	220.0	240.1
104	67.8	19.0	42.4	215.7	210.7
105	53.4	18.1	39.5	176.1	159.4
106	121.3	17.3	40.7	354.4	406.8
107	110.2	17.9	44.1	334.8	357.9
108	96.1	22.2	44.7	302.6	302.0
109	55.9	40.1	21.8	160.9	189.8
110	54.6	38.4	22.9	168.5	174.9
111	44.1	40.4	30.9	136.6	140.6

run	Resultant (lbs force)	measured shear angle (degrees)	Psi (measured degrees)	Friction Force (Newtons)	Normal Force (Newtons)
112	89.0	30.0	32.7	249.6	307.3
113	85.0	26.4	30.4	246.8	286.6
114	76.8	34.0	30.9	232.6	249.9
115	54.4	30.1	33.2	159.6	182.1
116	48.8	29.0	37.8	152.9	154.4
117	44.0	30.7	30.9	142.2	134.7
118	101.0	26.9	35.0	271.8	357.5
119	90.3	31.8	33.8	258.0	307.7
120	82.9	31.2	32.7	251.4	269.9
121	57.4	34.9	36.1	171.7	188.7
122	51.4	26.0	32.7	160.1	163.5
123	44.5	31.2	35.0	142.0	138.2
124	100.5	27.4	30.9	281.9	347.2
125	88.0	26.8	36.1	251.7	300.0
126	83.1	29.1	32.7	250.8	271.7
127	75.2	21.5	36.7	205.4	264.3
128	66.5	25.5	36.7	186.3	229.9
129	62.8	28.5	37.8	183.1	211.1
130	125.1	22.9	39.5	333.1	445.8
131	113.1	24.8	38.4	309.2	396.6
132	104.2	28.6	35.0	291.7	360.0
133	77.4	18.5	35.5	212.9	270.4
134	70.2	23.3	35.0	202.9	237.2
135	65.5	26.6	35.5	191.1	220.0
136	141.5	22.7	30.9	362.0	515.0
137	123.6	23.1	35.5	327.7	441.2
138	110.8	26.7	35.0	314.1	380.0
139	73.9	21.0	32.7	198.1	262.4
140	70.7	25.3	37.8	204.3	238.9
141	62.7	29.7	36.7	183.5	209.9
142	128.6	24.1	34.4	338.6	461.3
143	128.3	24.3	35.5	353.3	448.0
144	110.5	27.6	32.1	310.8	380.8
145	196.4	22.0	33.8	573.2	659.3
146	194.9	24.9	32.7	609.7	616.6
147	160.5	30.4	34.4	527.9	480.6
148	357.4	23.5	38.4	1027.7	1213.0

run	Resultant (lbs force)	measured shear angle (degrees)	Psi (measured degrees)	Friction Force (Newtons)	Normal Force (Newtons)
149	333.9	24.9	35.5	1036.9	1063.2
150	303.5	32.3	36.1	1004.8	901.8
151	224.0	20.6	37.8	669.1	738.3
152	209.5	26.3	39.0	688.3	628.1
153	183.7	32.1	31.5	625.3	525.8
154	377.2	24.2	15.5	1105.0	1262.7
155	365.6	18.8	33.2	1160.3	1139.7
156	328.5	26.6	30.9	1101.5	960.3
157	206.7	23.6	23.5	622.9	676.5
158	219.1	26.8	30.9	717.1	659.9
159	172.2	28.6	25.8	590.7	487.3
160	399.3	25.5	22.3	1180.5	1327.1
161	382.3	20.6	31.5	1214.5	1190.6
162	320.5	30.7	32.1	1050.3	964.3
163	225.0	27.6	39.0	695.7	719.7
164	200.1	30.9	33.8	629.1	629.8
165	172.2	32.2	37.2	567.2	514.9
166	426.4	24.9	37.8	1278.9	1401.0
167	362.8	29.3	28.1	1124.2	1157.6
168	319.2	27.1	35.5	1030.0	977.1
169	229.7	20.2	29.8	717.9	727.0
170	245.8	24.0	34.4	814.4	729.8
171	201.7	26.0	30.9	691.4	571.5
172	393.2	27.7	33.2	1135.2	1330.4
173	377.2	29.4	29.2	1177.2	1195.3
174	345.2	28.9	26.9	1139.5	1029.0
175	297.7	23.7	29.8	952.1	920.4
176	245.7	24.5	35.0	809.3	734.4
177	196.8	24.0	40.7	677.7	554.3
178	398.2	22.5	37.8	1166.3	1332.9
179	408.7	25.7	40.1	1282.5	1288.6
180	347.6	27.8	35.0	1130.1	1055.4
181	220.3	30.4	24.1	665.4	719.2
182	180.8	21.2	28.1	571.3	566.1
183	165.5	31.0	29.2	540.3	500.1
184	412.3	32.3	30.4	1247.9	1344.2
185	367.8	29.3	34.4	1132.8	1180.1

run	Resultant (lbs force)	measured shear angle (degrees)	Psi (measured degrees)	Friction Force (Newtons)	Normal Force (Newtons)
186	359.0	33.5	29.8	1151.0	1106.7
187	264.2	27.5	35.0	866.5	794.0
188	210.3	30.7	26.9	681.6	640.5
189	218.3	34.9	26.4	773.7	586.7
190	438.6	28.8	32.1	1347.9	1410.8
191	366.8	28.2	37.2	1168.7	1138.4
192	364.4	28.3	21.8	1215.0	1073.2
193	234.8	27.1	30.9	754.1	722.8
194	207.0	30.0	35.5	690.6	608.7
195	188.8	35.8	19.5	664.2	513.8
196	426.1	28.7	23.5	1338.8	1341.9
197	379.3	26.4	26.9	1197.4	1188.4
198	386.9	28.2	30.9	1324.4	1099.3
199	26.0	53.5	-0.6	68.4	93.5
200	26.8	47.3	2.8	92.7	75.2
201	24.5	51.5	-1.4	71.8	81.9
202	39.6	51.0	5.6	84.3	154.6
203	38.6	53.1	1.7	91.7	145.1
204	38.5	52.8	2.6	100.1	139.0
205	24.2	45.7	3.6	60.8	89.1
206	25.4	47.1	5.9	70.0	88.7
207	25.3	50.6	-0.6	72.1	86.6
208	39.4	51.8	-2.1	78.3	157.0
209	38.7	55.3	-3.2	86.3	148.8
210	38.8	50.6	3.7	98.6	141.4
211	24.0	50.1	2.7	60.6	88.1
212	25.2	52.9	-0.7	70.0	87.4
213	25.5	45.0	-4.0	72.9	86.6
214	39.3	54.1	2.1	77.9	156.4
215	38.3	52.9	-5.3	86.6	146.5
216	38.3	56.1	0.5	97.7	139.5
217	25.1	55.4	-20.2	75.5	82.3
218	26.6	55.1	7.2	87.4	79.8
219	25.5	56.9	7.0	90.6	68.0
220	44.0	60.7	-2.0	101.4	167.4
221	41.9	60.7	-3.2	118.3	143.8
222	40.6	65.7	1.9	122.7	132.7

run	Resultant (lbs force)	measured shear angle (degrees)	Psi (measured degrees)	Friction Force (Newtons)	Normal Force (Newtons)
223	25.8	64.8	-1.2	72.4	89.1
224	24.8	57.9	0.8	82.8	73.2
225	24.7	49.7	7.5	86.4	67.8
226	41.4	63.2	-4.3	93.0	159.0
227	39.8	60.4	-0.4	113.5	135.9
228	40.0	58.1	-1.7	118.7	132.4
229	23.4	59.4	7.3	69.0	78.2
230	24.3	58.7	-1.2	82.6	70.0
231	25.1	56.6	4.4	87.8	69.2
232	39.3	59.0	0.8	90.1	149.6
233	41.4	62.0	-0.5	116.6	142.3
234	41.3	62.0	1.2	121.0	138.4
235	76.2	11.9	44.7	231.9	246.9
236	66.9	22.1	41.8	212.0	209.0
237	53.2	16.8	44.1	171.7	162.9
238	125.2	13.6	47.0	365.4	420.2
239	100.3	18.7	47.6	303.7	327.1
240	95.8	19.8	47.0	298.5	304.3
241	76.7	16.4	39.5	231.7	250.4
242	70.2	18.0	42.4	222.1	219.4
243	54.1	21.9	38.4	176.6	163.8
244	127.1	19.8	45.8	376.7	421.7
245	112.0	16.5	45.8	341.9	362.6
246	87.7	22.3	39.0	262.5	288.4
247	73.6	17.6	44.1	216.9	245.5
248	71.7	20.4	39.5	227.3	223.6
249	57.9	19.4	41.8	189.3	174.6
250	123.2	15.6	43.0	355.0	417.4
251	118.8	17.0	41.8	361.0	386.0
252	96.0	18.5	41.8	301.7	302.5
253	51.3	31.2	25.2	152.4	169.8
254	53.3	36.0	30.4	165.3	169.9
255	44.6	32.5	29.8	136.9	143.6
256	98.9	26.7	34.4	280.6	338.8
257	88.4	32.8	35.5	256.6	298.1
258	82.6	31.9	30.4	249.7	269.6
259	54.5	30.3	35.0	162.8	179.6

run	Resultant (lbs force)	measured shear angle (degrees)	Psi (measured degrees)	Friction Force (Newtons)	Normal Force (Newtons)
260	54.8	32.1	29.2	170.1	174.6
261	45.5	29.5	34.4	146.4	139.7
262	99.8	25.3	31.5	276.9	347.1
263	90.4	28.3	30.9	259.3	307.4
264	85.5	29.0	29.8	257.7	279.5
265	52.7	30.8	35.0	158.2	172.9
266	48.0	30.4	34.4	150.5	151.1
267	44.3	30.6	31.5	143.0	135.7
268	100.3	28.6	37.8	279.5	347.7
269	91.0	29.1	30.4	258.8	311.3
270	83.9	31.4	30.9	254.0	273.6
271	69.5	21.1	39.0	190.1	243.6
272	70.5	23.0	29.2	204.1	238.3
273	60.7	29.3	34.4	179.5	201.6
274	139.3	24.8	30.4	367.5	499.0
275	118.6	26.2	30.9	306.2	429.7
276	108.5	28.5	36.7	302.7	376.2
277	77.3	20.6	31.5	213.8	269.4
278	70.7	24.4	31.5	206.1	237.8
279	58.9	25.4	30.4	171.8	197.7
280	132.5	23.8	39.5	349.5	474.8
281	126.2	28.6	33.2	346.3	441.9
282	109.5	28.7	36.7	309.3	376.0
283	76.6	23.6	30.9	209.5	268.8
284	68.7	26.8	33.8	199.1	232.0
285	57.8	26.4	39.5	169.7	193.1
286	133.4	23.7	33.2	350.7	478.4
287	128.2	27.6	33.2	354.6	446.7
288	111.9	28.9	30.4	315.1	385.2
289	193.3	19.7	40.7	562.6	649.9
290	200.1	33.1	26.4	629.1	629.7
291	157.6	25.9	35.5	519.8	470.8
292	358.1	18.8	39.5	1043.6	1203.3
293	344.1	25.2	31.5	1068.9	1095.6
294	302.2	33.7	33.2	1004.5	893.6
295	211.8	21.4	39.0	638.5	692.9
296	215.1	22.6	35.5	702.2	650.0

run	Resultant (lbs force)	measured shear angle (degrees)	Psi (measured degrees)	Friction Force (Newtons)	Normal Force (Newtons)
297	170.5	31.4	39.5	581.8	486.6
298	385.4	22.1	21.2	1135.3	1284.7
299	354.9	22.1	33.2	1134.9	1097.6
300	310.2	27.1	32.1	1060.1	883.0
301	210.5	24.0	27.5	634.8	688.1
302	205.8	27.0	29.8	670.5	623.6
303	188.3	32.5	22.3	636.1	544.9
304	362.8	20.0	27.5	1040.9	1233.2
305	369.9	20.1	27.5	1177.9	1149.2
306	328.8	28.1	29.2	1092.2	972.9
307	231.3	26.2	40.1	711.3	743.6
308	193.7	26.3	33.2	617.3	601.4
309	169.4	31.4	35.0	552.4	512.4
310	399.4	26.1	33.8	1155.7	1349.3
311	369.5	29.4	33.2	1131.6	1191.9
312	329.6	31.6	34.4	1062.3	1010.2
313	218.7	19.2	32.1	695.6	680.3
314	238.6	26.3	37.8	787.4	711.5
315	210.7	25.4	34.4	725.0	594.1
316	405.9	26.6	34.4	1196.1	1352.4
317	360.4	25.0	30.4	1121.7	1145.1
318	346.9	29.2	31.5	1144.4	1034.9
319	242.1	22.8	34.4	773.5	749.4
320	240.9	28.6	36.1	802.8	710.0
321	196.1	24.9	27.5	671.2	557.1
322	396.9	27.7	28.1	1164.3	1327.3
323	357.9	24.9	36.7	1114.7	1136.4
324	357.7	26.8	33.2	1200.9	1043.5
325	199.9	27.7	25.8	622.0	635.2
326	200.5	21.0	27.5	627.8	633.2
327	179.1	31.5	25.2	586.3	539.7
328	408.5	31.8	35.5	1230.4	1336.9
329	372.6	30.0	25.8	1147.4	1195.9
330	352.0	29.8	23.5	1138.0	1075.5
331	233.7	28.8	53.9	767.2	701.2
332	197.2	27.0	36.1	650.2	588.9
333	224.0	34.6	33.2	788.3	609.8

run	Resultant (lbs force)	measured shear angle (degrees)	Psi (measured degrees)	Friction Force (Newtons)	Normal Force (Newtons)
334	440.9	22.8	19.5	1372.7	1401.0
335	385.2	24.9	35.0	1241.9	1180.3
336	374.3	29.9	26.9	1255.2	1093.9
337	244.9	26.8	32.1	797.9	742.0
338	210.9	28.4	38.4	696.2	629.1
339	204.2	32.8	29.2	718.2	556.4
340	433.9	34.8	24.6	1343.8	1385.7
341	383.6	25.6	26.4	1221.0	1192.2
342	364.6	31.8	32.1	1242.6	1042.2
343	24.8	51.2	-0.2	66.9	87.6
344	24.1	51.7	-0.1	70.7	80.7
345	23.2	50.0	7.6	70.1	75.8
346	38.1	52.4	1.9	83.5	147.6
347	38.0	53.5	3.6	90.8	142.5
348	37.6	51.8	-5.5	100.1	134.2
349	24.5	49.8	1.4	61.3	90.3
350	23.8	47.5	3.2	66.7	82.2
351	26.2	47.9	-3.4	73.4	90.5
352	37.2	52.5	-1.6	74.7	147.7
353	36.9	56.2	-2.0	85.1	140.5
354	36.6	49.4	-0.5	95.1	132.2
355	25.0	50.3	-2.9	61.9	92.5
356	23.5	46.3	-8.3	67.2	80.0
357	25.4	46.7	-2.4	72.5	86.6
358	37.1	52.4	-5.8	74.4	147.5
359	37.2	52.6	-7.8	85.0	142.0
360	36.6	54.9	-1.3	94.8	132.4
361	23.9	50.0	-6.8	72.1	78.4
362	25.3	53.6	-3.5	85.4	73.3
363	27.5	54.1	8.2	95.4	76.9
364	41.1	60.2	-0.5	100.2	153.1
365	41.5	61.3	3.5	120.2	140.0
366	41.0	60.4	6.4	124.5	133.5
367	25.3	58.8	-4.5	71.8	86.4
368	25.3	60.5	3.0	84.1	74.6
369	27.1	55.3	-2.5	92.0	77.6
370	38.0	60.2	-1.0	88.9	143.8

run	Resultant (lbs force)	measured shear angle (degrees)	Psi (measured degrees)	Friction Force (Newtons)	Normal Force (Newtons)
371	41.9	59.4	-2.3	118.4	144.1
372	39.9	60.2	4.5	118.0	132.5
373	26.3	61.0	-1.7	73.9	90.9
374	25.9	61.5	-1.3	85.9	76.5
375	26.0	54.3	-0.5	90.3	72.0
376	40.8	60.3	0.3	92.9	156.1
377	41.0	59.4	-0.7	115.8	141.1
378	41.5	61.3	4.0	122.2	138.1
379	75.1	10.5	47.0	230.6	241.9
380	70.4	22.2	39.5	223.5	219.6
381	55.4	17.3	45.8	181.8	166.3
382	121.9	12.0	45.3	361.9	404.1
383	113.8	20.1	45.3	343.3	372.0
384	92.7	16.7	37.8	295.0	288.2
385	73.3	13.1	39.0	220.9	239.9
386	69.2	21.8	36.7	220.3	215.1
387	57.8	23.0	42.4	187.0	176.4
388	118.5	16.9	45.3	345.6	397.7
389	116.3	17.0	44.1	350.6	380.4
390	88.5	17.9	41.8	278.3	278.7
391	75.3	14.0	41.3	228.3	245.1
392	66.7	20.3	45.3	212.4	207.0
393	61.2	22.9	42.4	200.3	184.5
394	124.8	15.9	39.0	365.9	417.6
395	116.1	18.9	39.5	354.0	375.9
396	96.0	22.6	40.1	299.8	303.8
397	54.7	40.5	20.1	163.1	180.6
398	51.1	41.6	21.2	160.5	161.1
399	44.0	38.6	33.2	142.4	134.2
400	99.6	30.2	31.5	280.6	342.6
401	92.8	36.0	33.2	267.5	314.6
402	83.3	32.1	34.4	253.3	270.3
403	53.9	31.2	30.9	160.8	177.6
404	48.9	29.0	30.4	153.2	154.1
405	45.8	31.7	33.2	141.1	147.0
406	90.9	28.1	30.9	255.6	313.6
407	87.2	31.4	30.4	251.3	295.6

run	Resultant (lbs force)	measured shear angle (degrees)	Psi (measured degrees)	Friction Force (Newtons)	Normal Force (Newtons)
408	82.6	34.6	38.4	250.7	268.7
409	55.8	28.4	33.8	165.8	184.6
410	53.0	31.6	266.4	163.8	169.3
411	46.7	34.8	33.2	151.1	142.3
412	104.2	29.0	39.0	290.2	361.7
413	88.2	28.4	35.5	252.7	300.3
414	82.6	31.0	29.8	252.0	267.4
415	75.5	19.0	35.0	208.2	263.4
416	70.2	21.2	33.2	204.7	236.0
417	55.6	28.6	31.5	165.1	183.9
418	139.5	22.2	34.4	367.9	499.9
419	120.5	25.1	37.8	332.6	420.4
420	112.5	23.6	33.2	316.0	387.8
421	79.8	20.9	38.4	219.6	279.1
422	69.5	23.1	36.7	198.6	237.2
423	58.4	31.8	33.8	172.2	194.3
424	138.5	19.8	37.8	365.3	496.4
425	127.2	24.4	33.8	351.3	443.6
426	113.9	27.6	34.4	322.4	390.7
427	75.4	21.1	37.2	206.9	263.8
428	71.1	25.8	37.8	206.4	239.6
429	60.4	28.5	39.0	177.8	201.4
430	139.6	22.5	31.5	366.7	501.0
431	128.9	25.5	35.0	355.2	450.3
432	112.1	24.0	34.4	318.3	383.6

Appendix D
Calculated Values

run	Beta (degrees)	Shear Area, As Merchant (in ²)	Shear Area, As Vishnu (in ²)	Shear Stress Ts Merchant (Mpa)	Shear Stress, Ts Vishnu (MPa)
1	40.1	0.000880017	0.000712921	1023.0	584.0
2	44.9	0.001082605	0.001886242	881.3	178.1
3	48.2	0.00080213	0.000952629	756.2	253.9
4	38.8	0.002209448	0.00171359	820.9	447.4
5	44.2	0.001884624	0.001399652	876.5	463.9
6	48.1	0.001533822	0.001365286	740.6	349.6
7	42.7	0.002019703	0.001597725	602.4	228.8
8	47.0	0.001020059	0.001506541	978.6	216.0
9	49.6	0.000887799	0.001350358	883.7	196.8
10	41.2	0.002172895	0.001571608	876.5	469.2
11	45.8	0.00271451	0.002279649	796.1	293.2
12	49.3	0.001751531	0.001501884	802.3	325.7
13	42.1	0.001628345	0.001410352	711.8	266.2
14	47.1	0.001414522	0.002164938	846.5	155.8
15	49.7	0.000815094	0.001262406	937.5	220.1
16	42.5	0.002313431	0.001728226	838.1	398.2
17	45.4	0.001779653	0.001649482	913.4	382.9
18	49.6	0.001793878	0.001508831	860.4	344.5
19	43.9	0.001071952	0.001226581	980.7	295.6
20	45.7	0.001230582	0.001187126	821.6	274.8
21	47.8	0.000669039	0.000636738	862.6	485.5
22	40.3	0.001488708	0.000724198	960.3	1100.0
23	42.9	0.001758965	0.001747281	977.6	431.4
24	46.4	0.001711074	0.001676549	920.5	385.7
25	45.2	0.001085169	0.001053915	967.8	315.7
26	48.4	0.00129321	0.001169343	929.7	275.4
27	51.0	0.000818781	0.000794005	982.0	343.8
28	40.4	0.001649629	0.001553648	998.5	518.7
29	45.5	0.002175028	0.002016531	922.9	342.0
30	47.6	0.00183676	0.001792917	897.4	339.3

run	Beta (degrees)	Shear Area, As Merchant (in ²)	Shear Area, As Vishnu (in ²)	Shear Stress Ts Merchant (Mpa)	Shear Stress, Ts Vishnu (MPa)
31	45.6	0.001124057	0.001247626	1039.5	283.6
32	48.8	0.000911636	0.000870952	1069.8	355.4
33	50.5	0.000826659	0.000771283	1008.7	373.0
34	40.7	0.001759286	0.001640088	1018.6	498.1
35	45.8	0.002154263	0.001878888	968.5	377.3
36	47.7	0.001556934	0.001397544	899.9	425.5
37	42.8	0.000851997	0.000913259	1072.6	423.9
38	44.6	0.001001011	0.000870361	981.8	417.7
39	47.0	0.000746862	0.000726123	978.6	451.8
40	42.4	0.001687257	0.001571718	1050.7	491.6
41	43.4	0.001857362	0.001824261	1020.5	423.4
42	48.7	0.001664016	0.001355193	932.4	427.0
43	47.0	0.000786211	0.000743267	1044.3	414.7
44	46.8	0.000856511	0.000813378	970.3	378.5
45	52.1	0.00069668	0.000626805	906.5	389.8
46	43.2	0.001657951	0.001480582	989.4	474.3
47	45.0	0.001654769	0.001598123	1017.0	438.7
48	48.2	0.001692565	0.001459749	942.8	410.2
49	46.9	0.000832447	0.000802561	1064.6	386.3
50	48.5	0.000746033	0.000753166	1006.7	397.0
51	51.0	0.000767696	0.000750741	1019.3	371.8
52	44.0	0.001594034	0.001587347	1030.7	447.8
53	45.1	0.001770643	0.001631502	959.6	409.0
54	50.3	0.002158342	0.002065478	882.8	264.6
55	35.9	0.000646251	0.000732912	124.7	88.3
56	50.5	0.000588277	0.000629535	51.8	47.0
57	38.1	0.000605019	0.000712986	153.7	108.4
58	27.9	0.001338799	0.00157646	123.8	84.9
59	30.9	0.001266187	0.001425353	126.7	93.7
60	34.4	0.001263547	0.001400761	128.7	90.7
61	35.3	0.000574982	0.000511749	86.6	121.5
62	40.1	0.000600007	0.000708894	103.4	79.4
63	38.0	0.000671361	0.00076652	165.4	97.9
64	26.7	0.00140288	0.001683295	124.8	79.8
65	30.8	0.001438612	0.001568668	122.7	78.7
66	35.0	0.001300557	0.001491318	124.6	80.4
67	34.4	0.000635752	0.000725054	122.8	91.3

run	Beta (degrees)	Shear Area, As Merchant (in ²)	Shear Area, As Vishnu (in ²)	Shear Stress Ts Merchant (Mpa)	Shear Stress, Ts Vishnu (MPa)
68	39.2	0.001013507	0.001362641	124.7	42.5
69	40.2	0.000672502	0.000880934	154.6	76.7
70	27.7	0.00136264	0.001543836	120.0	83.5
71	31.1	0.001434561	0.001838157	127.5	69.5
72	35.5	0.00142864	0.001844311	126.4	63.8
73	40.5	0.000562764	0.00051104	38.3	101.5
74	49.2	0.000632854	0.000600449	71.8	52.9
75	53.5	0.000642299	0.000654417	80.1	41.1
76	31.6	0.001202698	0.001152352	96.3	109.8
77	37.3	0.001197827	0.001223054	94.7	93.8
78	41.1	0.001220039	0.001352121	104.5	80.1
79	41.9	0.000659733	0.000768459	87.5	56.1
80	48.3	0.000689773	0.000841648	97.1	41.6
81	51.2	0.000719855	0.000743223	113.4	46.4
82	30.7	0.001250415	0.001339786	102.5	91.8
83	39.0	0.001281703	0.001477872	98.3	67.9
84	41.7	0.00123999	0.001294543	97.9	75.1
85	39.9	0.000705433	0.000855866	112.6	60.6
86	48.1	0.000631526	0.000735159	78.7	49.1
87	51.9	0.00061877	0.00067895	78.9	48.2
88	31.2	0.001242209	0.001241743	99.6	97.4
89	39.1	0.001235101	0.001391941	93.9	74.4
90	42.3	0.001278093	0.001490376	103.1	64.5
91	41.9	0.001836614	0.00266779	219.6	48.2
92	44.4	0.002088248	0.002443861	184.9	48.2
93	47.7	0.001551603	0.001908336	200.5	48.8
94	41.0	0.003278183	0.004225981	202.3	53.6
95	39.0	0.003633638	0.004066415	156.8	55.3
96	45.3	0.003029791	0.003851666	179.9	48.0
97	42.9	0.001960428	0.002949046	221.6	44.1
98	45.4	0.001188754	0.002224009	291.8	51.3
99	47.2	0.001411034	0.002494109	225.5	40.1
100	41.8	0.003000713	0.004299532	231.1	54.0
101	43.0	0.002202986	0.003504583	246.2	59.0
102	45.5	0.002944748	0.003011441	195.0	64.7
103	42.5	0.001554407	0.001970257	262.2	66.3
104	45.7	0.002149495	0.002565018	190.1	45.1

run	Beta (degrees)	Shear Area, As Merchant (in ²)	Shear Area, As Vishnu (in ²)	Shear Stress Ts Merchant (Mpa)	Shear Stress, Ts Vishnu (MPa)
105	47.9	0.001518863	0.001566182	205.6	59.4
106	41.1	0.003506738	0.004144077	201.1	57.1
107	43.1	0.003559507	0.004412627	186.1	50.1
108	45.1	0.002467181	0.002600155	223.2	76.4
109	40.3	0.000869315	0.001876246	288.6	60.8
110	43.9	0.000610555	0.001402311	241.1	74.4
111	44.2	0.000657845	0.000670305	251.2	142.6
112	39.1	0.001728278	0.002995824	235.5	64.7
113	40.7	0.001621963	0.002276671	243.1	84.9
114	42.9	0.001490046	0.001305926	233.6	135.6
115	41.2	0.000884771	0.00087803	274.4	119.8
116	44.7	0.00068613	0.000597139	245.1	148.8
117	46.6	0.000910053	0.000797587	240.0	104.6
118	37.2	0.00204739	0.002068221	257.7	116.5
119	40.0	0.001712773	0.001618258	258.2	131.7
120	43.0	0.001940758	0.001805309	231.6	105.9
121	42.3	0.000722233	0.000892284	275.3	116.1
122	44.4	0.000886302	0.000881293	268.7	108.2
123	45.8	0.000810154	0.000804726	254.6	109.9
124	39.1	0.001871227	0.00189381	259.6	115.7
125	40.0	0.001674073	0.001582431	253.4	131.2
126	42.7	0.001730609	0.001835778	246.0	105.7
127	37.8	0.001599791	0.001909573	276.5	91.4
128	39.0	0.001323654	0.001590969	294.6	103.2
129	40.9	0.00123202	0.001691963	303.0	94.1
130	36.8	0.003194346	0.003306205	232.7	92.3
131	37.9	0.002842896	0.002945187	239.7	99.4
132	39.0	0.002632301	0.002580041	243.3	110.9
133	38.2	0.001639694	0.001861087	277.7	94.7
134	40.6	0.001460221	0.001541717	283.8	104.5
135	41.0	0.001192413	0.001471744	323.3	112.6
136	35.1	0.002873664	0.003259104	291.1	114.1
137	36.6	0.002590258	0.002625538	285.1	128.8
138	39.6	0.002088359	0.002085854	303.6	142.7
139	37.1	0.00133116	0.001906938	314.9	93.4
140	40.5	0.001359608	0.001611277	301.8	100.8
141	41.2	0.001292563	0.001413403	291.0	111.3

run	Beta (degrees)	Shear Area, As Merchant (in ²)	Shear Area, As Vishnu (in ²)	Shear Stress Ts Merchant (Mpa)	Shear Stress, Ts Vishnu (MPa)
142	36.3	0.002421841	0.002519955	295.2	127.4
143	38.3	0.002546506	0.002588218	294.6	126.6
144	39.2	0.002345097	0.002500112	281.1	120.5
145	41.0	0.001240508	0.001286284	839.0	298.9
146	44.7	0.00094671	0.001494202	976.3	237.7
147	47.7	0.000831056	0.00121448	861.7	233.0
148	40.3	0.002276804	0.001816747	812.8	401.7
149	44.3	0.002433876	0.001855014	739.8	336.2
150	48.1	0.001534529	0.001382804	806.2	376.5
151	42.2	0.001486725	0.001284959	831.4	317.5
152	47.6	0.000918558	0.001416397	998.0	218.6
153	49.9	0.000988023	0.001282151	900.9	214.8
154	41.2	0.002065313	0.00149318	888.1	489.2
155	45.5	0.002146234	0.002073403	855.1	304.1
156	48.9	0.001533079	0.001443349	855.2	368.5
157	42.6	0.001652581	0.001210513	704.3	302.0
158	47.4	0.001271173	0.001793745	903.0	184.0
159	50.5	0.000699656	0.000831311	820.0	297.3
160	41.7	0.002406523	0.00169933	860.7	442.3
161	45.6	0.001601109	0.00160768	962.6	408.6
162	47.4	0.001276759	0.001111456	758.8	516.6
163	44.0	0.001236781	0.00120836	916.3	299.1
164	45.0	0.000665679	0.000662566	902.7	540.0
165	47.8	0.000680729	0.000691547	858.1	436.7
166	42.4	0.002020128	0.001765494	986.6	434.1
167	44.2	0.001982991	0.001861708	896.4	366.7
168	46.5	0.001767626	0.001683768	860.5	360.0
169	44.6	0.000972844	0.000858009	1028.0	410.8
170	48.1	0.000778322	0.00080195	1138.0	434.5
171	50.4	0.000972693	0.001067703	981.6	272.5
172	40.5	0.001664902	0.001595112	985.9	497.6
173	44.6	0.001744413	0.001520615	960.9	455.2
174	47.9	0.001745303	0.001779232	908.9	336.7
175	46.0	0.001258191	0.001324373	1161.9	309.8
176	47.8	0.000854081	0.000868294	1167.4	413.0
177	50.7	0.000788936	0.000707614	976.2	391.6
178	41.2	0.001875363	0.001663287	966.1	463.6

run	Beta (degrees)	Shear Area, As Merchant (in ²)	Shear Area, As Vishnu (in ²)	Shear Stress Ts Merchant (Mpa)	Shear Stress, Ts Vishnu (MPa)
179	44.9	0.001900268	0.001921489	1013.2	382.9
180	47.0	0.001649569	0.001423081	941.2	451.3
181	42.8	0.000772494	0.00082359	1055.5	468.7
182	45.3	0.001012356	0.000892612	878.8	355.4
183	47.2	0.000727173	0.000619989	899.9	485.2
184	42.9	0.001554809	0.001470072	987.2	488.4
185	43.8	0.001750396	0.001615842	965.6	437.0
186	46.1	0.001385953	0.00131411	983.3	531.0
187	47.5	0.001157579	0.001160383	1057.9	272.6
188	46.8	0.000704892	0.000712969	988.5	465.0
189	52.8	0.00077765	0.000817132	1046.5	309.5
190	43.7	0.001999491	0.002126649	1006.1	339.4
191	45.8	0.001648893	0.001488593	932.3	418.1
192	48.5	0.001718989	0.001504223	966.1	402.8
193	46.2	0.000884899	0.000924966	1045.6	342.6
194	48.6	0.000674104	0.000620906	870.0	454.0
195	52.3	0.000756269	0.000696264	910.5	331.8
196	44.9	0.001600003	0.001308289	971.3	488.6
197	45.2	0.001730783	0.001527947	970.6	436.7
198	50.3	0.001818294	0.001710407	977.6	329.4
199	36.2	0.000670812	0.000813514	132.2	80.3
200	50.9	0.000639244	0.000714731	81.8	40.7
201	41.2	0.000678664	0.000787085	143.7	77.8
202	28.6	0.001233718	0.001303571	113.8	101.2
203	32.3	0.001297758	0.001444953	121.0	85.6
204	35.8	0.001282364	0.001463551	124.2	81.6
205	34.3	0.000632448	0.000666704	121.1	98.8
206	38.3	0.000614578	0.000726103	124.9	89.4
207	39.8	0.000670882	0.000806488	153.0	83.6
208	26.5	0.001374201	0.001615651	129.3	86.7
209	30.1	0.001398324	0.001751988	130.8	75.9
210	34.9	0.001264033	0.001429916	126.1	86.6
211	34.5	0.000639687	0.000714382	121.4	90.7
212	38.7	0.000671987	0.00088689	137.6	71.1
213	40.1	0.000708407	0.000785638	156.2	85.1
214	26.5	0.001289938	0.0014533	125.1	96.1
215	30.6	0.00144975	0.001892073	128.4	68.4

run	Beta (degrees)	Shear Area, As Merchant (in ²)	Shear Area, As Vishnu (in ²)	Shear Stress Ts Merchant (Mpa)	Shear Stress, Ts Vishnu (MPa)
216	35.0	0.001320771	0.00158491	127.7	76.9
217	42.5	0.000891199	0.001273724	116.3	35.1
218	47.6	0.000582703	0.000617259	50.6	63.9
219	53.1	0.000583713	0.000550471	46.6	52.1
220	31.2	0.001285854	0.001372593	117.4	98.0
221	39.4	0.001306425	0.001622585	103.1	62.5
222	42.7	0.001228907	0.001401772	94.3	67.5
223	39.1	0.000636438	0.000844877	100.7	66.5
224	48.5	0.000621928	0.000672757	70.1	50.6
225	51.9	0.000581539	0.000643055	49.3	48.7
226	30.3	0.001325404	0.001628476	117.3	80.1
227	39.9	0.00126089	0.001345909	90.5	70.2
228	41.9	0.001281502	0.001395695	103.9	69.6
229	41.4	0.000582494	0.000594769	50.0	75.3
230	49.7	0.000636994	0.000688726	70.7	43.6
231	51.7	0.000598118	0.000668765	64.5	48.4
232	31.0	0.001244325	0.001209787	99.6	99.7
233	39.3	0.001262938	0.001469824	96.3	68.5
234	41.2	0.00123758	0.001467201	103.3	70.7
235	43.2	0.002205811	0.002844011	203.6	45.6
236	45.4	0.001566379	0.002080254	244.5	55.9
237	46.5	0.001227372	0.001536987	243.6	65.8
238	41.0	0.003301873	0.004761954	217.9	51.4
239	42.9	0.00331954	0.004717104	179.9	43.2
240	44.4	0.00249262	0.002901634	222.4	70.6
241	42.8	0.001239698	0.002540132	319.9	52.9
242	45.3	0.00108026	0.002086574	329.0	58.7
243	47.1	0.001372949	0.001978644	227.1	49.9
244	41.8	0.002686663	0.003622191	255.3	65.6
245	43.3	0.003196149	0.003971493	206.2	55.8
246	42.3	0.002821646	0.003268389	189.2	63.8
247	41.5	0.001772288	0.002410239	241.0	58.2
248	45.5	0.00137655	0.001724553	288.1	71.9
249	47.3	0.001834762	0.002891454	192.0	36.2
250	40.4	0.003155534	0.004006614	223.8	62.4
251	43.1	0.002732124	0.003725355	247.3	64.0
252	44.9	0.00318476	0.003430038	183.4	58.3

run	Beta (degrees)	Shear Area, As Merchant (in ²)	Shear Area, As Vishnu (in ²)	Shear Stress Ts Merchant (Mpa)	Shear Stress, Ts Vishnu (MPa)
253	41.9	0.000912246	0.001470625	253.1	64.7
254	44.2	0.000779763	0.001140074	283.9	87.7
255	43.6	0.000797013	0.000834995	266.1	119.1
256	39.6	0.002142796	0.00432175	237.5	48.4
257	40.7	0.001783013	0.00336693	246.3	59.8
258	42.8	0.001540038	0.00134956	251.6	142.2
259	42.2	0.001158191	0.001205736	240.7	82.3
260	44.2	0.000960249	0.000938447	279.3	109.3
261	46.3	0.000775894	0.000825921	258.2	105.7
262	38.6	0.002143286	0.002162964	243.6	103.2
263	40.1	0.001617186	0.001535391	261.6	137.9
264	42.7	0.001879029	0.001969375	243.8	101.5
265	42.5	0.001000858	0.00100389	249.2	93.9
266	44.9	0.000750995	0.00065772	249.8	131.0
267	46.5	0.00079666	0.000865357	250.2	97.3
268	38.8	0.001972158	0.001834877	254.5	120.9
269	39.7	0.001770954	0.001801277	258.4	120.7
270	42.9	0.001684603	0.001801869	250.1	107.8
271	38.0	0.001577947	0.001804558	257.7	88.7
272	40.6	0.001552588	0.001728819	271.8	93.6
273	41.7	0.001162993	0.001277123	302.4	116.4
274	36.4	0.002876815	0.003440556	282.5	100.6
275	35.5	0.002344389	0.002662071	297.9	127.5
276	38.8	0.002554428	0.002843542	260.0	105.7
277	38.4	0.001600007	0.001833643	282.3	95.0
278	40.9	0.001201891	0.001400864	327.7	113.8
279	41.0	0.001065972	0.000955198	313.1	155.7
280	36.4	0.002747537	0.002793112	278.2	118.0
281	38.1	0.002615405	0.002826373	284.8	114.9
282	39.4	0.002291541	0.002190894	282.3	134.9
283	37.9	0.001612661	0.002106887	279.5	84.0
284	40.6	0.001063677	0.001183248	344.2	132.8
285	41.3	0.000983457	0.001380313	320.6	104.3
286	36.2	0.002432769	0.002817541	305.2	118.3
287	38.4	0.002395707	0.002654796	306.8	122.4
288	39.3	0.002205687	0.002468035	296.7	123.2
289	40.9	0.001056993	0.001044115	905.1	365.0

run	Beta (degrees)	Shear Area, As Merchant (in ²)	Shear Area, As Vishnu (in ²)	Shear Stress Ts Merchant (Mpa)	Shear Stress, Ts Vishnu (MPa)
290	45.0	0.00113541	0.001685143	915.7	212.3
291	47.8	0.001016989	0.001258506	790.8	218.7
292	40.9	0.002390212	0.001637379	783.5	429.9
293	44.3	0.001705748	0.001495898	890.6	429.3
294	48.3	0.001590709	0.001418735	801.2	359.2
295	42.7	0.001529641	0.001170955	765.1	319.4
296	47.2	0.001249685	0.001939454	898.5	169.3
297	50.1	0.001050724	0.001446566	811.5	174.6
298	41.5	0.002210829	0.001548735	873.9	473.9
299	46.0	0.002353522	0.002230225	783.5	266.2
300	50.2	0.001618883	0.001322998	788.4	344.1
301	42.7	0.001615796	0.001559107	729.2	237.9
302	47.1	0.000976205	0.001440188	975.0	220.5
303	49.4	0.000764022	0.001023841	967.5	287.1
304	40.2	0.001662381	0.000809244	923.3	920.8
305	45.7	0.001799213	0.001722436	921.2	365.6
306	48.3	0.001638303	0.001417639	872.3	392.2
307	43.7	0.000996335	0.000937032	1047.7	405.2
308	45.7	0.001032884	0.001021263	915.2	322.0
309	47.2	0.000699562	0.000755527	878.6	409.2
310	40.6	0.001607588	0.001410758	996.8	568.1
311	43.5	0.001744404	0.001756893	961.7	411.5
312	46.4	0.001826336	0.001924767	880.7	326.6
313	45.6	0.000937503	0.000865687	964.6	358.1
314	47.9	0.000911411	0.000970339	1124.2	355.4
315	50.7	0.000912478	0.000843798	1040.4	353.0
316	41.5	0.00199337	0.001760685	959.8	438.3
317	44.4	0.001848493	0.001700094	908.9	392.8
318	47.9	0.001828967	0.00159705	903.1	378.1
319	45.9	0.001112774	0.001121314	1006.9	299.2
320	48.5	0.000796996	0.000849675	1112.7	389.5
321	50.3	0.000707667	0.000723622	934.3	394.6
322	41.3	0.001723646	0.00149784	976.5	511.1
323	44.4	0.001843743	0.001501503	902.6	440.6
324	49.0	0.001955275	0.001799469	891.1	319.6
325	44.4	0.00075135	0.000741275	902.9	421.3
326	44.8	0.001017943	0.000957412	980.2	379.6

run	Beta (degrees)	Shear Area, As Merchant (in ²)	Shear Area, As Vishnu (in ²)	Shear Stress Ts Merchant (Mpa)	Shear Stress, Ts Vishnu (MPa)
327	47.4	0.000799662	0.000653616	982.0	493.2
328	42.6	0.00176651	0.001606229	989.6	450.1
329	43.8	0.001543544	0.001467478	987.3	488.0
330	46.6	0.001679362	0.001502663	973.5	442.0
331	47.6	0.000706114	0.000643758	892.6	431.4
332	47.8	0.00084378	0.000789232	954.7	363.1
333	52.3	0.000650746	0.000681826	940.4	402.2
334	44.4	0.001722271	0.001565298	1027.1	439.7
335	46.5	0.001862993	0.001546508	944.8	402.1
336	48.9	0.001637781	0.001428637	991.0	423.9
337	47.1	0.000813257	0.000816957	1054.5	374.0
338	47.9	0.001017463	0.000980711	975.9	311.0
339	52.2	0.000588305	0.000570473	645.9	439.8
340	44.1	0.001641143	0.001659541	1015.9	417.2
341	45.7	0.001716587	0.001499357	973.4	436.2
342	50.0	0.001869013	0.001884261	918.6	288.5
343	37.4	0.000667142	0.000751063	120.5	78.4
344	41.2	0.000665655	0.000861989	121.2	62.0
345	42.8	0.000603059	0.000635432	111.4	85.0
346	29.5	0.00129452	0.001457865	112.9	84.6
347	32.5	0.001265774	0.00141536	116.0	85.4
348	36.7	0.001452843	0.001734522	123.9	65.1
349	34.1	0.000651684	0.000759998	128.4	88.2
350	39.1	0.000635721	0.000721724	120.8	81.3
351	39.1	0.000700763	0.000835074	163.9	86.0
352	26.8	0.001361437	0.001497868	120.8	87.3
353	31.2	0.001370694	0.001600662	121.8	76.7
354	35.7	0.001339605	0.001482575	121.0	76.7
355	33.8	0.00069498	0.000841164	139.7	82.5
356	40.0	0.000766109	0.000923329	131.3	59.8
357	39.9	0.000689772	0.000766357	155.0	87.6
358	26.8	0.001460708	0.001751955	122.1	74.7
359	30.9	0.001516772	0.001920156	123.8	65.0
360	35.6	0.001355914	0.001637649	121.8	69.8
361	42.6	0.00068704	0.000599508	94.7	70.8
362	49.4	0.000656384	0.000733512	83.2	43.9
363	51.1	0.00057787	0.000575323	55.7	65.2

run	Beta (degrees)	Shear Area, As Merchant (in ²)	Shear Area, As Vishnu (in ²)	Shear Stress Ts Merchant (Mpa)	Shear Stress, Ts Vishnu (MPa)
364	33.2	0.001263556	0.00128992	99.8	90.5
365	40.7	0.001207854	0.001199871	80.6	78.9
366	43.0	0.001174204	0.001224639	81.1	77.1
367	39.7	0.000664925	0.000806224	105.8	65.9
368	48.4	0.000606891	0.000615263	62.6	56.8
369	49.8	0.00064743	0.000772093	106.7	52.9
370	31.7	0.001270329	0.001339276	97.9	85.1
371	39.4	0.001291182	0.00144491	101.4	70.3
372	41.7	0.001195797	0.001211806	89.4	80.6
373	39.1	0.000641097	0.00089234	104.7	64.2
374	48.3	0.000637584	0.000855555	81.9	42.2
375	51.4	0.000631298	0.000836374	88.2	41.1
376	30.8	0.00125057	0.001256919	105.6	100.8
377	39.4	0.001265618	0.001436683	95.8	69.4
378	41.5	0.001201435	0.00128301	95.0	79.8
379	43.6	0.002183059	0.003090451	201.7	40.2
380	45.5	0.001246941	0.002497746	302.7	48.7
381	47.5	0.001524077	0.001954245	213.5	50.4
382	41.8	0.003930211	0.004842787	182.4	46.9
383	42.7	0.003642104	0.005046833	189.3	46.2
384	45.7	0.002684635	0.003325237	201.1	55.7
385	42.6	0.00157919	0.002601089	259.0	49.9
386	45.7	0.001349619	0.002579893	281.3	45.7
387	46.7	0.001990901	0.00247485	179.7	43.9
388	41.0	0.003233323	0.004126764	209.7	56.2
389	42.7	0.002698877	0.003574892	245.5	66.8
390	45.0	0.00295094	0.003352315	179.8	54.9
391	43.0	0.001903925	0.002406956	228.4	54.1
392	45.7	0.001781961	0.002214746	218.9	51.1
393	47.4	0.001724469	0.002176618	213.9	50.7
394	41.2	0.003269528	0.004229802	218.4	57.0
395	43.3	0.003344299	0.004160826	206.0	55.3
396	44.6	0.002677149	0.003320537	210.9	61.2
397	42.1	0.000829002	0.001860968	272.9	53.9
398	44.9	0.000704549	0.00137052	259.6	67.0
399	46.7	0.000647678	0.000480436	229.9	171.8
400	39.3	0.002186063	0.004628121	237.5	46.3

run	Beta (degrees)	Shear Area, As Merchant (in ²)	Shear Area, As Vishnu (in ²)	Shear Stress Ts Merchant (Mpa)	Shear Stress, Ts Vishnu (MPa)
401	40.4	0.001848165	0.003884401	256.3	55.3
402	43.1	0.001402714	0.001369333	250.7	139.0
403	42.2	0.000821206	0.000793406	268.3	123.9
404	44.8	0.000928329	0.000825093	249.6	106.9
405	43.8	0.000802559	0.000806689	272.1	125.4
406	39.2	0.001946612	0.001797715	230.6	109.6
407	40.4	0.001958338	0.0017793	234.3	113.5
408	43.0	0.00183518	0.002006279	237.2	94.7
409	41.9	0.000796367	0.000865584	278.9	119.2
410	44.1	0.000850959	0.000931413	281.2	107.7
411	46.7	0.000689409	0.000587965	255.7	148.9
412	38.7	0.002070309	0.002036413	258.5	113.5
413	40.1	0.001756022	0.001647055	249.9	125.8
414	43.3	0.001861771	0.001845466	234.7	101.5
415	38.3	0.001480906	0.001954309	292.9	87.5
416	40.9	0.001553549	0.001617554	269.4	97.8
417	41.9	0.001144354	0.001151745	279.2	116.9
418	36.3	0.002638421	0.002970217	301.6	116.9
419	38.4	0.002381087	0.002496647	289.9	122.8
420	39.2	0.002393405	0.002628838	282.0	116.8
421	38.2	0.001639165	0.001912892	286.6	95.1
422	39.9	0.001161146	0.001300753	333.6	126.4
423	41.6	0.00095696	0.001118492	327.3	128.6
424	36.3	0.0027638	0.00284596	289.5	121.1
425	38.4	0.002541768	0.002632956	292.2	122.8
426	39.5	0.00214823	0.002290781	306.5	133.7
427	38.1	0.001632922	0.001990771	271.7	86.7
428	40.7	0.001274989	0.001584373	317.1	102.0
429	41.4	0.001249881	0.001307096	286.7	114.4
430	36.2	0.002682427	0.002888099	298.7	121.0
431	38.3	0.002643876	0.002724347	288.0	120.8
432	39.7	0.002615622	0.002657734	261.5	112.7

run	Friction Co-efficient	Shear Strain Y Merchant	Resulatant force (newtons) Merchant	Resulatant force (lbf) Merchant	Shear Strain Y Vishnu
1	0.7	1.6	898.5	202.0	1.0
2	0.8	1.9	834.3	187.6	0.8
3	0.8	1.3	632.4	142.2	1.1
4	0.7	2.0	1544.0	347.1	0.8
5	0.8	1.6	1542.1	346.7	0.8
6	0.8	1.3	1241.9	279.2	1.2
7	0.7	3.7	926.5	208.3	0.4
8	0.8	1.8	932.9	209.7	0.9
9	0.9	1.5	770.2	173.2	1.0
10	0.7	2.0	1697.6	381.6	0.8
11	0.8	2.4	1754.7	394.5	0.6
12	0.9	1.4	1386.3	311.6	1.0
13	0.7	3.0	912.9	205.2	0.6
14	0.8	2.5	978.2	219.9	0.6
15	0.9	1.3	811.1	182.3	1.3
16	0.7	2.1	1713.0	385.1	0.8
17	0.8	1.5	1618.4	363.8	1.0
18	0.9	1.5	1502.2	337.7	1.0
19	0.8	1.9	992.9	223.2	0.9
20	0.8	2.1	849.4	191.0	0.7
21	0.8	1.1	783.9	176.2	1.4
22	0.7	1.4	1735.2	390.1	1.3
23	0.7	1.5	1653.6	371.7	1.2
24	0.8	1.4	1503.7	338.0	1.1
25	0.8	2.0	1010.8	227.2	0.8
26	0.8	2.2	1033.1	232.2	0.7
27	0.9	1.3	882.0	198.3	1.1
28	0.7	1.5	1768.6	397.6	1.2
29	0.8	1.9	1772.8	398.6	0.8
30	0.8	1.5	1528.2	343.5	1.1
31	0.8	2.0	1111.3	249.8	0.8
32	0.9	1.6	1031.2	231.8	0.8
33	0.9	1.3	896.3	201.5	1.1
34	0.7	1.6	1823.9	410.0	1.2
35	0.8	1.9	1860.9	418.4	0.8
36	0.8	1.3	1504.7	338.3	1.1
37	0.7	1.6	985.6	221.6	1.2

run	Friction Co-efficient	Shear Strain Y Merchant	Resulatant force (newtons) Merchant	Resulatant force (lbf) Merchant	Shear Strain Y Vishnu
38	0.8	1.8	884.2	198.8	0.8
39	0.8	1.2	790.5	177.7	1.4
40	0.7	1.6	1909.9	429.4	1.2
41	0.8	1.6	1746.5	392.6	1.0
42	0.8	1.4	1559.7	350.6	1.1
43	0.8	1.5	1089.4	244.9	1.3
44	0.8	1.5	872.0	196.0	1.2
45	0.9	1.2	876.6	197.1	1.6
46	0.8	1.6	1835.5	412.6	1.2
47	0.8	1.5	1751.5	393.8	1.1
48	0.8	1.4	1567.4	352.4	1.0
49	0.8	1.6	1088.4	244.7	1.2
50	0.8	1.3	968.2	217.7	1.2
51	0.9	1.3	904.3	203.3	1.4
52	0.8	1.5	1960.8	440.8	1.5
53	0.8	1.6	1670.1	375.5	1.1
54	0.9	1.8	1668.5	375.1	0.8
55	0.6	1.3	113.5	25.5	10.0
56	0.9	1.2	116.1	26.1	5.1
57	0.7	1.1	120.8	27.2	3.3
58	0.5	1.3	174.9	39.3	14.9
59	0.5	1.2	177.3	39.9	5.1
60	0.6	1.1	174.1	39.1	4.3
61	0.6	1.3	106.4	23.9	4.3
62	0.7	1.2	106.4	23.9	6.1
63	0.7	1.1	116.9	26.3	4.1
64	0.5	1.3	169.3	38.1	10.7
65	0.5	1.3	163.2	36.7	3.9
66	0.6	1.1	167.4	37.6	4.4
67	0.6	1.3	108.7	24.4	7.2
68	0.7	1.7	105.4	23.7	1.9
69	0.7	1.1	114.8	25.8	2.9
70	0.5	1.3	167.3	37.6	6.1
71	0.5	1.3	170.5	38.3	6.8
72	0.6	1.2	167.3	37.6	4.9
73	0.7	1.3	114.5	25.7	-82.7
74	0.9	1.2	109.3	24.6	5.1

run	Friction Co-efficient	Shear Strain Y Merchant	Resulatant force (newtons) Merchant	Resulatant force (lbf) Merchant	Shear Strain Y Vishnu
75	0.9	1.1	110.4	24.8	5.1
76	0.6	1.3	186.8	42.0	-12.0
77	0.7	1.2	191.7	43.1	37.7
78	0.7	1.0	191.3	43.0	348.9
79	0.7	1.3	103.6	23.3	-5.6
80	0.8	1.2	111.7	25.1	22.7
81	0.9	1.2	114.0	25.6	3.5
82	0.5	1.3	175.9	39.5	-21.5
83	0.7	1.2	180.8	40.6	-36.9
84	0.7	1.1	176.9	39.8	-267.0
85	0.7	1.3	110.4	24.8	-31.1
86	0.8	1.2	113.0	25.4	20.0
87	0.9	1.1	115.2	25.9	11.4
88	0.5	1.3	176.0	39.6	-23.3
89	0.7	1.2	187.6	42.2	-20.1
90	0.7	1.1	179.8	40.4	106.0
91	0.7	3.4	309.0	69.5	0.4
92	0.8	3.8	282.6	63.5	0.3
93	0.8	2.7	235.0	52.8	0.4
94	0.7	3.0	513.6	115.5	0.5
95	0.7	3.3	405.1	91.1	0.4
96	0.8	2.6	403.8	90.8	0.5
97	0.7	3.6	332.7	74.8	0.4
98	0.8	2.1	292.8	65.8	0.6
99	0.8	2.4	244.1	54.9	0.5
100	0.7	2.7	554.1	124.6	0.5
101	0.7	1.9	455.3	102.4	0.7
102	0.8	2.5	428.7	96.4	0.5
103	0.7	2.9	325.6	73.2	0.5
104	0.8	3.9	301.5	67.8	0.4
105	0.8	2.6	237.5	53.4	0.5
106	0.7	3.2	539.6	121.3	0.4
107	0.8	3.2	490.1	110.2	0.4
108	0.8	2.1	427.6	96.1	0.6
109	0.7	1.6	248.9	55.9	1.9
110	0.8	1.2	242.9	54.6	2.2
111	0.8	1.1	196.1	44.1	2.0

run	Friction Co-efficient	Shear Strain Y Merchant	Resulatant force (newtons) Merchant	Resulatant force (lbf) Merchant	Shear Strain Y Vishnu
112	0.7	1.6	395.9	89.0	1.2
113	0.7	1.4	378.2	85.0	1.1
114	0.7	1.3	341.4	76.8	1.4
115	0.7	1.7	242.2	54.4	1.2
116	0.8	1.3	217.3	48.8	1.4
117	0.8	1.5	195.8	44.0	1.0
118	0.7	1.9	449.1	101.0	0.9
119	0.7	1.5	401.5	90.3	1.2
120	0.8	1.6	368.9	82.9	1.0
121	0.7	1.4	255.1	57.4	1.8
122	0.8	1.6	228.8	51.4	1.0
123	0.8	1.4	198.1	44.5	1.2
124	0.7	1.7	447.2	100.5	1.0
125	0.7	1.5	391.6	88.0	1.1
126	0.7	1.5	369.8	83.1	1.0
127	0.7	2.8	334.7	75.2	0.5
128	0.7	2.3	295.9	66.5	0.7
129	0.7	2.0	279.4	62.8	0.7
130	0.6	2.8	556.5	125.1	0.6
131	0.7	2.4	502.9	113.1	0.6
132	0.7	2.2	463.4	104.2	0.7
133	0.7	2.9	344.2	77.4	0.5
134	0.7	2.5	312.1	70.2	0.6
135	0.7	1.9	291.4	65.5	0.7
136	0.6	2.5	629.5	141.5	0.6
137	0.6	2.2	549.6	123.6	0.7
138	0.7	1.7	493.0	110.8	0.8
139	0.6	2.4	328.8	73.9	0.6
140	0.7	2.3	314.4	70.7	0.7
141	0.7	2.1	278.8	62.7	0.7
142	0.6	2.1	572.2	128.6	0.8
143	0.7	2.2	570.5	128.3	0.7
144	0.7	1.9	491.5	110.5	0.8
145	0.7	2.2	873.6	196.4	0.7
146	0.8	1.6	867.1	194.9	0.9
147	0.8	1.4	713.9	160.5	1.1
148	0.7	2.1	1589.8	357.4	0.8

run	Friction Co-efficient	Shear Strain Y Merchant	Resulatant force (newtons) Merchant	Resulatant force (lbf) Merchant	Shear Strain Y Vishnu
149	0.8	2.1	1485.2	333.9	0.7
150	0.8	1.3	1350.1	303.5	1.3
151	0.7	2.7	996.4	224.0	0.6
152	0.8	1.6	931.8	209.5	1.0
153	0.9	1.6	817.0	183.7	1.0
154	0.7	1.9	1677.9	377.2	0.9
155	0.8	1.9	1626.4	365.6	0.7
156	0.9	1.3	1461.3	328.5	1.1
157	0.7	3.0	919.5	206.7	0.5
158	0.8	2.2	974.5	219.1	0.7
159	0.9	1.2	765.8	172.2	1.3
160	0.7	2.2	1776.2	399.3	0.8
161	0.8	1.4	1700.7	382.3	1.0
162	0.8	1.1	1425.8	320.5	1.5
163	0.8	2.2	1001.0	225.0	0.8
164	0.8	1.2	890.2	200.1	1.6
165	0.8	1.1	766.1	172.2	1.5
166	0.7	1.8	1896.9	426.4	0.9
167	0.8	1.7	1613.7	362.8	1.0
168	0.8	1.4	1419.7	319.2	1.0
169	0.8	1.8	1021.8	229.7	0.9
170	0.8	1.4	1093.5	245.8	1.1
171	0.9	1.6	897.1	201.7	0.9
172	0.7	1.5	1748.9	393.2	1.2
173	0.8	1.5	1677.7	377.2	1.1
174	0.8	1.4	1535.3	345.2	1.0
175	0.8	2.3	1324.2	297.7	0.7
176	0.8	1.5	1092.8	245.7	1.0
177	0.9	1.3	875.5	196.8	1.0
178	0.7	1.7	1771.1	398.2	0.9
179	0.8	1.6	1818.0	408.7	0.9
180	0.8	1.3	1546.3	347.6	1.1
181	0.7	1.5	979.8	220.3	1.4
182	0.8	1.8	804.3	180.8	0.8
183	0.8	1.2	736.2	165.5	1.3
184	0.7	1.5	1834.2	412.3	1.5
185	0.8	1.5	1635.8	367.8	1.1

run	Friction Co-efficient	Shear Strain Y Merchant	Resulatant force (newtons) Merchant	Resulatant force (lbf) Merchant	Shear Strain Y Vishnu
186	0.8	1.2	1596.8	359.0	1.5
187	0.8	2.1	1175.3	264.2	0.9
188	0.8	1.3	935.3	210.3	1.4
189	0.9	1.3	971.0	218.3	1.4
190	0.8	1.8	1951.2	438.6	1.0
191	0.8	1.5	1631.5	366.8	1.1
192	0.8	1.4	1621.1	364.4	1.0
193	0.8	1.6	1044.6	234.8	1.1
194	0.8	1.2	920.6	207.0	1.5
195	0.9	1.3	839.7	188.8	1.5
196	0.8	1.5	1895.6	426.1	1.3
197	0.8	1.5	1687.0	379.3	1.0
198	0.9	1.5	1721.2	386.9	1.0
199	0.6	1.3	115.9	26.0	10.9
200	0.9	1.2	119.3	26.8	3.6
201	0.7	1.1	108.9	24.5	3.9
202	0.5	1.3	176.1	39.6	7.2
203	0.6	1.2	171.6	38.6	6.5
204	0.6	1.1	171.3	38.5	4.7
205	0.6	1.3	107.9	24.2	3.9
206	0.7	1.2	113.0	25.4	3.7
207	0.7	1.1	112.7	25.3	3.7
208	0.5	1.3	175.4	39.4	7.5
209	0.5	1.2	172.0	38.7	8.8
210	0.6	1.1	172.4	38.8	3.9
211	0.6	1.3	106.9	24.0	6.1
212	0.7	1.2	112.0	25.2	6.1
213	0.7	1.2	113.2	25.5	2.4
214	0.5	1.3	174.7	39.3	13.3
215	0.5	1.3	170.2	38.3	5.7
216	0.6	1.1	170.3	38.3	6.9
217	0.7	1.6	111.7	25.1	15.6
218	0.8	1.2	118.4	26.6	10.4
219	0.9	1.0	113.3	25.5	9.2
220	0.5	1.3	195.7	44.0	-14.3
221	0.7	1.2	186.2	41.9	-65.2
222	0.7	1.1	180.7	40.6	-15.3

run	Friction Co-efficient	Shear Strain Y Merchant	Resulatant force (newtons) Merchant	Resulatant force (lbf) Merchant	Shear Strain Y Vishnu
223	0.7	1.3	114.8	25.8	-6.4
224	0.8	1.2	110.5	24.8	22.8
225	0.9	1.0	109.9	24.7	4.0
226	0.5	1.3	184.2	41.4	-7.9
227	0.7	1.2	177.0	39.8	-112.5
228	0.7	1.1	177.8	40.0	10.6
229	0.7	1.3	104.3	23.4	-27.2
230	0.9	1.2	108.3	24.3	37.1
231	0.9	1.0	111.8	25.1	8.4
232	0.5	1.3	174.6	39.3	-31.1
233	0.7	1.2	184.0	41.4	-23.8
234	0.7	1.1	183.8	41.3	92.6
235	0.8	4.1	338.8	76.2	0.3
236	0.8	2.8	297.7	66.9	0.5
237	0.8	2.1	236.7	53.2	0.6
238	0.7	3.0	556.8	125.2	0.4
239	0.7	3.0	446.3	100.3	0.5
240	0.8	2.1	426.2	95.8	0.6
241	0.7	2.3	341.2	76.7	0.6
242	0.8	1.9	312.2	70.2	0.7
243	0.8	2.3	240.8	54.1	0.6
244	0.7	2.5	565.4	127.1	0.6
245	0.8	2.8	498.3	112.0	0.5
246	0.7	2.4	389.9	87.7	0.5
247	0.7	3.3	327.6	73.6	0.4
248	0.8	2.4	318.8	71.7	0.6
249	0.8	3.2	257.5	57.9	0.4
250	0.7	2.9	547.9	123.2	0.5
251	0.8	2.4	528.5	118.8	0.5
252	0.8	2.7	427.2	96.0	0.4
253	0.7	1.7	228.2	51.3	1.2
254	0.8	1.4	237.0	53.3	1.5
255	0.8	1.3	198.4	44.6	1.2
256	0.7	2.0	439.9	98.9	0.9
257	0.7	1.6	393.4	88.4	1.2
258	0.7	1.3	367.4	82.6	1.2
259	0.7	2.2	242.5	54.5	0.9

run	Friction Co-efficient	Shear Strain Y Merchant	Resulatant force (newtons) Merchant	Resulatant force (lbf) Merchant	Shear Strain Y Vishnu
260	0.8	1.7	243.8	54.8	1.1
261	0.8	1.3	202.4	45.5	1.2
262	0.7	2.0	444.0	99.8	0.9
263	0.7	1.4	402.2	90.4	1.1
264	0.7	1.6	380.2	85.5	0.9
265	0.7	1.9	234.4	52.7	1.1
266	0.8	1.4	213.3	48.0	1.3
267	0.8	1.3	197.1	44.3	1.2
268	0.7	1.8	446.1	100.3	1.0
269	0.7	1.6	404.8	91.0	1.1
270	0.7	1.4	373.3	83.9	1.1
271	0.7	2.8	309.0	69.5	0.5
272	0.7	2.7	313.8	70.5	0.5
273	0.7	1.9	269.9	60.7	0.8
274	0.6	2.6	619.7	139.3	0.7
275	0.6	2.0	527.7	118.6	0.8
276	0.7	2.1	482.8	108.5	0.7
277	0.7	2.8	344.0	77.3	0.5
278	0.7	2.0	314.6	70.7	0.7
279	0.7	1.7	261.9	58.9	0.8
280	0.6	2.4	589.6	132.5	0.7
281	0.7	2.2	561.4	126.2	0.8
282	0.7	1.9	486.9	109.5	0.8
283	0.7	2.9	340.8	76.6	0.6
284	0.7	1.8	305.7	68.7	0.9
285	0.7	1.6	257.0	57.8	0.9
286	0.6	2.2	593.2	133.4	0.8
287	0.7	2.0	570.3	128.2	0.8
288	0.7	1.8	497.7	111.9	0.8
289	0.7	1.9	859.6	193.3	0.8
290	0.8	2.0	890.1	200.1	1.0
291	0.8	1.7	701.3	157.6	0.8
292	0.7	2.2	1592.8	358.1	0.7
293	0.8	1.5	1530.6	344.1	1.0
294	0.8	1.3	1344.4	302.2	1.3
295	0.7	2.8	942.2	211.8	0.6
296	0.8	2.2	956.9	215.1	0.7

run	Friction Co-efficient	Shear Strain Y Merchant	Resulatant force (newtons) Merchant	Resulatant force (lbf) Merchant	Shear Strain Y Vishnu
297	0.9	1.7	758.5	170.5	0.9
298	0.7	2.0	1714.4	385.4	0.8
299	0.8	2.0	1578.8	354.9	0.7
300	0.9	1.3	1379.7	310.2	1.1
301	0.7	3.0	936.2	210.5	0.6
302	0.8	1.7	915.7	205.8	0.9
303	0.9	1.3	837.5	188.3	1.3
304	0.7	1.5	1613.8	362.8	1.0
305	0.8	1.6	1645.6	369.9	0.9
306	0.8	1.3	1462.7	328.8	1.1
307	0.8	1.8	1029.0	231.3	1.0
308	0.8	1.8	861.8	193.7	0.9
309	0.8	1.2	753.4	169.4	1.4
310	0.7	1.5	1776.5	399.4	1.2
311	0.8	1.5	1643.5	369.5	1.1
312	0.8	1.5	1466.0	329.6	1.1
313	0.8	1.7	973.0	218.7	0.9
314	0.8	1.6	1061.2	238.6	1.0
315	0.9	1.5	937.3	210.7	0.9
316	0.7	1.8	1805.4	405.9	1.0
317	0.8	1.6	1602.9	360.4	1.0
318	0.8	1.5	1543.0	346.9	1.0
319	0.8	2.0	1076.9	242.1	0.8
320	0.8	1.4	1071.7	240.9	1.2
321	0.9	1.2	872.3	196.1	1.2
322	0.7	1.6	1765.6	396.9	1.2
323	0.8	1.6	1591.8	357.9	1.0
324	0.9	1.6	1590.9	357.7	0.9
325	0.8	1.4	889.0	199.9	1.3
326	0.8	1.8	891.7	200.5	0.8
327	0.8	1.3	796.9	179.1	1.2
328	0.7	1.6	1816.9	408.5	1.3
329	0.8	1.4	1657.3	372.6	1.3
330	0.8	1.4	1565.8	352.0	1.1
331	0.8	1.4	1039.4	233.7	1.5
332	0.8	1.5	877.2	197.2	1.1
333	0.9	1.1	996.6	224.0	1.6

run	Friction Co-efficient	Shear Strain Y Merchant	Resulatant force (newtons) Merchant	Resulatant force (lbf) Merchant	Shear Strain Y Vishnu
334	0.8	1.6	1961.4	440.9	1.0
335	0.8	1.6	1713.3	385.2	0.9
336	0.9	1.4	1665.0	374.3	1.1
337	0.8	1.5	1089.6	244.9	1.2
338	0.8	1.8	938.3	210.9	0.9
339	0.9	1.1	908.5	204.2	1.7
340	0.8	1.5	1930.2	433.9	1.6
341	0.8	1.5	1706.5	383.6	1.0
342	0.9	1.6	1621.8	364.6	1.0
343	0.7	1.3	110.3	24.8	7.0
344	0.7	1.2	107.3	24.1	5.3
345	0.7	1.1	103.2	23.2	3.9
346	0.5	1.3	169.6	38.1	8.8
347	0.6	1.2	169.0	38.0	7.1
348	0.6	1.2	167.4	37.6	3.8
349	0.6	1.3	109.1	24.5	5.8
350	0.7	1.2	105.9	23.8	3.7
351	0.7	1.2	116.5	26.2	2.9
352	0.5	1.3	165.5	37.2	8.5
353	0.5	1.2	164.3	36.9	11.2
354	0.6	1.1	162.8	36.6	3.4
355	0.6	1.3	111.3	25.0	5.9
356	0.7	1.3	104.4	23.5	2.8
357	0.7	1.1	112.9	25.4	2.7
358	0.5	1.4	165.2	37.1	7.8
359	0.5	1.3	165.5	37.2	5.2
360	0.6	1.1	162.8	36.6	5.6
361	0.7	1.3	106.5	23.9	5.8
362	0.9	1.2	112.6	25.3	7.2
363	0.9	1.0	122.5	27.5	6.2
364	0.6	1.3	183.0	41.1	-17.5
365	0.7	1.2	184.5	41.5	-38.0
366	0.8	1.0	182.5	41.0	23.7
367	0.7	1.3	112.4	25.3	-33.9
368	0.8	1.2	112.3	25.3	-98.2
369	0.9	1.1	120.4	27.1	6.4
370	0.6	1.3	169.1	38.0	-17.4

run	Friction Co-efficient	Shear Strain Y Merchant	Resulatant force (newtons) Merchant	Resulatant force (lbf) Merchant	Shear Strain Y Vishnu
371	0.7	1.2	186.5	41.9	72.1
372	0.7	1.0	177.4	39.9	21.5
373	0.7	1.3	117.1	26.3	-13.2
374	0.8	1.2	115.0	25.9	-30.3
375	0.9	1.1	115.5	26.0	5.7
376	0.5	1.3	181.7	40.8	-17.0
377	0.7	1.2	182.6	41.0	78.5
378	0.7	1.0	184.4	41.5	40.7
379	0.8	4.1	334.2	75.1	0.3
380	0.8	2.2	313.3	70.4	0.7
381	0.8	2.6	246.4	55.4	0.5
382	0.7	3.6	542.5	121.9	0.4
383	0.7	3.3	506.2	113.8	0.4
384	0.8	2.3	412.4	92.7	0.5
385	0.7	2.9	326.1	73.3	0.4
386	0.8	2.4	307.9	69.2	0.6
387	0.8	3.5	257.1	57.8	0.4
388	0.7	3.0	526.9	118.5	0.5
389	0.7	2.4	517.4	116.3	0.5
390	0.8	2.5	393.9	88.5	0.5
391	0.7	3.5	334.9	75.3	0.4
392	0.8	3.2	296.5	66.7	0.4
393	0.8	3.0	272.3	61.2	0.5
394	0.7	3.0	555.3	124.8	0.5
395	0.8	3.0	516.3	116.1	0.5
396	0.8	2.3	426.8	96.0	0.6
397	0.7	1.6	243.4	54.7	2.0
398	0.8	1.3	227.4	51.1	2.2
399	0.8	1.1	195.7	44.0	1.9
400	0.7	2.0	442.8	99.6	1.0
401	0.7	1.6	413.0	92.8	1.3
402	0.8	1.2	370.4	83.3	1.4
403	0.7	1.6	239.6	53.9	1.3
404	0.8	1.6	217.3	48.9	1.0
405	0.8	1.3	203.8	45.8	1.2
406	0.7	1.8	404.6	90.9	1.0
407	0.7	1.7	388.0	87.2	1.0

run	Friction Co-efficient	Shear Strain Y Merchant	Resulatant force (newtons) Merchant	Resulatant force (lbf) Merchant	Shear Strain Y Vishnu
408	0.8	1.5	367.5	82.6	1.1
409	0.7	1.5	248.2	55.8	1.3
410	0.8	1.5	235.6	53.0	1.2
411	0.8	1.2	207.6	46.7	1.5
412	0.7	1.9	463.7	104.2	1.0
413	0.7	1.6	392.5	88.2	1.1
414	0.8	1.6	367.5	82.6	1.0
415	0.7	2.6	335.8	75.5	0.6
416	0.7	2.7	312.4	70.2	0.5
417	0.7	1.9	247.2	55.6	0.8
418	0.6	2.3	620.7	139.5	0.7
419	0.7	2.0	536.1	120.5	0.8
420	0.7	1.9	500.3	112.5	0.7
421	0.7	2.9	355.1	79.8	0.5
422	0.7	2.0	309.3	69.5	0.7
423	0.7	1.5	259.7	58.4	1.0
424	0.6	2.5	616.3	138.5	0.6
425	0.7	2.2	565.9	127.2	0.7
426	0.7	1.7	506.5	113.9	0.8
427	0.7	2.9	335.2	75.4	0.5
428	0.7	2.2	316.2	71.1	0.7
429	0.7	2.0	268.6	60.4	0.7
430	0.6	2.4	620.9	139.6	0.7
431	0.7	2.3	573.5	128.9	0.7
432	0.7	2.1	498.5	112.1	0.6

run	Resultant Shear Stress Merchant (MPa)	Resultant Shear Stress Payton (MPa)	Resultant Shear Stress Vishnu (MPa)	Specific Horsepower (hp*min/in ³)	Coefficient of Friction μ (μ)
1	1582.4946	1582.5230	1953.4031	12.15587879	1.072176907
2	1194.4807	1194.5022	685.5702	3.364212121	0.868017149
3	1222.1008	1222.1228	1029.0308	3.2118	0.963009285
4	1083.1947	1083.2142	1396.6366	11.76466667	1.215245804
5	1268.2853	1268.3081	1707.7391	10.41636364	1.101362887
6	1254.9858	1255.0084	1409.9061	2.613878788	1.055736922
7	710.9989	711.0117	898.7820	12.73569697	1.077815699
8	1417.6063	1417.6319	959.8426	4.211490909	0.855197725
9	1344.7332	1344.7574	884.1010	1.350751515	0.89783108
10	1210.9768	1210.9986	1674.2892	3.251569697	1.098473231
11	1001.9182	1001.9362	1193.0421	1.590139394	0.781698252
12	1226.7555	1226.7775	1430.6701	1.502763636	0.853980983
13	868.9648	868.9804	1003.2777	1.406206061	1.158221442
14	1071.9049	1071.9242	700.3585	2.868054545	1.002023494
15	1542.4135	1542.4413	995.8859	11.81842424	0.842227771
16	1147.7074	1147.7281	1536.3401	3.786945455	0.867083538
17	1409.5445	1409.5699	1520.7806	11.37206061	1.0661282
18	1297.9453	1297.9686	1543.1517	13.75830303	1.06902359
19	1435.7595	1435.7853	1254.7610	4.180824242	0.855725793
20	1069.8691	1069.8884	1109.0325	1.192172727	0.605319712
21	1816.0648	1816.0974	1908.1919	3.61330303	0.894983602
22	1806.5954	1806.6279	3713.7523	3.845236364	1.015665563
23	1457.1515	1457.1777	1466.8955	11.52369697	1.001186249
24	1362.1257	1362.1503	1390.1754	2.693939394	0.838521252
25	1443.8231	1443.8491	1486.6400	3.823	0.734043891
26	1238.2075	1238.2298	1369.3690	13.29769697	1.143651719
27	1669.7260	1669.7560	1721.8281	2.989939394	0.760321017
28	1661.7702	1661.8001	1764.4316	3.955290909	1.02365251
29	1263.3943	1263.4170	1362.6959	10.32493939	1.136276019
30	1289.5737	1289.5970	1321.1081	3.846212121	0.788609002
31	1532.3837	1532.4112	1380.6122	2.627184848	0.839038155
32	1753.3009	1753.3325	1835.2008	4.027393939	0.898234942
33	1680.5471	1680.5774	1801.2060	12.80121212	0.961447316
34	1606.9588	1606.9878	1723.7485	1.161075758	0.603161112
35	1338.9537	1338.9778	1535.1947	13.35593939	1.126249856
36	1497.9546	1497.9815	1668.7963	10.15351515	1.176602036
37	1793.0415	1793.0738	1672.7636	10.15893939	1.164261602

run	Resultant Shear Stress Merchant (MPa)	Resultant Shear Stress Payton (MPa)	Resultant Shear Stress Vishnu (MPa)	Specific Horsepower (hp*min/in ³)	Coefficient of Friction μ (Mu)
38	1369.1770	1369.2016	1574.7048	1.138587879	0.525247463
39	1640.5144	1640.5439	1687.3700	2.863490909	0.989762649
40	1754.5663	1754.5979	1883.5466	11.84266667	1.23542832
41	1457.4843	1457.5105	1483.9302	1.190175758	0.530284709
42	1452.7984	1452.8246	1783.8645	11.61554545	0.851141164
43	2147.8285	2147.8672	2271.9258	3.719242424	0.742738816
44	1578.0758	1578.1042	1661.7598	12.78418182	0.926654232
45	1950.2055	1950.2406	2167.6092	4.446054545	0.77705307
46	1715.9705	1716.0013	1921.5379	12.63184848	0.96484302
47	1640.6371	1640.6666	1698.7903	11.65751515	0.986730703
48	1435.3904	1435.4162	1664.3215	1.417236364	0.816816663
49	2026.6246	2026.6611	2102.0930	1.444624242	1.123189343
50	2011.5914	2011.6276	1992.5385	8.388727273	1.118950093
51	1825.7813	1825.8142	1867.0145	4.221939394	0.702997403
52	1906.6306	1906.6649	1914.6626	1.518072727	0.724175269
53	1461.9762	1462.0025	1586.6590	4.380969697	0.754999922
54	1198.2231	1198.2447	1252.0956	4.231224242	0.916180723
55	272.1559	272.1608	239.9759	1.216181818	0.810626247
56	305.9802	305.9857	285.9270	2.303663636	0.930739476
57	309.4853	309.4909	262.6205	9.998333333	1.100130614
58	202.5343	202.5380	172.0010	2.488615152	0.931622055
59	217.0918	217.0957	192.8495	1.428084848	0.840686073
60	213.5250	213.5288	192.6087	10.68781818	1.180514504
61	286.7429	286.7481	322.1734	2.652036364	1.027199364
62	274.9925	274.9974	232.7535	3.39330303	0.779602708
63	269.8254	269.8303	236.3283	2.706372727	1.010570825
64	187.0501	187.0535	155.8900	1.296133333	0.871376333
65	175.7943	175.7975	161.2195	12.50939394	1.130538873
66	199.4687	199.4723	173.9538	11.14369697	1.023002169
67	264.9957	265.0004	232.3570	1.5014	1.277301431
68	161.1734	161.1763	119.8778	1.111406061	0.596118358
69	264.4911	264.4958	201.9117	14.16860606	1.022785029
70	190.3290	190.3324	167.9906	12.02187879	0.924365535
71	184.1849	184.1882	143.7442	3.022781818	0.931302118
72	181.5601	181.5634	140.6402	3.148757576	0.810423443
73	315.2454	315.2511	347.1525	1.463927273	1.114546452
74	267.6603	267.6651	282.1055	11.50339394	1.027290277

run	Resultant Shear Stress Merchant (MPa)	Resultant Shear Stress Payton (MPa)	Resultant Shear Stress Vishnu (MPa)	Specific Horsepower (hp*min/in ³)	Coefficient of Friction μ (μ)
75	266.4894	266.4942	261.5549	3.339545455	0.816052302
76	240.7695	240.7738	251.2888	3.53230303	0.871171975
77	248.0244	248.0289	242.9087	3.728957576	0.979802711
78	243.0798	243.0842	219.3345	1.557151515	0.844221
79	243.4582	243.4625	209.0123	10.53581818	1.071259131
80	250.9815	250.9860	205.6920	10.04181818	1.049796975
81	245.5677	245.5721	237.8468	10.96348485	1.204599324
82	218.0140	218.0179	203.4712	3.168266667	0.876428834
83	218.6045	218.6085	189.5875	9.902878788	1.174976723
84	221.1308	221.1348	211.8123	1.192224242	0.593609836
85	242.6597	242.6640	200.0082	10.98242424	0.998121473
86	277.4431	277.4481	238.3332	10.98651515	1.002106994
87	288.5634	288.5686	262.9864	1.26430303	0.614830876
88	219.6417	219.6457	219.7242	3.982315152	0.810279899
89	235.4428	235.4470	208.9138	2.637333333	0.97138619
90	218.0573	218.0612	186.9981	1.152781818	0.503582908
91	260.7676	260.7723	179.5229	12.92212121	1.008337118
92	209.7498	209.7535	179.2285	1.425678788	0.70929057
93	234.8043	234.8085	190.9114	3.251569697	1.078498938
94	242.8572	242.8615	188.3894	1.461206061	0.683491372
95	172.8167	172.8198	154.4243	3.777169697	0.874080391
96	206.5691	206.5728	162.4910	11.88709091	0.904032492
97	263.0168	263.0216	174.8449	10.98072727	0.929178803
98	381.7762	381.7831	204.0631	2.616233333	0.812187467
99	268.1752	268.1800	151.7192	10.21430303	0.804456839
100	286.2343	286.2395	199.7675	11.96145455	0.860296449
101	320.3607	320.3665	201.3792	1.643478788	0.784542883
102	225.6267	225.6308	220.6299	11.57278788	0.946434942
103	324.6935	324.6994	256.1624	13.76436364	1.071696475
104	217.4169	217.4208	182.1962	3.347545455	0.826533538
105	242.3502	242.3546	235.0281	3.019357576	0.979558149
106	238.4951	238.4994	201.8158	1.139966667	0.714056041
107	213.4073	213.4111	172.1480	11.64006061	1.016360347
108	268.6244	268.6292	254.8868	11.87778788	0.939379229
109	443.7516	443.7596	205.6020	10.39442424	1.119618522
110	616.5564	616.5675	268.4437	1.454406061	0.834813763
111	461.9859	461.9942	453.3987	3.948945455	0.868691813

run	Resultant Shear Stress Merchant (MPa)	Resultant Shear Stress Payton (MPa)	Resultant Shear Stress Vishnu (MPa)	Specific Horsepower (hp*min/in ³)	Coefficient of Friction μ (Mu)
112	355.0989	355.1053	204.8549	3.251909091	0.935302116
113	361.4451	361.4516	257.5033	12.20021212	1.02728082
114	355.1746	355.1810	405.2499	10.15893939	1.095831262
115	424.2882	424.2958	427.5455	1.295190909	0.761428935
116	490.8583	490.8672	564.0105	12.41784848	0.912181365
117	333.5117	333.5177	380.5394	11.40315152	0.847206912
118	340.0101	340.0163	336.5856	3.270927273	0.847645887
119	363.3656	363.3721	384.5881	1.261821212	0.81401596
120	294.6031	294.6084	316.7067	1.196833333	0.891839497
121	547.5157	547.5256	443.1704	3.711333333	0.747292704
122	400.1429	400.1501	402.4171	1.427187879	1.349266473
123	379.0802	379.0870	381.6371	10.62824242	1.014738776
124	370.4515	370.4582	366.0340	11.55278788	1.234176349
125	362.5726	362.5791	383.5700	3.318478788	0.910291341
126	331.1829	331.1888	312.2099	2.496293939	0.922923536
127	324.2860	324.2919	271.6786	3.154581818	1.104826322
128	346.5491	346.5553	288.3217	11.10418182	0.876270123
129	351.5625	351.5688	255.9939	2.871618182	1.016218335
130	270.0280	270.0329	260.8921	2.725815152	0.810215787
131	274.2075	274.2124	264.6838	1.207954545	0.599297066
132	272.8403	272.8452	278.3669	4.565715152	0.787379766
133	325.3917	325.3976	286.6834	8.238545455	1.116258633
134	331.3267	331.3327	313.8126	1.185727273	0.685278824
135	378.8152	378.8220	306.9177	11.13069697	0.915685685
136	339.5491	339.5552	299.3921	2.955160606	0.812041029
137	328.8769	328.8828	324.4577	11.41242424	1.28647597
138	365.8827	365.8893	366.3222	1.2149	0.910764605
139	382.8460	382.8529	267.2501	2.531490909	0.861326543
140	358.4357	358.4422	302.4507	10.18260606	0.973751452
141	334.3717	334.3777	305.7842	1.140175758	0.699194336
142	366.2371	366.2437	351.9777	4.313254545	0.928970221
143	347.2552	347.2615	341.6588	1.491806061	1.245865092
144	324.8894	324.8953	304.7451	1.481739394	1.214431425
145	1091.5689	1091.5886	1052.7227	1.45029697	0.682223435
146	1419.7414	1419.7669	899.5325	12.09969697	1.095926672
147	1331.5147	1331.5387	911.1424	1.197536364	0.545375924
148	1082.3048	1082.3242	1356.3780	1.188333333	0.834736208

run	Resultant Shear Stress Merchant (MPa)	Resultant Shear Stress Payton (MPa)	Resultant Shear Stress Vishnu (MPa)	Specific Horsepower (hp*min/in ³)	Coefficient of Friction μ (μ)
149	945.8128	945.8298	1240.9563	2.63189697	1.054207471
150	1363.7537	1363.7783	1513.3885	4.102187879	1.012059193
151	1038.7986	1038.8173	1201.9123	11.97072727	0.995267745
152	1572.3139	1572.3422	1019.6731	10.82090909	0.959959666
153	1281.7050	1281.7281	987.6794	12.594	1.318760528
154	1259.2792	1259.3019	1741.7902	10.67348485	1.03997641
155	1174.6112	1174.6323	1215.8706	1.17189697	0.57948572
156	1477.4712	1477.4978	1569.3226	3.598909091	0.850491612
157	862.4690	862.4846	1177.4352	1.536563636	0.842239231
158	1188.2993	1188.3207	842.1118	11.59233333	0.889567863
159	1696.4695	1696.5001	1427.7988	12.96975758	0.906150187
160	1144.0021	1144.0227	1620.0898	10.05490909	1.212272003
161	1646.4199	1646.4495	1639.6911	2.703551515	1.047696502
162	1730.9946	1731.0258	1988.4385	1.458284848	1.26804947
163	1254.4519	1254.4745	1283.9569	4.138818182	0.736542834
164	2072.7616	2072.7989	2082.5005	11.78224242	1.101562961
165	1744.3241	1744.3555	1717.0377	4.525781818	0.779129567
166	1455.4805	1455.5067	1665.4018	10.97751515	0.87509148
167	1261.3185	1261.3412	1343.4886	9.804757576	0.975239628
168	1244.9360	1244.9584	1306.9383	2.718172727	0.83120659
169	1627.9349	1627.9642	1845.8161	1.174636364	0.69737942
170	2177.7261	2177.7653	2113.5647	10.69736364	1.026574928
171	1429.4955	1429.5212	1302.2924	3.380757576	0.818122087
172	1628.1953	1628.2246	1699.4329	1.236842424	0.819080381
173	1490.7076	1490.7345	1710.1047	1.52990303	0.833182681
174	1363.5220	1363.5466	1337.5203	10.75521212	1.189175104
175	1631.3577	1631.3871	1549.8355	11.93969697	0.920735977
176	1983.3142	1983.3499	1950.8491	2.8998	0.82828446
177	1720.0823	1720.1132	1917.7636	3.207921212	1.053872993
178	1463.8392	1463.8656	1650.4851	4.28010303	0.883522131
179	1482.9296	1482.9563	1466.5518	1.159366667	0.591527063
180	1452.9487	1452.9749	1684.1902	11.48236364	0.912788311
181	1965.8757	1965.9111	1843.9105	1.220078788	0.924263918
182	1231.3934	1231.4156	1396.5862	2.808424242	0.996319932
183	1569.3193	1569.3476	1840.6235	10.30527273	1.070809451
184	1828.5392	1828.5721	1933.9389	10.7360303	1.132137342
185	1448.5581	1448.5842	1569.1816	10.57163636	1.009062179

run	Resultant Shear Stress Merchant (MPa)	Resultant Shear Stress Payton (MPa)	Resultant Shear Stress Vishnu (MPa)	Specific Horsepower (hp*min/in ³)	Coefficient of Friction μ (Mu)
186	1785.7693	1785.8014	1883.3982	2.47989697	0.926235971
187	1573.6977	1573.7260	1569.8945	12.13969697	0.997710682
188	2056.7288	2056.7659	2033.4294	9.803939394	1.080488988
189	1935.3212	1935.3560	1841.8100	3.306787879	0.822622142
190	1512.5647	1512.5919	1422.1242	11.44139394	0.86942078
191	1533.6946	1533.7222	1698.8519	9.485272727	1.089108351
192	1461.6955	1461.7218	1670.3894	3.281939394	0.804648471
193	1829.6509	1829.6838	1750.3948	11.58721212	0.875032063
194	2116.7330	2116.7711	2298.0915	14.79412121	1.091252185
195	1721.0294	1721.0604	1869.3510	2.951542424	0.803808508
196	1836.3426	1836.3756	2245.7979	14.15878788	0.998970144
197	1510.7973	1510.8244	1711.3574	3.652812121	0.890412424
198	1467.2068	1467.2333	1559.7531	1.427660606	1.131638517
199	267.7445	267.7493	220.7784	2.974260606	0.897264891
200	289.3109	289.3161	258.7553	4.186272727	1.016683906
201	248.7084	248.7129	214.4487	1.518187879	1.23269293
202	221.2927	221.2966	209.4344	1.244760606	0.874213313
203	204.9440	204.9477	184.0667	1.202524242	0.896454673
204	207.0324	207.0362	181.4020	3.937878788	0.736131904
205	264.3534	264.3581	250.7709	1.437212121	0.687126361
206	284.9773	284.9824	241.2066	9.489515152	1.098339023
207	260.3433	260.3480	216.5681	3.155836364	0.906490361
208	197.8286	197.8322	168.2642	3.786272727	0.783639671
209	190.6842	190.6877	152.1919	9.477272727	1.054125417
210	211.4359	211.4397	186.9074	3.219115152	0.973960983
211	259.1467	259.1513	232.0507	3.909860606	1.014436259
212	258.2589	258.2636	195.6799	4.426666667	0.925133066
213	247.7408	247.7453	223.3868	2.566887879	0.922091442
214	209.9545	209.9583	186.3539	2.940424242	0.797677852
215	181.9638	181.9671	139.4248	1.325690909	0.605376819
216	199.9035	199.9071	166.5879	2.864190909	0.980854728
217	194.3447	194.3482	135.9791	10.44781818	0.84725874
218	314.8432	314.8489	297.2177	1.249184848	0.584759791
219	300.8782	300.8836	319.0477	3.687848485	0.893388032
220	235.9518	235.9560	221.0410	4.558036364	0.793537685
221	220.9236	220.9276	177.8767	4.102466667	0.78027099
222	227.9730	227.9772	199.8596	1.507963636	0.801065051

run	Resultant Shear Stress Merchant (MPa)	Resultant Shear Stress Payton (MPa)	Resultant Shear Stress Vishnu (MPa)	Specific Horsepower (hp*min/in ³)	Coefficient of Friction μ (Mu)
223	279.5877	279.5927	210.6108	1.388648485	1.1792437
224	275.4339	275.4389	254.6242	12.71175758	0.925181293
225	292.7926	292.7979	264.7833	1.363078788	0.882080802
226	215.3696	215.3735	175.2876	1.183051515	0.601848806
227	217.6444	217.6483	203.8960	11.89239394	0.928349028
228	215.0511	215.0549	197.4561	3.506757576	0.935125626
229	277.5264	277.5314	271.7989	11.16069697	1.020096656
230	263.4255	263.4302	243.6391	2.6722	0.953201674
231	289.6437	289.6489	259.0463	4.202909091	0.856399546
232	217.5310	217.5349	223.7412	12.67175758	1.08666468
233	225.8067	225.8108	194.0231	11.7169697	0.998970144
234	230.1764	230.1805	194.1531	11.42921212	0.988782165
235	238.0420	238.0463	184.6251	11.88709091	1.134540182
236	294.5570	294.5623	221.7940	10.19451515	1.147086915
237	298.8613	298.8667	238.6578	4.384406061	0.939310661
238	261.3992	261.4039	181.2506	11.06178788	0.971087721
239	208.4111	208.4149	146.6639	10.65890909	0.971087721
240	265.0381	265.0428	227.6783	11.30933333	1.204772393
241	426.5816	426.5892	208.1909	2.634851515	0.910185751
242	447.9739	447.9819	231.9247	3.646272727	0.869619463
243	271.8996	271.9045	188.6668	1.194421212	0.498545205
244	326.2002	326.2061	241.9502	1.517066667	0.81239598
245	241.6611	241.6654	194.4823	2.632863636	0.86094227
246	214.2046	214.2085	184.9259	11.08957576	1.007614005
247	286.4832	286.4884	210.6557	1.166754545	0.719932214
248	358.9823	358.9888	286.5423	1.432060606	1.275386303
249	217.5506	217.5546	138.0460	10.92472727	1.292785736
250	269.1365	269.1413	211.9668	10.17951515	1.101562961
251	299.8154	299.8208	219.8805	1.537309091	1.094465153
252	207.9391	207.9428	193.0696	4.093951515	0.858090695
253	387.6535	387.6605	240.4661	3.548854545	0.869351197
254	471.1683	471.1768	322.2594	1.467321212	1.332279565
255	385.7879	385.7948	368.2393	12.89248485	0.966697168
256	318.2317	318.2374	157.7846	11.48260606	1.222495879
257	341.9499	341.9560	181.0852	3.045951515	0.915170777
258	369.8104	369.8171	422.0058	4.209472727	0.866710351
259	324.4804	324.4863	311.6855	12.2010303	1.064198695

run	Resultant Shear Stress Merchant (MPa)	Resultant Shear Stress Payton (MPa)	Resultant Shear Stress Vishnu (MPa)	Specific Horsepower (hp*min/in ³)	Coefficient of Friction μ (Mu)
260	393.4748	393.4819	402.6159	1.251354545	0.822388842
261	404.2862	404.2935	379.7981	14.17884848	1.10193589
262	321.1254	321.1312	318.2039	3.578393939	0.71264154
263	385.4545	385.4614	405.9887	12.59118182	0.9553611
264	313.6307	313.6364	299.2428	1.474921212	0.876415645
265	362.9505	362.9570	361.8541	1.523563636	0.788504719
266	440.2210	440.2289	502.6517	1.451757576	0.917274708
267	383.5517	383.5586	353.1030	3.303424242	0.942881597
268	350.6283	350.6347	376.8616	3.480793939	0.878718073
269	354.3236	354.3300	348.3590	2.964193939	0.928464146
270	343.5145	343.5207	321.1585	3.427915152	1.084184487
271	303.5067	303.5121	265.3932	3.963545455	0.733006983
272	313.2845	313.2901	281.3491	2.696830303	0.843484921
273	359.7607	359.7672	327.6106	13.26739394	1.043277787
274	333.8955	333.9015	279.1862	12.3320303	0.912788311
275	348.8812	348.8875	307.2470	3.843181818	0.793717405
276	292.9796	292.9848	263.1913	1.189918182	0.498004306
277	333.2012	333.2072	290.7459	1.168018182	0.63185196
278	405.7843	405.7916	348.1484	3.207921212	1.077952565
279	380.8315	380.8383	424.9964	3.130684848	0.972810233
280	332.6144	332.6204	327.1872	1.548836364	0.731202361
281	332.6912	332.6972	307.8581	8.958515152	1.114315793
282	329.3197	329.3256	344.4482	13.11133333	0.966697168
283	327.5636	327.5695	250.7249	2.867030303	0.997352641
284	445.5095	445.5175	400.4894	1.160421212	0.70051194
285	405.0998	405.1071	288.6288	10.19451515	1.054125417
286	377.9459	377.9527	326.3325	16.84763636	1.034359188
287	368.9925	368.9992	332.9816	2.519354545	0.928610911
288	349.7194	349.7257	312.5449	10.67624242	1.018117655
289	1260.5935	1260.6162	1276.1417	1.585878788	1.185352847
290	1215.1346	1215.1565	818.7298	11.19263636	1.024146029
291	1068.7978	1068.8170	863.6874	11.5469697	0.877177699
292	1032.8876	1032.9062	1507.7877	2.632548485	0.841470302
293	1390.8780	1390.9030	1585.9950	12.296	1.220454717
294	1310.0056	1310.0292	1468.8001	1.253330303	0.82215989
295	954.7501	954.7673	1247.2085	10.43375758	0.867274439
296	1186.8120	1186.8334	764.7211	2.993969697	0.996453186

run	Resultant Shear Stress Merchant (MPa)	Resultant Shear Stress Payton (MPa)	Resultant Shear Stress Vishnu (MPa)	Specific Horsepower (hp*min/in ³)	Coefficient of Friction μ (Mu)
297	1118.8503	1118.8704	812.6859	3.624490909	1.08587027
298	1201.9715	1201.9931	1715.8217	4.038872727	1.024393778
299	1039.8110	1039.8297	1097.2961	1.127521212	0.598442152
300	1320.9680	1320.9917	1616.3988	3.430115152	1.060032068
301	898.0923	898.1085	930.7468	2.862272727	0.993826153
302	1453.8591	1453.8853	985.4723	1.467460606	0.763383517
303	1699.1552	1699.1858	1267.9620	3.34290303	0.897913732
304	1504.6935	1504.7206	3091.0019	4.451751515	0.790501975
305	1417.6538	1417.6793	1480.8452	10.10448485	0.975642701
306	1383.8348	1383.8597	1599.2377	9.315939394	1.104070256
307	1600.8128	1600.8416	1702.1241	3.430115152	1.092935281
308	1293.2832	1293.3064	1308.0002	10.61075758	0.844114344
309	1669.3016	1669.3317	1545.6486	4.113369697	1.01766769
310	1712.8983	1712.9291	1951.8843	1.248327273	0.885110045
311	1460.3348	1460.3611	1449.9546	2.767221212	0.850474456
312	1244.1478	1244.1702	1180.5236	4.710448485	0.786972947
313	1608.6559	1608.6848	1742.1069	12.60218182	0.979764304
314	1804.8144	1804.8469	1695.2100	2.642660606	0.998604328
315	1592.1850	1592.2137	1721.7794	1.509527273	1.253521408
316	1403.8744	1403.8997	1589.4043	1.548012121	0.812710207
317	1344.1067	1344.1309	1461.4316	2.498015152	0.937043764
318	1307.6235	1307.6470	1497.5109	3.1194	0.905191776
319	1500.1005	1500.1275	1488.6757	10.2469697	1.20057728
320	2084.2712	2084.3087	1955.0487	10.67121212	1.192309284
321	1910.5489	1910.5833	1868.4247	3.399151515	0.814884786
322	1587.7178	1587.7464	1827.0731	10.60533333	1.086398394
323	1338.2111	1338.2352	1643.2309	10.51557576	1.150879045
324	1261.1826	1261.2053	1370.3819	13.70721212	1.032132898
325	1834.0727	1834.1057	1858.9985	10.79181818	1.024955575
326	1357.7422	1357.7666	1443.5846	1.151724242	0.566001223
327	1544.6250	1544.6528	1889.7613	12.16606061	1.106530681
328	1594.2524	1594.2811	1753.3378	3.234569697	0.898352961
329	1664.2164	1664.2464	1750.4802	11.05212121	1.167290854
330	1445.2154	1445.2414	1615.1588	1.383472727	0.919514238
331	2281.6029	2281.6440	2502.6040	1.433854545	0.876673981
332	1611.4774	1611.5064	1722.8538	1.452236364	1.127447286
333	2373.8327	2373.8755	2265.6266	1.603787879	1.239470124

run	Resultant Shear Stress Merchant (MPa)	Resultant Shear Stress Payton (MPa)	Resultant Shear Stress Vishnu (MPa)	Specific Horsepower (hp*min/in ³)	Coefficient of Friction μ (μ)
334	1765.2294	1765.2612	1942.2525	3.613060606	0.791306505
335	1425.4680	1425.4936	1717.1834	1.498145455	0.668788709
336	1575.7910	1575.8194	1806.4776	11.46290909	1.204852736
337	2076.6648	2076.7022	2067.2585	10.50118182	0.980862222
338	1429.4527	1429.4784	1483.0209	1.126633333	0.505739128
339	2393.4924	2393.5355	2468.3063	11.79672727	0.920324832
340	1823.0493	1823.0821	1802.8394	10.88621212	0.94935895
341	1540.9080	1540.9357	1764.1575	13.07654545	1.094162591
342	1344.9853	1345.0095	1334.1017	13.84666667	1.130597351
343	256.1715	256.1761	227.5480	3.068545455	0.802323988
344	249.8443	249.8488	192.9376	2.671960606	0.815101968
345	265.3367	265.3414	251.8190	1.118890909	0.605372873
346	203.0575	203.0612	180.3061	1.480872727	0.831238471
347	206.9103	206.9140	185.0425	3.536909091	0.895444559
348	178.6387	178.6419	149.6285	1.231251515	0.595104007
349	259.5769	259.5815	222.5823	4.145575758	0.735913139
350	258.1297	258.1344	227.3699	11.79345455	0.884433819
351	257.7344	257.7391	216.2811	3.113363636	0.96761863
352	188.3817	188.3851	171.2232	2.477115152	0.942229486
353	185.7690	185.7723	159.0796	12.45333333	1.080275398
354	188.4099	188.4133	170.2409	12.15236364	0.922525432
355	248.1400	248.1444	205.0165	1.447084848	1.165136832
356	211.2994	211.3032	175.3205	4.151072727	0.837199145
357	253.7977	253.8022	228.4347	4.234569697	0.92051102
358	175.2721	175.2753	146.1347	12.406	1.022472391
359	169.1572	169.1602	133.6209	3.423212121	0.941711679
360	186.1551	186.1584	154.1297	1.401127273	0.840429594
361	240.3306	240.3349	275.4202	1.143760606	0.61804004
362	265.8417	265.8465	237.8884	11.26533333	0.865646737
363	328.6272	328.6331	330.0819	10.44854545	1.058097856
364	224.4910	224.4950	219.9027	1.12469697	0.504576942
365	236.7719	236.7762	238.3472	1.149966667	0.637548882
366	240.9086	240.9129	230.9871	1.231163636	0.932503583
367	261.9813	261.9860	216.0665	4.448533333	0.784149731
368	286.9403	286.9455	283.0359	2.478966667	0.933143173
369	288.2902	288.2954	241.7424	1.424478788	0.811378803
370	206.2737	206.2774	195.6545	4.149393939	0.731935139

run	Resultant Shear Stress Merchant (MPa)	Resultant Shear Stress Payton (MPa)	Resultant Shear Stress Vishnu (MPa)	Specific Horsepower (hp*min/in ³)	Coefficient of Friction μ (μ)
371	223.8796	223.8836	200.0603	2.769351515	1.061682606
372	229.9559	229.9600	226.9181	1.468066667	0.67817758
373	283.2313	283.2364	203.4860	3.637012121	0.883108644
374	279.6908	279.6958	208.4334	12.96618182	1.292680386
375	283.5902	283.5953	214.0550	11.30115152	1.02652553
376	225.1477	225.1517	224.0103	4.178981818	0.867191725
377	223.5994	223.6034	196.9755	11.19360606	1.052186773
378	237.9430	237.9473	222.8143	11.74842424	0.991401974
379	237.2696	237.2739	167.6045	2.599912121	0.85038881
380	389.4467	389.4537	194.4221	1.200321212	0.890794835
381	250.6153	250.6198	195.4499	9.977393939	1.195590525
382	213.9357	213.9395	173.6216	3.16949697	0.902875421
383	215.4291	215.4330	155.4668	3.450515152	0.86913365
384	238.1320	238.1363	192.2563	13.75933333	1.106708683
385	320.0884	320.0941	194.3342	1.227148485	0.820751402
386	353.6261	353.6324	184.9923	3.384454545	0.829780502
387	200.1392	200.1428	161.0026	2.743733333	0.959605647
388	252.5902	252.5948	197.9047	10.0350303	1.078021339
389	297.1280	297.1333	224.3178	1.109306061	0.715487965
390	206.8756	206.8793	182.1063	3.888606061	1.026103551
391	272.6588	272.6637	215.6757	1.533115152	0.837325715
392	257.9244	257.9290	207.5233	13.27739394	0.956615234
393	244.7792	244.7836	193.9312	4.314630303	0.953116004
394	263.2336	263.2383	203.4728	10.96354545	0.959407403
395	239.2959	239.3003	192.3361	4.233018182	0.861606167
396	247.1250	247.1295	199.2420	12.42418182	0.969741472
397	455.0114	455.0196	202.6932	10.57642424	0.979561028
398	500.2531	500.2621	257.1672	2.866915152	0.986577531
399	468.3136	468.3220	631.3356	1.583618182	0.811466425
400	313.9962	314.0019	148.3141	1.109209091	0.719164874
401	346.3400	346.3462	164.7856	2.923048485	0.819229695
402	409.3122	409.3196	419.2902	11.71593939	0.998996995
403	452.2487	452.2568	468.0949	12.23224242	0.921562779
404	362.8357	362.8422	408.2336	2.610733333	1.061470289
405	393.5799	393.5870	391.5648	13.75684848	1.075293474
406	322.1283	322.1341	348.8087	3.631909091	0.876314444
407	307.0909	307.0965	337.9912	11.00933333	1.147449844

run	Resultant Shear Stress Merchant (MPa)	Resultant Shear Stress Payton (MPa)	Resultant Shear Stress Vishnu (MPa)	Specific Horsepower (hp*min/in ³)	Coefficient of Friction μ (Mu)
408	310.3792	310.3848	283.9094	3.5146	0.8864074
409	483.0136	483.0223	444.3889	1.393593939	0.925397477
410	429.0704	429.0781	392.0079	2.761172727	1.023706069
411	466.7067	466.7151	547.2294	9.78830303	1.051510251
412	347.1699	347.1761	352.9484	9.696848485	1.1225446
413	346.4454	346.4517	369.3659	1.488	1.123469973
414	305.9297	305.9352	308.6325	10.2469697	1.105783294
415	351.4480	351.4544	266.3149	8.911393939	1.124089214
416	311.6746	311.6802	299.3420	3.813878788	0.791934384
417	334.7671	334.7731	332.6188	3.439939394	0.825242167
418	364.6298	364.6363	323.8978	11.37806061	1.104096069
419	348.9527	348.9590	332.8010	11.20021212	0.883708951
420	323.9979	324.0037	294.9813	3.866606061	0.78893061
421	335.7953	335.8014	287.7443	10.34118182	1.034041012
422	412.8954	412.9029	368.5804	4.116212121	0.735890428
423	420.5644	420.5720	359.8268	1.140157576	0.746046959
424	345.6200	345.6262	335.6423	4.340654545	0.931425064
425	345.0823	345.0885	333.1309	11.82163636	1.290838236
426	365.4775	365.4840	342.7345	3.438666667	0.921776341
427	318.2066	318.2123	261.0077	1.233936364	0.654474343
428	384.4446	384.4515	309.3733	11.92575758	1.075122447
429	333.1464	333.1524	318.5636	1.235242424	0.858903663
430	358.7914	358.7979	333.2406	3.364060606	0.922825626
431	336.2491	336.2551	326.3171	11.65775758	0.856503744
432	295.3937	295.3990	290.7131	11.42527273	0.97930927

Appendix E

T-Tests of mean cutting and thrust forces for tool wear analysis. These are comparing the replicate runs

t-Test: Two-Sample Assuming Equal Variances

Cutting force 1 vs 2

	<i>cutting force (lbs force)</i>	<i>cutting force (lbs force)</i>
Mean	142.9032	143.9929
Variance	14542.34	14488.71
Observations	144	144
Pooled Variance	14515.53	
Hypothesized Mean Difference	0	
df	286	
t Stat	-0.07674	
P(T<=t) one-tail	0.469441	
t Critical one-tail	1.650199	
P(T<=t) two-tail	0.938881	
t Critical two-tail	1.968293	

t-Test: Two-Sample Assuming Equal Variances

Cutting force 2 vs 3

	<i>cutting force (lbs force)</i>	<i>cutting force (lbs force)</i>
Mean	143.9929	142.8826
Variance	14488.71	14077.31
Observations	144	144
Pooled Variance	14283.01	
Hypothesized Mean Difference	0	
df	286	
t Stat	0.078833	
P(T<=t) one-tail	0.46861	
t Critical one-tail	1.650199	
P(T<=t) two-tail	0.93722	
t Critical two-tail	1.968293	

t-Test: Two-Sample Assuming Equal Variances

Cutting force 1 vs 3

	<i>cutting force (lbs force)</i>	<i>cutting force (lbs force)</i>
Mean	142.9032	142.8826
Variance	14542.34	14077.31
Observations	144	144
Pooled Variance	14309.83	
Hypothesized Mean Difference	0	
df	286	
t Stat	0.001466	
P(T<=t) one-tail	0.499416	
t Critical one-tail	1.650199	
P(T<=t) two-tail	0.998831	
t Critical two-tail	1.968293	

t-Test: Two-Sample Assuming Equal Variances

Thrust force 1 vs 2

	<i>thrust force (lbs force)</i>	<i>thrust force (lbs force)</i>
Mean	36.67969	37.21594
Variance	1345.852	1381.035
Observations	144	144
Pooled Variance	1363.444	
Hypothesized Mean Difference	0	
df	286	
t Stat	-0.12323	
P(T<=t) one-tail	0.451006	
t Critical one-tail	1.650199	
P(T<=t) two-tail	0.902012	
t Critical two-tail	1.968293	

t-Test: Two-Sample Assuming Equal Variances

Thrust force 2 vs 3

	<i>thrust force (lbs force)</i>	<i>thrust force (lbs force)</i>
Mean	37.21594	37.21509
Variance	1381.035	1333.457
Observations	144	144
Pooled Variance	1357.246	
Hypothesized Mean Difference	0	
df	286	
t Stat	0.000196	
P(T<=t) one-tail	0.499922	
t Critical one-tail	1.650199	
P(T<=t) two-tail	0.999844	
t Critical two-tail	1.968293	

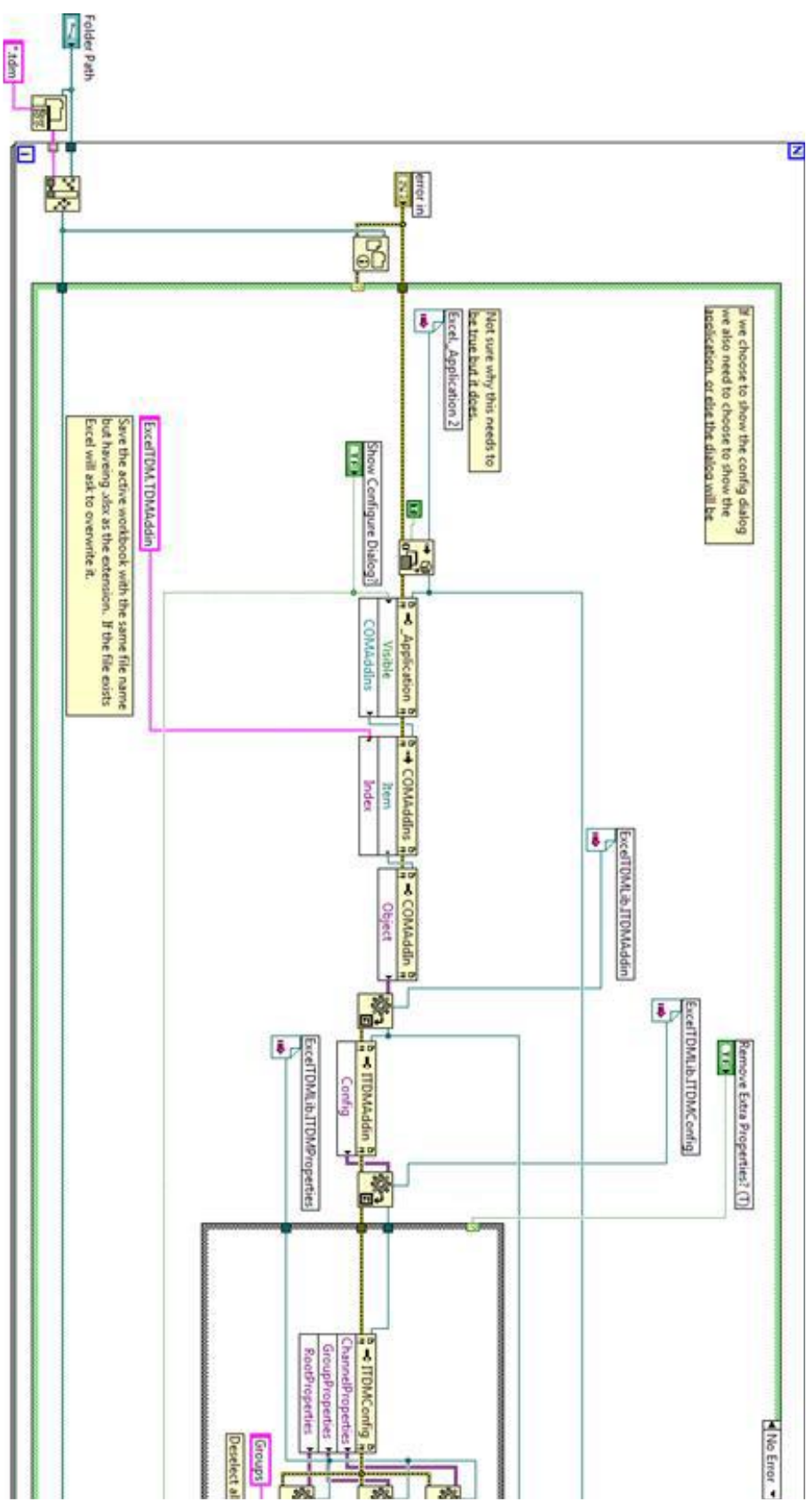
t-Test: Two-Sample Assuming Equal Variances

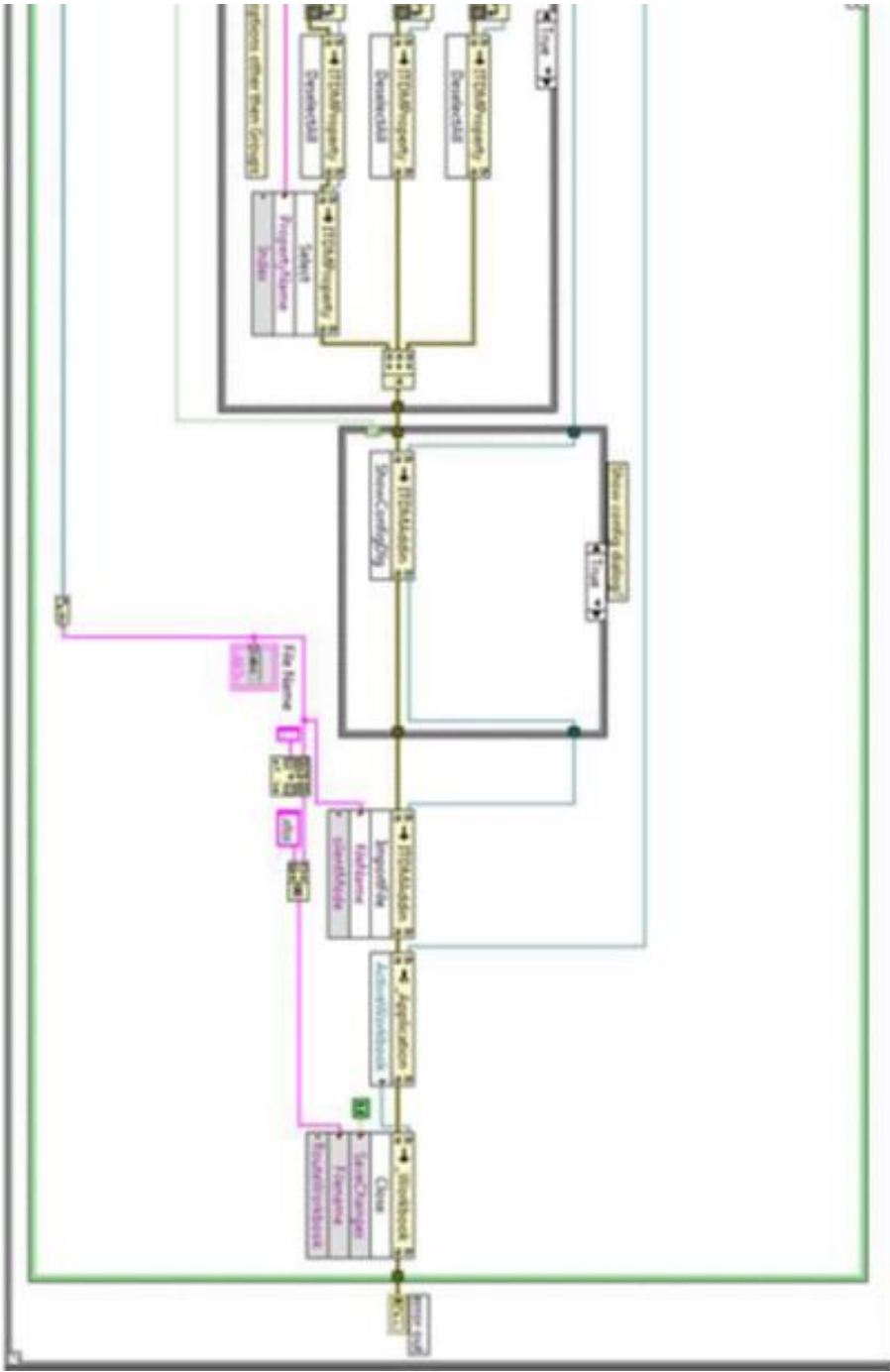
Thrust Force 1 vs 3

	<i>thrust force (lbs force)</i>	<i>thrust force (lbs force)</i>
Mean	36.67969	37.21509
Variance	1345.852	1333.457
Observations	144	144
Pooled Variance	1339.655	
Hypothesized Mean Difference	0	
df	286	
t Stat	-0.12412	
P(T<=t) one-tail	0.450653	
t Critical one-tail	1.650199	
P(T<=t) two-tail	0.901306	
t Critical two-tail	1.968293	

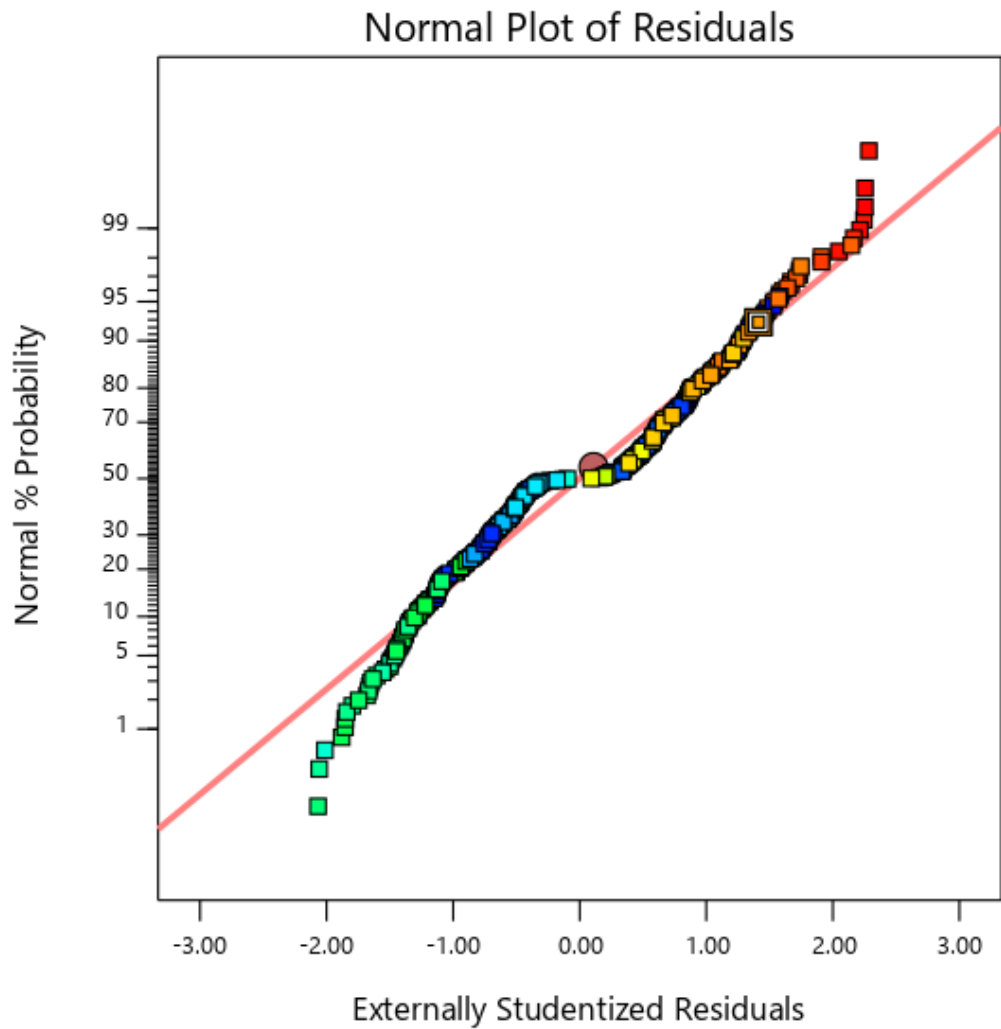
Appendix F Program Files

The figure below shows the LabVIEW file used to convert the force data from collection into an Excel file for further analysis.





Appendix G
Normal Plot of Residuals



cutting force

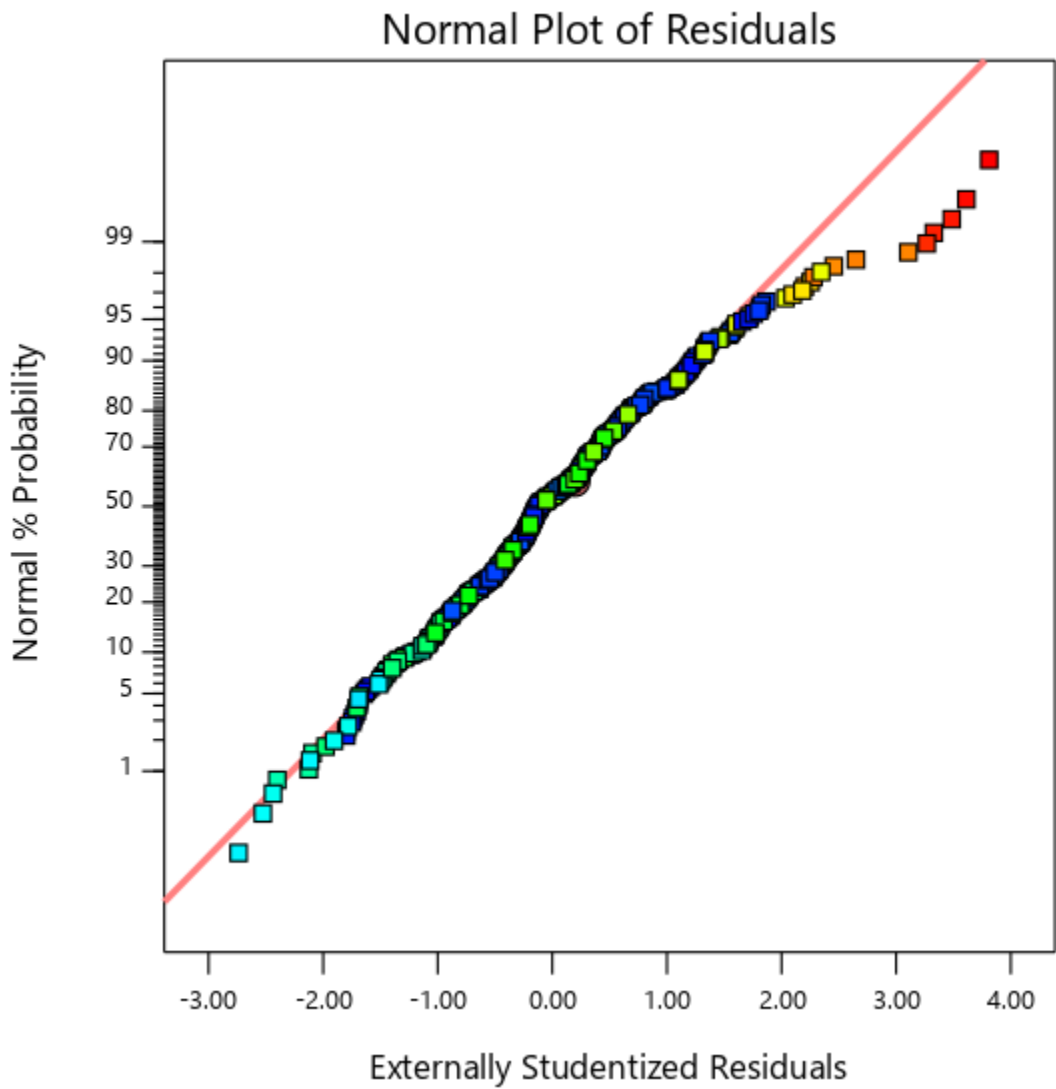
Color points by value of
cutting force:

22.2874  416.851

Std # 258 Run # 325

X: 1.414

Y: 92.7

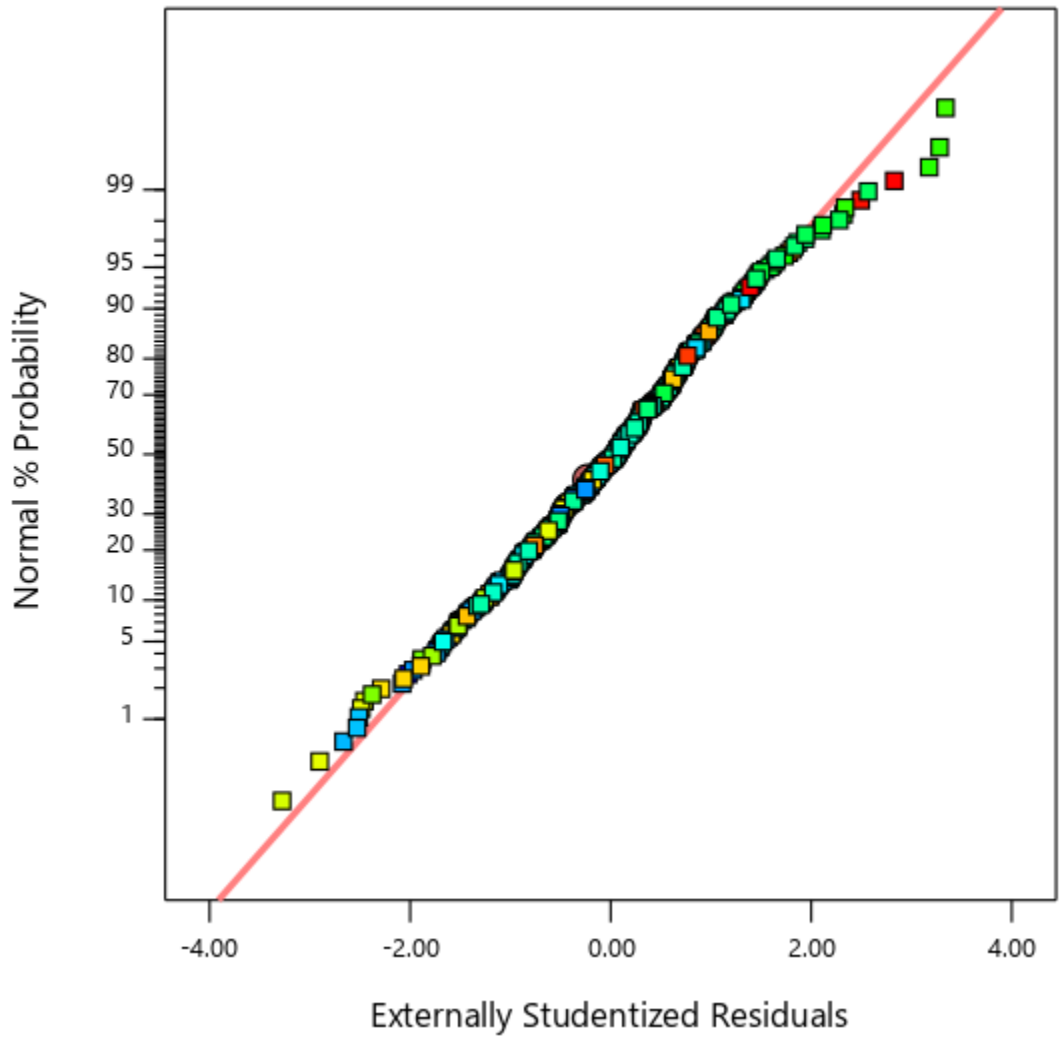


thrust force

Color points by value of
thrust force:

-0.394737  146.569

Normal Plot of Residuals

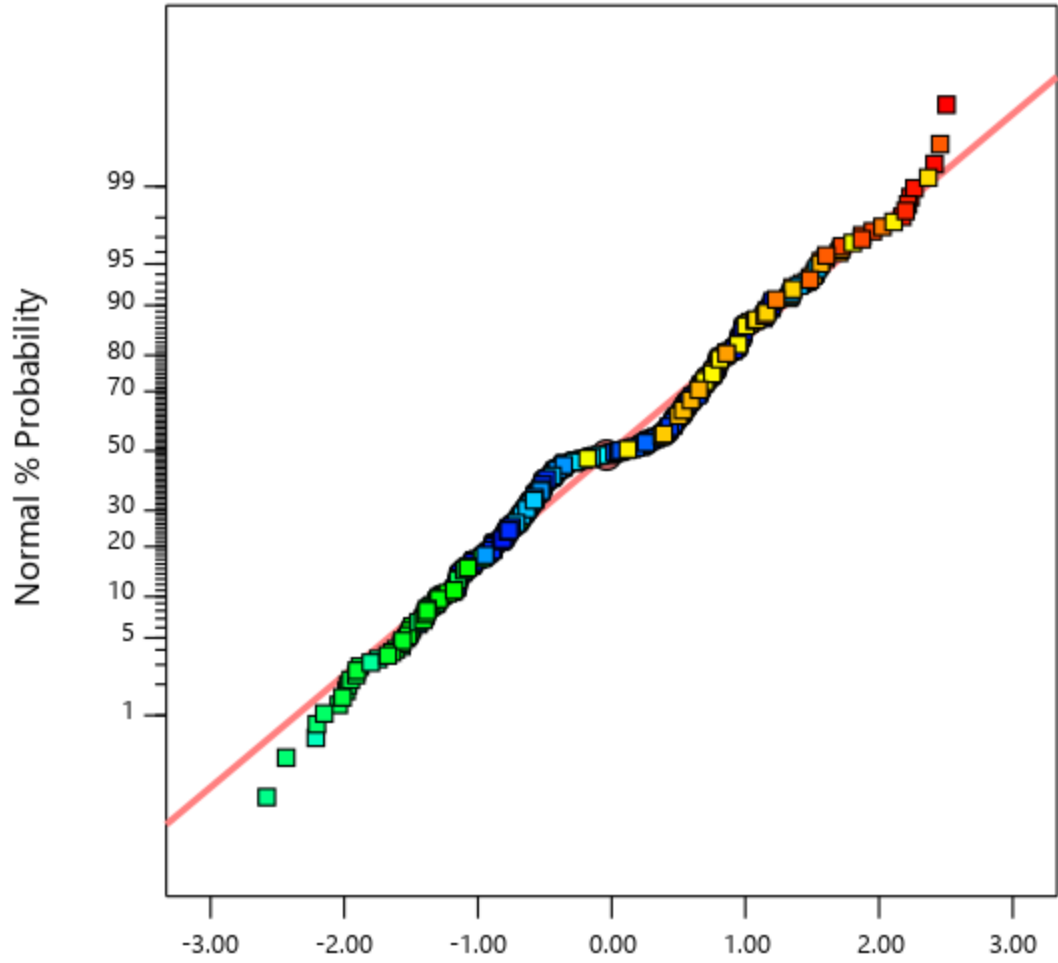


Shear Angle

Color points by value of Shear Angle:

10.5  65.7

Normal Plot of Residuals

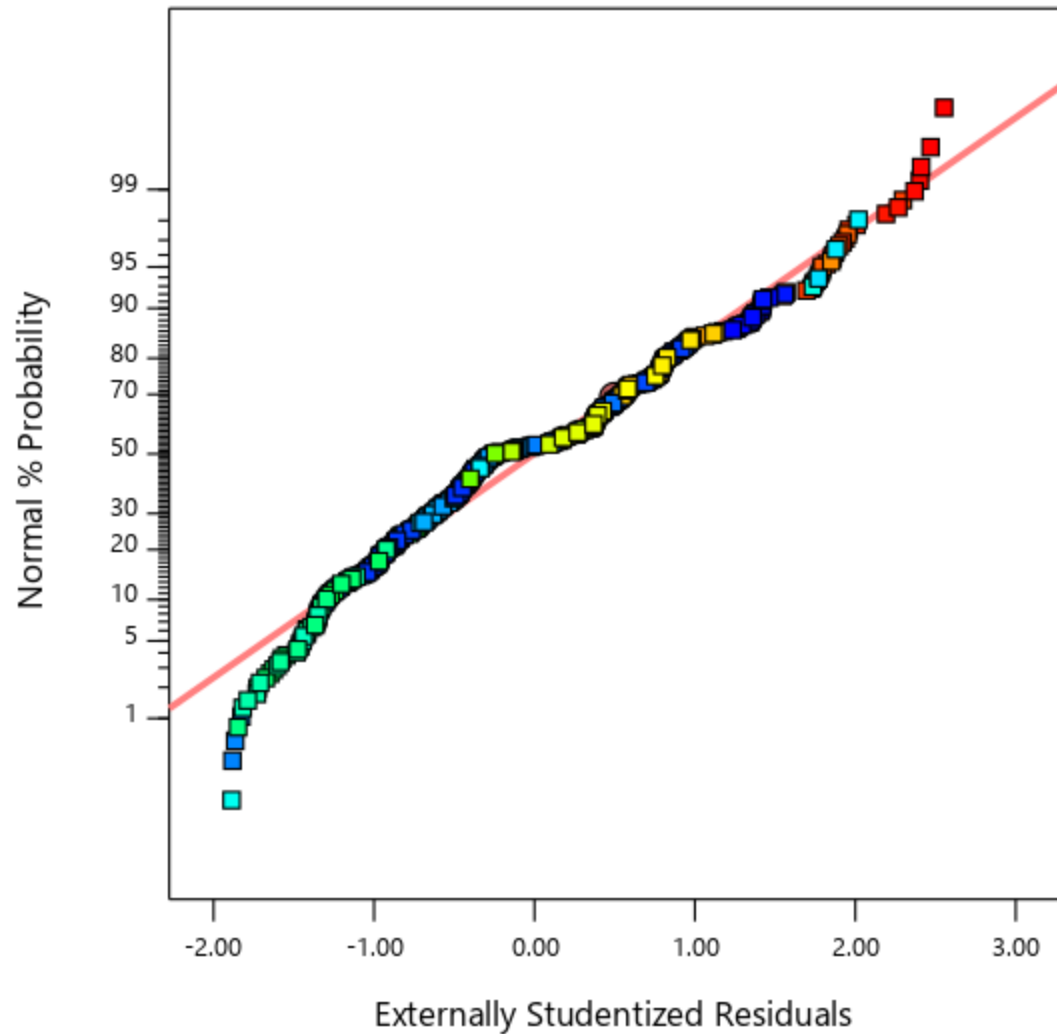


Friction Force

Color points by value of Friction Force:

60.568  1372.684

Normal Plot of Residuals

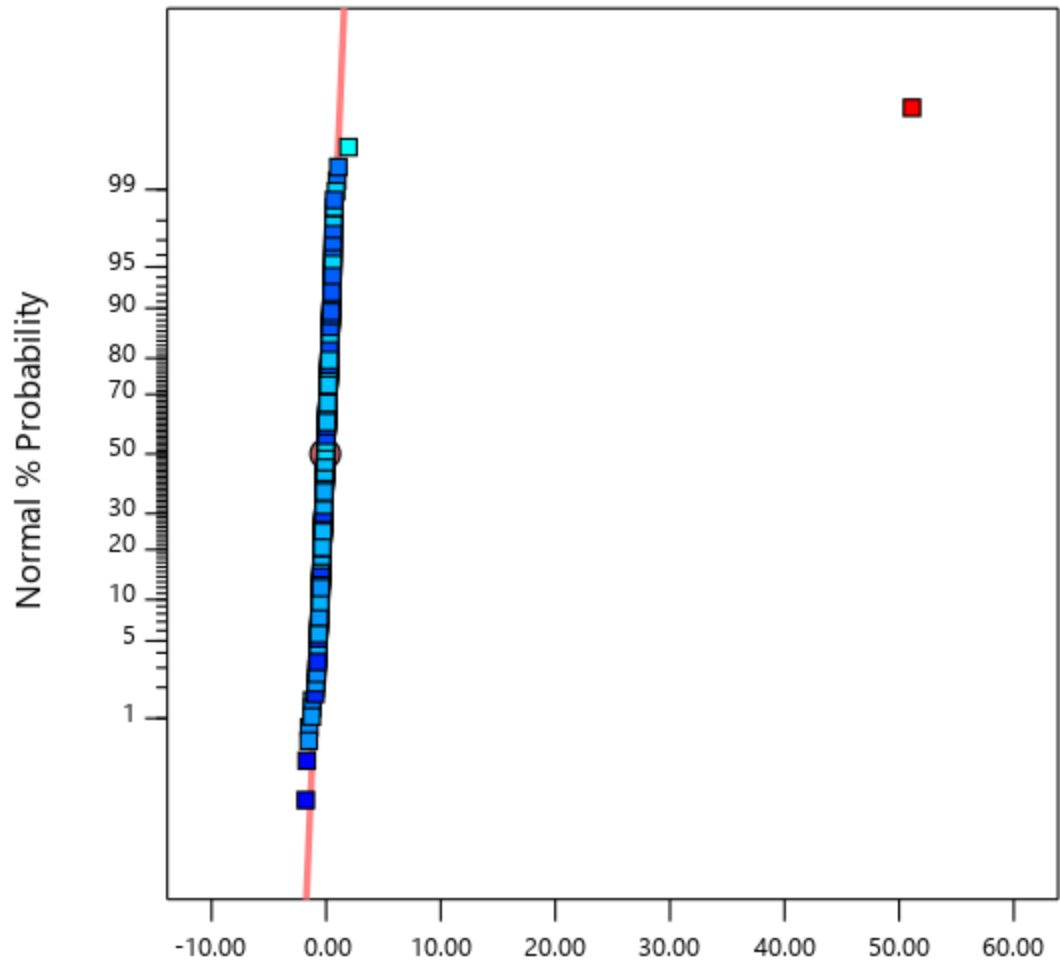


Normal Force

Color points by value of
Normal Force:

65.754  1411.072

Normal Plot of Residuals



Externally Studentized Residuals

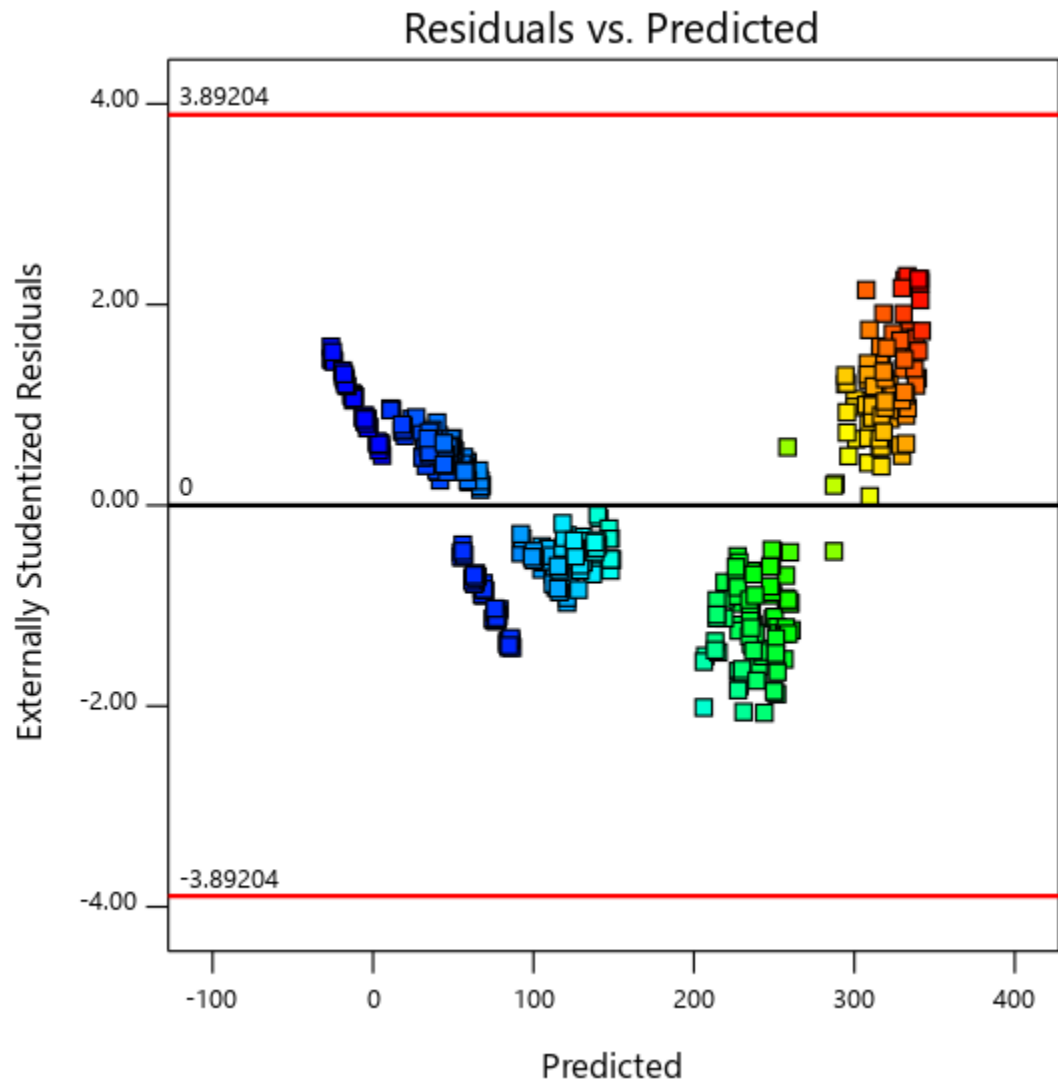
Psi

Color points by value of

Psi:

-20.2465  266.425

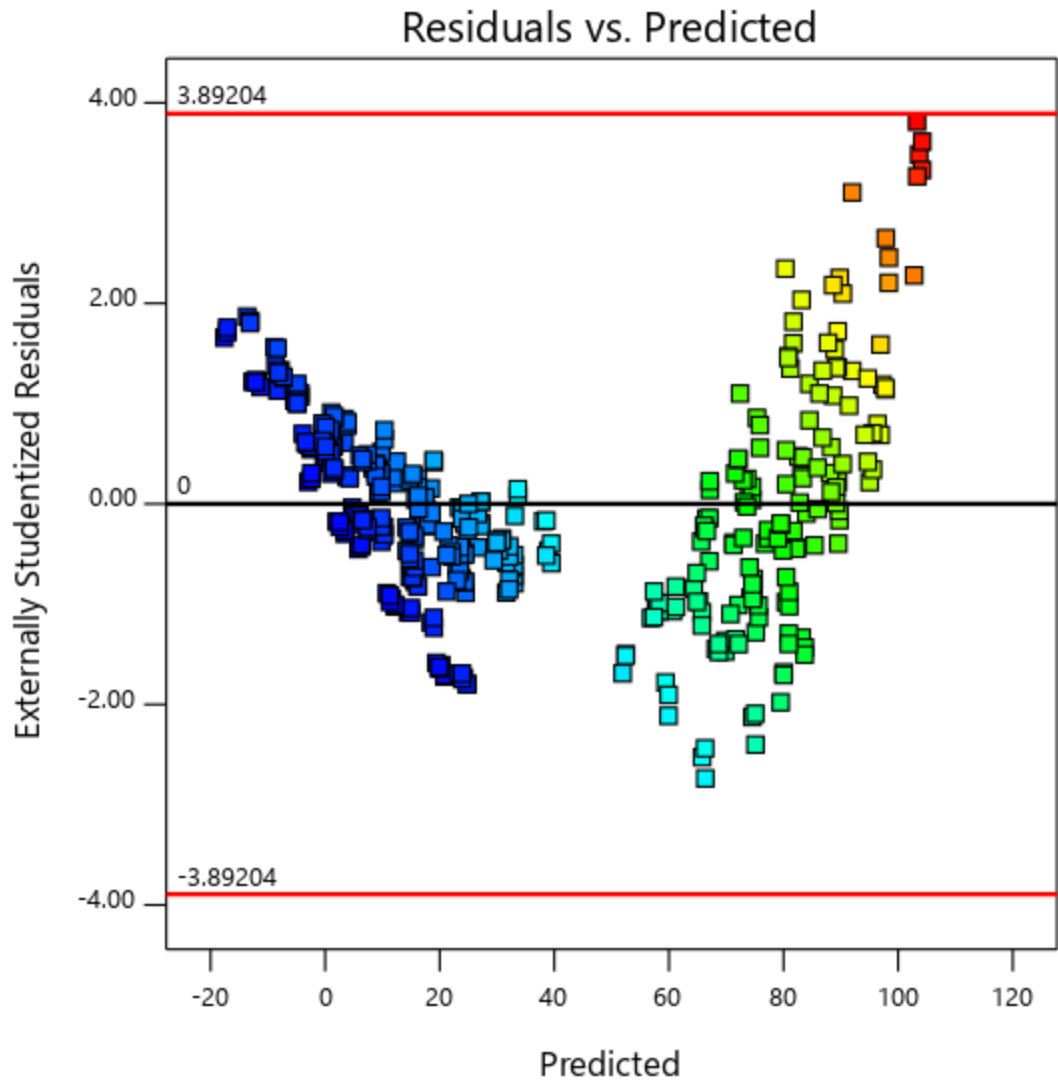
Appendix H
Residuals vs. Predicted



cutting force

Color points by value of
cutting force:

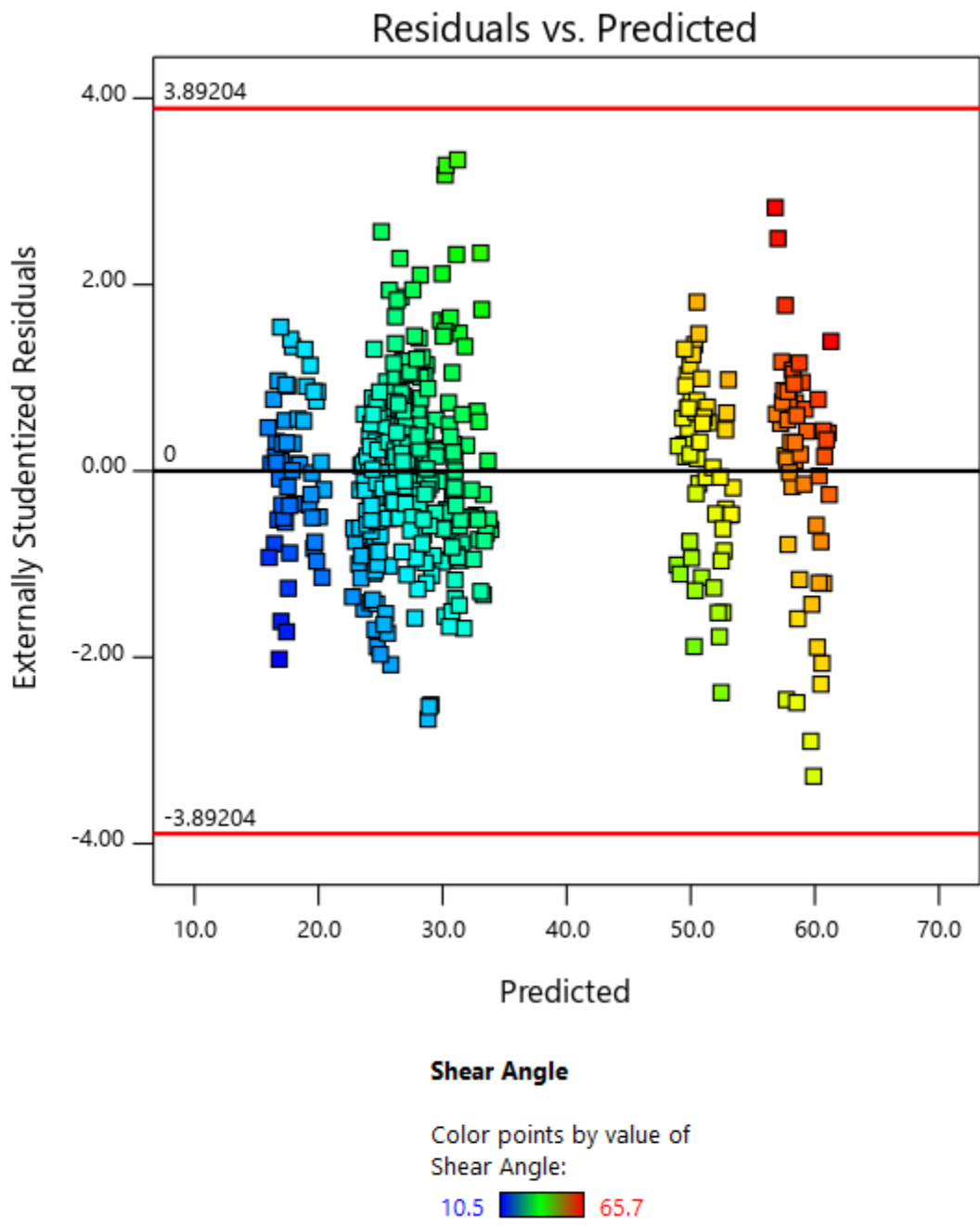


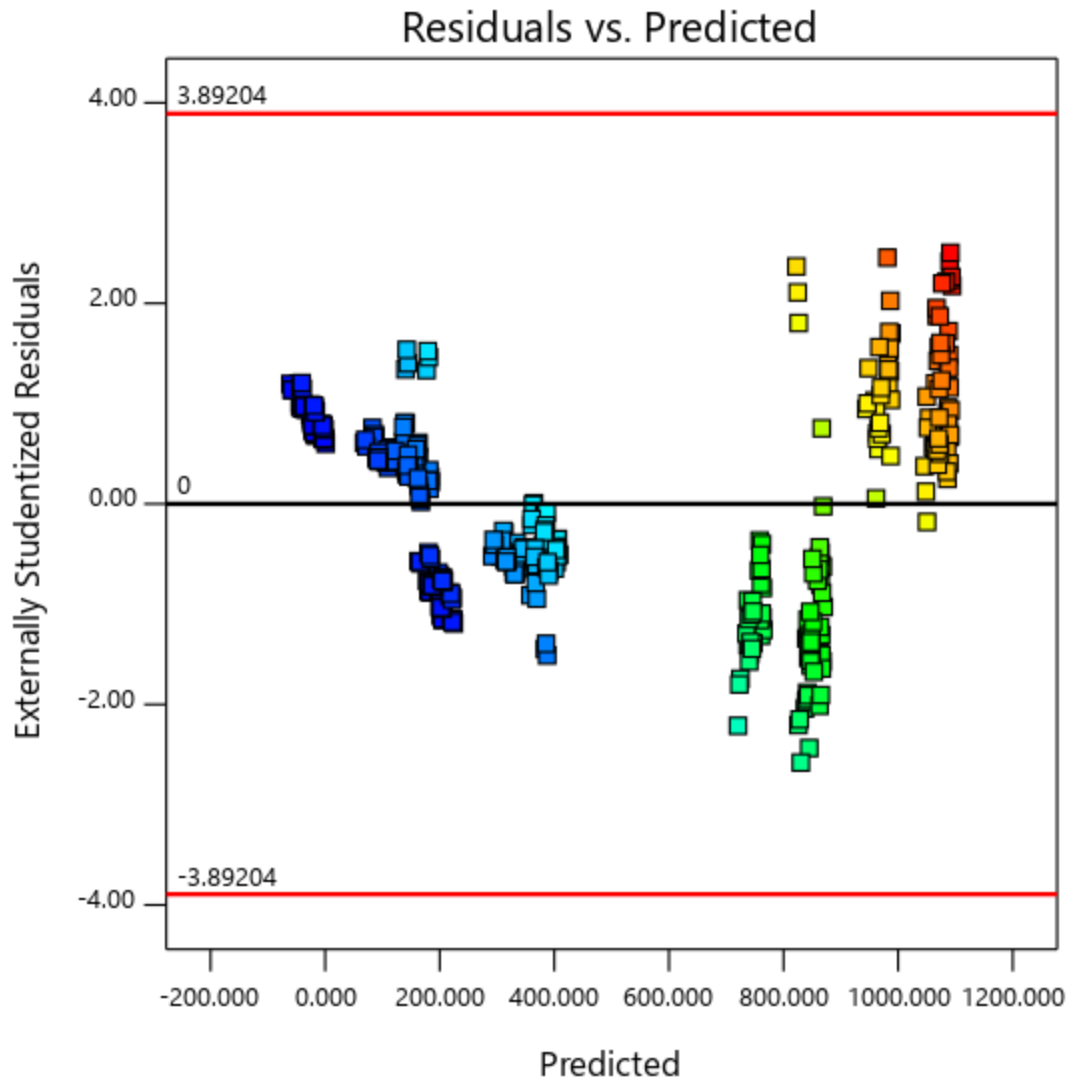


thrust force

Color points by value of
thrust force:

-0.394737  146.569

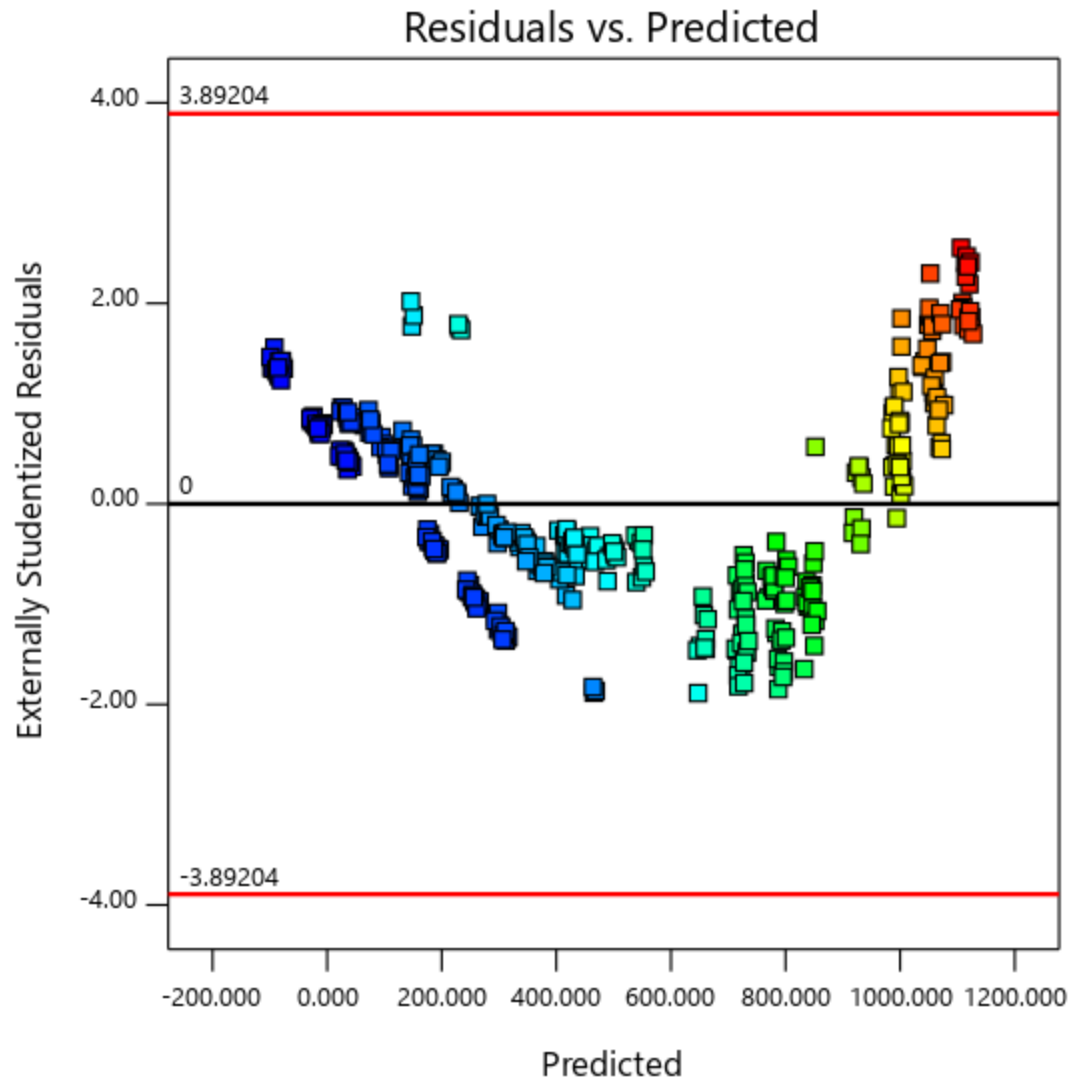




Friction Force

Color points by value of Friction Force:

60.568  1372.684



Normal Force

Color points by value of
Normal Force:

65.754  1411.072

